HOKKAIDO UNIVERSITY

Title	Development of Microfluidic Devices for Production of Size-Controlled Lipid Nanoparticles and Application to Nanomedicines
Author(s)	木村, 笑
Degree Grantor	北海道大学
Degree Name	博士(工学)
Dissertation Number	甲第14467号
Issue Date	2021-03-25
DOI	https://doi.org/10.14943/doctoral.k14467
Doc URL	https://hdl.handle.net/2115/81274
Type	doctoral thesis
File Information	KIMURA_Niko.pdf

Hokkaido University Collection of Scholarly and Academic Papers : HUSCAP

Development of Microfluidic Devices for Production of Size-Controlled Lipid Nanoparticles and Application to Nanomedicines

脂質ナノ粒子作製用マイクロ流体デバイスの開発と
ナノ医薬品作製への応用

Niko Kimura

Graduate School of Chemical Sciences Engineering

Hokkaido University

Title Development of Microfluidic Devices for Production of Size-Controlled Lipid Nanoparticles and Application to Nanomedicines

Author Niko Kimura

Degree Doctor of Philosophy (Engineering)

Supervisor Professor Manabu Tokeshi

CONTENTS

CHAPTER 1 General Introduction

1.1 Development of Lipid-Based Nanomedicines

Biocompatible carrier-assisted drug delivery systems (DDSs) are a novel breakthrough that could mitigate current problems in cancer chemotherapies and gene therapies. Carrier-assisted DDS enable the controlled delivery and release of encapsulated pharmaceutical products. Several drug carriers in the 10-nm to 5-μm diameter size range have been developed [1]. Natural materials, including phospholipids [2] and polysaccharides (chitosan, dextran, and hyaluronan) [3], which were expected to show high biocompatibility, were first used as the main components of carrier particles. In addition to these natural materials, synthesized lipids and biodegradable polymers have been developed to improve therapeutic efficiency and have been employed for the carrier materials [4-7]. In particular, lipid-based nanocarriers such as liposomes and lipid nanoparticles (LNPs) are most widely used as nanomedicines [8-12]. Their high biocompatibility, particle composition flexibility, and payloads are remarkable advantages of DDSs. Several liposomal drugs and LNP-based genetic nanomedicines have been approved for the treatment of cancer, infectious diseases, and gene therapies. In addition, extracellular vesicles, such as exosomes and artificial exosomes, have attracted attention as novel nanomedicines [13-16]. This section gives an overview of the advances of lipid-based nanomedicines.

1.1.1 Liposomal Drugs

In 1965, Bangham et al. described the first synthetic phospholipid vesicles called liposomes [17], and soon after, these were applied as DDSs. Extrusion techniques for size adjustment, remote drug loading methods, and surface modifications for long circulating times and targeted delivery, such as polyethylene-glycol modification (PEGylation) and ligand modification, have contributed to the development of liposomal drugs [18]. Viruses also have liposomal structures, and viral nanoparticles (VNPs) and virus-like particles (VLPs), which are genome-free VNP counterparts, have also been developed for effective drug delivery[19]. However, risk of adverse effects and time-consuming preparation have prevented their mass production and clinical application [20, 21]. In contrast, nonviral liposomes show low cytotoxicity and reduce the adverse effects of payloads [22].

Some of the approved liposomal drugs used to deliver anticancer and anti-fungal drugs are listed in Table 1.1. These liposomal drugs are mainly composed of phosphatidylcholine (PC), phosphatidylglycerol (PG), and sphingomyelin (SM) to construct the lipid bilayer structure [23]. Cholesterol stabilizes the membranes [24] and PEGylated-phosphatidylethanolamine (PE) enables long circulation times [25].

Table 1.1 Approved liposomal drugs

Name	**Encapsulated Drug**	**Lipids**	**Size [nm]**	**Indication**	**Year Approved**	**Company**
AmBisome®	Amphotericin B	HSPC, DSPG, and cholesterol	45-80	Aspergillosis	1997 (USA)	Gilead
Doxil®	Doxorubicin	HSPC, cholesterol, and DSPE-PEG 2K	~100	Kaposi's sarcoma, ovarian cancer, and breast cancer	1995 (USA) 1999 (USA) 2003 (Europe, Canada)	Johnson & Johnson
Myocet®	Doxorubicin, Cyclophosphadamide	EPC and cholesterol	190	Metastatic breast cancer	2000 (Europe)	Cephalon
Visudyne®	Verteporphin	EPG and DMPC	100	Ocular histoplasmosis	2000 (USA) 2003 (Japan)	QLT
Lipo-Dox®	Doxorubicin	DSPC, cholesterol, and DSPE-PEG 2K	20	Kaposi's sarcoma, ovarian cancer, and breast cancer	2001 (Taiwan) 2012 (USA)	Taiwan Liposome
Marqibo®	Vincristine	SM and cholesterol	100	Non-Hodgkin's lymphoma and leukemia	2012 (USA)	Acrotech Biopharma
Vyxeos™	Daunorubicin, Cytarabine	DSPC, DSPG, and cholesterol	100	Acute myeloid leukemia	2017 (USA)	Jazz Pharmaceuticals

HSPC: L-α-phosphatidylcholine, hydrogenated (Soy); DSPG: 1,2-distearoyl-sn-glycero-3-phospho-(1'-rac-glycerol); DSPE-PEG 2K: polyethylene-glycol 2000-distearoyl phosphatidylethanolamine; EPC: ethyl phosphatidylcholine; EPG: ethyl phosphatidylglycerol; DMPC: dimyristoyl phosphatidylcholine; DOPC: dioleoyl phosphatidylcholine; SM: Sphingomyelin

1.1.2 Lipid Nanoparticle-Based Genetic Nanomedicines

Genetic drugs such as small interfering RNA (siRNA), mRNA, or plasmids allow gene therapies for causal treatment of intractable diseases. However, naked nucleic acids are degradable in biological fluids and show no accumulation in tissues following systemic injection. Additionally, their genetic information could induce undesirable immunogenicity [26]. To overcome these issues, sophisticated genetic drug delivery technologies are required for the clinical application of gene therapies. The clinical potential of liposomal drugs has dramatically affected the generation of LNP-based genetic nanomedicines [5, 27, 28]. However, the conventional pH-gradient-assisted loading methods used to produce small molecule drug-loaded liposomes cannot be applied to the production of macromolecule negatively charged genetic drug-loaded LNPs. Therefore, novel methods for effective encapsulation of nucleic acids are required to develop LNP-based genetic nanomedicines.

Synthesized cationic lipids that have a quaternary amine provided a way forward. Dioleoyl-3-trimethylammonium propane (DOTAP) and 1,2-di-O-octadecenyl-3-trimethylammonium propane (DOTMA) are popular, permanently positively charged lipids used as the lipid components with phospholipids, cholesterol, and other lipids (Figure 1.1). Although cationic lipids allow effective encapsulation of nucleic acids, the permanently positively charged LNP surface induces high cytotoxicity [29, 30]. Instead of the cationic lipids, ionizable lipids, which have a tertiary amine, have been used for nucleic acid-loaded LNPs. 1,2-dioleoyl-3-dimethylammonium-propane (DODAP) is the first commercialized ionizable lipid [4]. In recent years, numerous ionizable lipids have been developed, and several LNP-based genetic nanomedicines have been approved or in clinical trials as shown in Table 1.2.

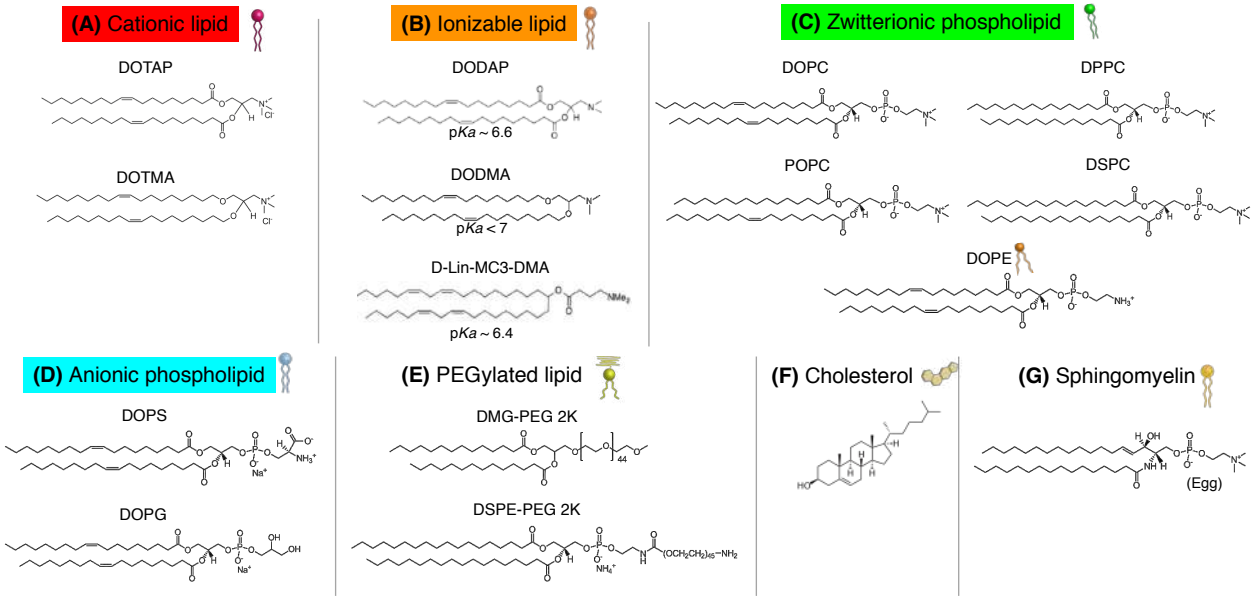

DOTAP: 1,2-dioleoyl-3-trimethylammonium-propane; DOTMA: 1,2-di-O-octadecenyl-3-trimethylammonium propane; DODAP: 1,2-dioleoyl-3-dimethylammonium-propane; DODMA: 1,2-dioleyloxy-3-dimethylaminopropane; D-Lin-MC3-DMA: (6Z,9Z,28Z,31Z)-heptatriacont-6,9,28,31 -tetraene-19-yl 4-(dimethylamino)butanoate; DOPC: 1,2-dioleoyl-sn-glycero-3-phosphocholine; POPC: 1-Palmitoyl-2-oleoyl-sn-glycero-3-phosphocholine; DPPC: 1,2-Dipalmitoyl-sn-glycero-3-phosphorylcholine; DSPC: 1,2-distearoyl-sn-glycero-3-phosphocholine; DOPE: 1,2-dioleoyl-sn-glycero-3-phosphoethanolamine; DOPS: 1,2-dioleoyl-sn-glycero-3-phospho-L-serine; DOPG: 1,2-dioleoyl-sn-glycero-3- phospho-(1'-rac-glycerol); DSPE-PEG 2K: polyethylene glycol 2000 - distearoyl phosphatidylethanolamine; DMG-PEG 2K: 1,2-dimyristoyl-rac-glycero-3-methoxypolyethylene glycol-2000

Figure 1.1 Popular lipids used for lipid-based nanomedicines

Table 1.2 LNP-based genetic nanomedicines approved and in clinical trials

Name	Genetic Drug	Indication	Status	Company
ONPATTRO®	siRNA	Transthyretin-induced amyloidosis	Approved 2018 (USA)	Alnylam
ARB-001467	siRNA	Hepatitis B	Phase II (completed)	Alnylam
TKM-080301	siRNA	Hepatocellular carcinoma	Phase I/II (completed)	Arbutus Biopharma
ALN-VSP02	siRNA	Liver cancer	Phase I (completed)	Arbutus Biopharma
ND-L02-s0201	siRNA	Idiopathic pulmonary fibrosis	Phase II	Nitto Denko Corporation
EPHARNA	siRNA	Advanced or recurrent solid tumors	Phase I	M.D. Anderson Cancer Center)
Lipo-MERIT	mRNAs	Melanoma	Phase I	Biotech RNA Pharmaceuticals

IVAC_W_brel_uID IVAC_M_uID	mRNAs	Triple negative breast cancer	Phase I	Biotech RNA Pharmaceuticals
SGT-53	pDNA	Metastatic pancreatic cancer	Phase II	SynerGene Therapeutics
MTL-CEBPA	saRNA	Advanced liver cancer	Phase I	Mina Alpha
NTLA-2001	sgRNA-TTR mRNA-Cas9	ATTRv amyloidosis	Phase I (planned)	Intellia Therapeutics/Regeneron

siRNA: small interfering RNA; mRNA: messenger RNA; pDNA: plasmid DNA; saRNA: small activating RNA; sgRNA: single-guide RNA

1.1.3 Application to Exosome-Inspired Nanomedicines

Small molecule drug-loaded liposomal nanomedicines and LNP-based genetic nanomedicines have shown progress over the past decades. In addition to these lipid-based nanomedicines, exosomes have provided a way forward for novel nanomedicines.

Since the first report concerning exosome-mediated microRNA transfer by Valadi et al. in 2007, exosomes have drawn attention in life sciences [31]. Exosomes are nanometer-sized extracellular vesicles and have a unilamellar phospholipid bilayer, as shown in Figure 1.2. Exosomes are a natural lipid-based nanocarrier for nucleic acid delivery. Exosome-inspired nanomedicines, including exosomal nanomedicines and artificial exosomes, are expected to have high biocompatibility and selective targeting. Exosomal nanomedicines are composed of purified exosomes obtained using differential centrifugation, size extrusion chromatography, precipitation, membrane filtration, and immunomagnetic isolation methods [32]. In the case of exosomal drugs, anticancer drugs and nucleic acids are loaded into the purified exosomes using incubation, electroporation, and sonication [33-36]. Exosomes labeled with fluorescent dyes and inorganic nanoparticles are also used for site-specific imaging technologies to analyze detailed in vivo behavior such as biodistribution, migration, and targeting mechanisms [16]. Artificial exosomes are composed of appropriate lipids [13, 37] and modified by membrane proteins [38]. The ease of manufacture and flexibility are expected to contribute to the clinical applications of exosome-inspired nanomedicines.

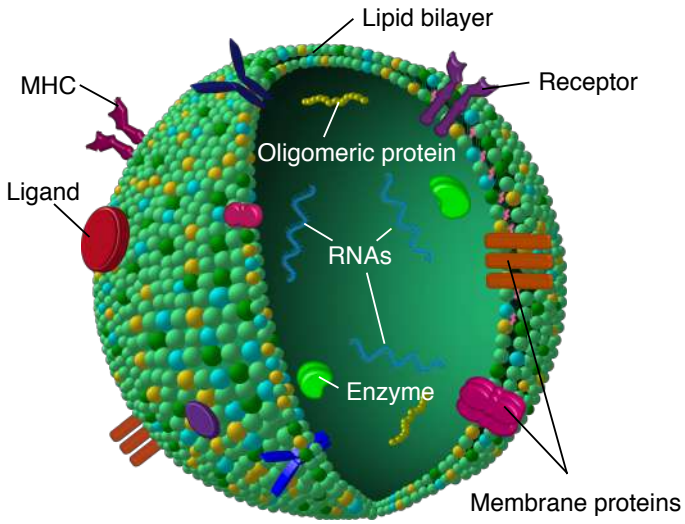

MHC: Major histocompatibility complex

Figure 1.2 Schematic representation of an exosome

1.2 Size-Depending Biodistribution of Biocompatible Nanoparticles (NP)

The effect of biocompatible NP size on biodistribution, bioavailability, and activity has been reported by several studies. In 2000, Saez et al. reported that 100-nm-sized and 160-nm-sized cyclosporine (CyA)-loaded NPs, an immunosuppressive drug, showed different organ distributions, such as in the liver, kidney, and spleen. They found that 160-nm-sized CyA-loaded NPs were accumulated in the liver. In contrast, 100-nm-sized CyA-loaded NPs were homogeneously distributed in each organ. These results indicate that the size difference of NPs may affect bioavailability [39]. In 2005, Hu-Lieskovan et al. were the first to report that the systemic application of small interfering RNA (siRNA)-loaded NPs in the 50–100 nm size range achieve safe and sequence-specific inhibition of tumor glowing in a disseminated tumor model. Their work provided a breakthrough in the conventional naked siRNA delivery [40].

In the past decade, the strategy of biocompatible NP size-based therapy has shifted to use sub-100-nm-sized NPs. In 2011, Cabral et al. revealed different accumulability and permeability in hypovascular tumors using polymer micelles loaded with 1,2-diaminocyclohexane-platinum(II) (DACHPt) with diameters of 30, 50, 70, and 100 nm. They demonstrated that the carrier particle size from 50 to 100 nm did not show any size

dependency on extravasation and penetration in highly permeable tumors. However, only 30-nm-sized carrier particles showed permeability in hypovascular tumors [41]. In 2013, Hirsjarvi et al. also reported that 25-nm-sized, lipid-based nanocarriers were more rapidly distributed in peripherical capillaries and accumulated in mice tissues than 50-nm-sized lipid-based nanocarriers [42]. In 2018, Mukhamadiyarov et al. reported that 70-nm-sized LNPs more effectively accumulated in rat ischemic myocardium than 100-nm-sized LNPs [43]. Ren et al. reported that 100 nm was a more appropriate size of LNPs for rheumatoid arthritis therapy than 70 nm [44]. Therefore, precisely size-controlled LNPs with various sizes in the range from 20 to 100 nm are necessary to develop highly effective lipid-based nanomedicines.

1.3 Lipid Nanoparticle Preparation Methods

There are several methods for preparing LNPs, and the Bangham method and organic solvent injection method are the most popular (Figure 1.3). These methods use lipid dissolved organic solvent (lipid solution) and an aqueous solution. The Bangham method is composed of two steps for LNP synthesis. Thin lipid film is formed by solvent evaporation, and then the film is hydrated using an aqueous solution to synthesize LNPs. This method is one of the most famous LNP production methods; however, it requires an additional process to adjust the LNP size using sonication and extrusion.

The organic solvent injection method allows a one-step production. In brief, a lipid solution dissolved in an organic solvent, such as alcohols, is injected into an aqueous solution. LNPs are formed by the self-assembly of lipid molecules. In this process, lipid molecules are spontaneously aggregated by decreasing their solubility and forming an intermediate structure. The intermediate structure finally turns into LNPs [45, 46]. When the organic solvent is diluted rapidly using the aqueous solution, the small-sized LNPs can form with narrow particle size distribution. In the batch method, LNPs are synthesized with low homogeneity in the macroscale reaction field, and the size adjustment process is needed, similar to the Bangham method.

The microfluidic device-assisted method enables precise size control of LNPs. A microfluidic device can flexibly operate the chemical reaction and continuously produce LNPs. The shorter diffusion length of the microchannel compared to the conventional macroscale methods allows the precise size control of LNPs; thus, the production of the small-sized LNPs is possible. In addition, a microfluidic device enables on-demand LNP production. Therefore, both the reduction of sample consumption for screening and the mass production of lipid-based nanomedicines for practical applications can be compatible using a microfluidic device. Owing to these unique features, microfluidic devices have been considered novel apparatus in the field of biocompatible carrier-assisted nanomedicine production [47]. A microchannel can promote the dilution rate of organic solvents through shorter diffusion lengths. Therefore, the microfluidic device-assisted organic solvent injections have significant advantages to produce the size-controlled, LNP-based nanomedicines. Several microfluidic devices have been developed. The chaotic micromixer (CM) device is a popular microfluidic device used for LNP production.

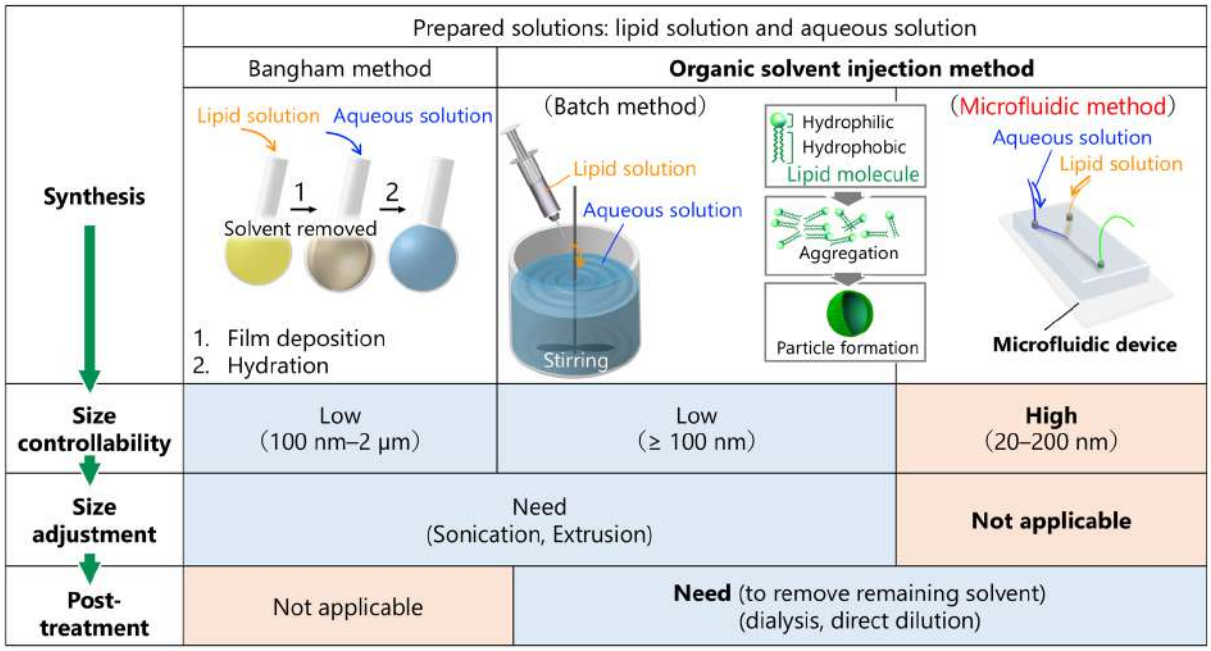

Figure 1.3 Methods for LNP production

1.3.1 CM device-based LNP synthesis method

In 2002, Strook et al. defined the innovative micromixer structure, called the CM (Figure 1.3) [48]. Before that innovation, stable laminar flow in microchannels made it difficult to mix solutions, which caused a bottleneck for microfluidic device-based chemical reactions. The CM consists of a rectangular microchannel with staggered herringbone grooves. These grooves cause asymmetric and transverse flow in the microchannel, resulting in two counter-rotating vortices and complete mixing. Therefore, the CM device is excellent at homogeneous mixing in the microchannel and is the current gold-standard device for LNP-based nanomedicine production [49-55], commercialized as NanoAssemblr® from Precision Nanosystems Inc.

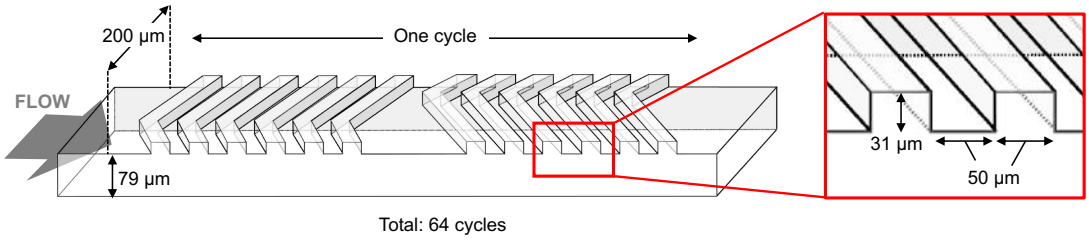

Figure 1.4 Schematic representation of the chaotic mixer (CM) structure

In 2012, Zhigaltsev et al. first reported the production of 20-nm-sized, phospholipid-based NPs using the CM device [49]. Twenty nanometer is the theoretical minimum size used in the lipid system. They found that LNP size could be controlled by flow rate and flow rate ratio (aqueous solution/lipid solution), which is one of the benefits of microfluidic LNP production. Uniform LNPs with various sizes can be produced by a simple procedure, namely controlling the flow conditions. For the liposomal drug application, an anticancer drug (doxorubicin; DOX) was loaded into the 20-nm-sized LNPs by the remote loading method, and the encapsulation efficiency and effects of the loading method on the product size were evaluated. They demonstrated the loading efficiency of 60%–100% and achieved 20-nm-sized DOX-loaded LNPs. Furthermore, in the same year, Chen et al. reported rapid screening of lipid formulations for siRNA-loaded LNPs using CMs

[56]. They indicated the high applicability of the CM device in developing LNP-based nanomedicines for siRNA delivery. They investigated various lipid-based systems, and several siRNA-loaded LNPs were prepared using the device. Also, the gene-silencing activity of the produced siRNA-LNPs was evaluated in vitro and in vivo. In addition, in 2018, the siRNA-loaded LNP-based nanomedicine (Onpattro®) was approved by the Food and Drug Administration (FDA), and this nanomedicine was produced using the CM device-assisted method.

1.3.2 Proposed LNP formation mechanism

Dilution of the organic solvent is the driving force of the LNP formation process, regardless of the synthesis methods. Understanding the LNP formation behavior in a microchannel is important for precise LNP size control. In 2017, Maeki et al. reported the LNP formation mechanism in microfluidic devices using the CM device [53]. From the relationship between the number of mixer structures and the LNP size, at least 10 cycles of mixer structures are needed to produce the LNPs smaller than 50 nm. However, the fluid dynamics visualization experiment using a confocal microscope and a fluorescent lipid revealed that the solutions were not completely mixed under the flow conditions in the microchannel. These results suggest that the rapid dilution of ethanol was more significant than complete mixing for precise LNP size control.

1.4 Indicating a Gap and Outline of Thesis

As described in Subsection 1.3, microfluidic device-based LNP synthesis methods allow effective production of various size-controlled LNPs and nanomedicines. CM device is excellent at homogeneous dilution of organic solvent and allows precise size control of LNPs with narrow size distributions. Nevertheless, despite the progress of microfluidic device-assisted methods for LNP-based nanomedicines, three challenges still remain: (1) narrow range of size controllability, (2) laborious and un-controlled post-treatment process, and (3) limited applicability to nucleic acid-loaded nanomedicines.

First, the chaotic mixing fluid dynamics is not appropriate for controlling lipid nanoparticles with various sizes because the solutions can be completely and homogeneously mixed at any flow conditions at specific dilution rates to some degree. Therefore, there is no microfluidic device developed for the production of size-controlled LNPs with various sizes. Second, conventional post-treatment methods such as overnight dialysis and direct dilution could affect the structure and size of the final products. The LNP synthesis process is strictly controlled using microfluidic devices; however, the post-treatment methods are not controlled, and conventional methods are laborious and time-consuming. Therefore, the seamless microfluidic process composed of the LNP synthesis process and post-treatment process are expected to allow more precise size controllability and high-throughput production of LNPs. Third, few reports have achieved the production of size-controlled, nucleic acid-loaded, noncationic LNPs with high encapsulation efficiency. Most nucleic acid-loaded LNPs prepared using microfluidic devices are composed of synthetic cationic lipid-based systems. Effective electrostatic interactions between negatively charged nucleic acids and positively charged synthesized cationic lipid molecules allow high encapsulation efficiency. Conversely, noncationic lipid systems often show low encapsulation efficiency because the driving force for effectively trapping nucleic acids is lacking and the applicability of microfluidic methods have not been sufficiently investigated. Artificial exosomes, which are nucleic acid-loaded noncationic LNPs composed of exosome-like lipid systems, are expected to be next-generation genetic nanomedicines. To address these three challenges, this study was carried out as follows:

In Chapter 2 and Chapter 3, the development of several novel microfluidic devices equipped with optimized baffle structures to prepare size-controlled LNPs based on the microfluid dynamics is described. In Chapter 4, the investigations pertaining to the on-device, post-treatment process for the development of integrated microfluidic devices are delineated. In Chapter 5, the applications of the developed microfluidic device to produce size-controlled artificial exosomes are narrated. Finally, in Chapter 6, conclusions, implications of this study, and future perspectives are discussed.

References

[1] W. H. De Jong and P. J. Borm, *Int J Nanomedicine*, **3**, 133-149 (2008)

[2] R. P. Singh, H. V. Gangadharappa and K. Mruthunjaya, *J. Drug Deliv. Sci. Technol.*, **39**, 166-179 (2017)

[3] T. Miao, J. Wang, Y. Zeng, G. Liu and X. Chen, *Adv Sci (Weinh)*, **5**, 1700513 (2018)

[4] A. L. Bailey and P. R. Cullis, *Biochemistry*, **33**, 12573-12580 (1994)

[5] P. R. Cullis and M. J. Hope, *Mol. Ther.*, **25**, 1467-1475 (2017)

[6] X. Zhang, W. Zhao, G. N. Nguyen, C. Zhang, C. Zeng, J. Yan, S. Du, X. Hou, W. Li, J. Jiang, B. Deng, D. W. McComb, R. Dorkin, A. Shah, L. Barrera, F. Gregoire, M. Singh, D. Chen, D. E. Sabatino and Y. Dong, *Sci Adv*, **6** (2020)

[7] E. Calzoni, A. Cesaretti, A. Polchi, A. Di Michele, B. Tancini and C. Emiliani, *J Funct Biomater*, **10** (2019)

[8] T. Sun, Y. S. Zhang, B. Pang, D. C. Hyun, M. Yang and Y. Xia, *Angew. Chem. Int. Ed. Engl.*, **53**, 12320-12364 (2014)

[9] P. Yingchoncharoen, D. S. Kalinowski and D. R. Richardson, *Pharmacol. Rev.*, **68**, 701-787 (2016)

[10] B. Garcia-Pinel, C. Porras-Alcala, A. Ortega-Rodriguez, F. Sarabia, J. Prados, C. Melguizo and J. M. Lopez-Romero, *Nanomaterials (Basel)*, **9** (2019)

[11] K. Zabielska-Koczywąs and R. Lechowski, *Molecules*, **22** (2017)

[12] Y. Duan, A. Dhar, C. Patel, M. Khimani, S. Neogi, P. Sharma, N. Siva Kumar and R. L. Vekariya, *RSC Advances*, **10**, 26777-26791 (2020)

[13] S. Stremersch, R. E. Vandenbroucke, E. Van Wonterghem, A. Hendrix, S. C. De Smedt and K. Raemdonck, *J. Control. Release*, **232**, 51-61 (2016)

[14] M. Maeki, N. Kimura, Y. Sato, H. Harashima and M. Tokeshi, *Adv Drug Deliv Rev*, **128**, 84-100 (2018)

[15] M. Zhang, X. Zang, M. Wang, Z. Li, M. Qiao, H. Hu and D. Chen, *J Mater Chem B*, **7**, 2421-2433 (2019)

[16] O. Betzer, E. Barnoy, T. Sadan, I. Elbaz, C. Braverman, Z. Liu and R. Popovtzer, *Wiley Interdiscip Rev Nanomed Nanobiotechnol*, **12**, e1594 (2020)

[17] A. Bangham, *Current Contents/Life Sciences*, 14-14 (1989)

[18] T. M. Allen and P. R. Cullis, *Adv. Drug Deliv. Rev.*, **65**, 36-48 (2013)

[19] Y. H. Chung, H. Cai and N. F. Steinmetz, *Adv. Drug Deliv. Rev.* (2020)

[20] S. Hacein-Bey-Abina, *Science*, **302**, 415-419 (2003)

[21] A. N. Lukashev and A. A. Zamyatnin, *Biochemistry (Moscow)*, **81**, 700-708 (2016)

[22] G. Lin, L. Li, N. Panwar, J. Wang, S. C. Tjin, X. Wang and K.-T. Yong, *Coord. Chem. Rev.*, **374**, 133-152 (2018)

[23] A. Uzman, *Biochem. Mol. Biol. Educ.*, **31**, 212-214 (2003)

[24] S. Raffy and J. Teissie, *Biophys. J.*, **76**, 2072-2080 (1999)

[25] P. Milla, F. Dosio and L. Cattel, *Curr. Drug Metab.*, **13**, 105-119 (2012)

[26] A. G. Bowie and L. Unterholzner, *Nat. Rev. Immunol.*, **8**, 911-922 (2008)

[27] S. C. Semple, A. Akinc, J. Chen, A. P. Sandhu, B. L. Mui, C. K. Cho, D. W. Sah, D. Stebbing, E. J. Crosley, E. Yaworski, I. M. Hafez, J. R. Dorkin, J. Qin, K. Lam, K. G. Rajeev, K. F. Wong, L. B. Jeffs, L. Nechev, M. L. Eisenhardt, M. Jayaraman, M. Kazem, M. A. Maier, M. Srinivasulu, M. J. Weinstein, Q. Chen, R. Alvarez, S. A. Barros, S. De, S. K. Klimuk, T. Borland, V. Kosovrasti, W. L. Cantley, Y. K. Tam, M. Manoharan, M. A. Ciufolini, M. A. Tracy, A. de Fougerolles, I. MacLachlan, P. R. Cullis, T. D. Madden and M. J. Hope, *Nat. Biotechnol.*, **28**, 172-176 (2010)

[28] A. Schroeder, C. G. Levins, C. Cortez, R. Langer and D. G. Anderson, *J. Intern. Med.*, **267**, 9-21 (2010)

[29] T. Ren, Y. K. Song, G. Zhang and D. Liu, *Gene Ther.*, **7**, 764-768 (2000)

[30] D. A. Balazs and W. Godbey, *J Drug Deliv*, **2011**, 326497 (2011)

[31] H. Valadi, K. Ekstrom, A. Bossios, M. Sjostrand, J. J. Lee and J. O. Lotvall, *Nat. Cell Biol.*, **9**, 654-U672 (2007)

[32] E. J. Bunggulawa, W. Wang, T. Y. Yin, N. Wang, C. Durkan, Y. Z. Wang and G. X. Wang, *Journal of Nanobiotechnology*, **16** (2018)

[33] M. J. Haney, N. L. Klyachko, Y. L. Zhaoa, R. Gupta, E. G. Plotnikova, Z. J. He, T. Patel, A. Piroyan, M. Sokolsky, A. V. Kabanov and E. V. Batrakova, *J. Control. Release*, **207**, 18-30 (2015)

[34] Y. Liu, D. Li, Z. Liu, Y. Zhou, D. Chu, X. Li, X. Jiang, D. Hou, X. Chen, Y. Chen, Z. Yang, L. Jin, W. Jiang, C. Tian, G. Zhou, K. Zen, J. Zhang, Y. Zhang, J. Li and C. Y. Zhang, *Sci. Rep.*, **5**, 17543 (2015)

[35] J. L. Hood, M. J. Scott and S. A. Wickline, *Anal. Biochem.*, **448**, 41-49 (2014)

[36] H. Saari, E. Lazaro-Ibanez, T. Viitala, E. Vuorimaa-Laukkanen, P. Siljander and M. Yliperttula, *J. Control. Release*, **220**, 727-737 (2015)

[37] M. Lu, X. Zhao, H. Xing, Z. Xun, S. Zhu, L. Lang, T. Yang, C. Cai, D. Wang and P. Ding, *Int. J. Pharm.*, **550**, 100-113 (2018)

[38] M. Lu, X. Zhao, H. Xing, H. Liu, L. Lang, T. Yang, Z. Xun, D. Wang and P. Ding, *Acta Biomater.*, **96**, 517-536 (2019)

[39] A. Saez, M. Guzmán, J. Molpeceres and M. R. Aberturas, *Eur. J. Pharm. Biopharm.*, **50**, 379-387 (2000)

[40] S. Hu-Lieskovan, J. D. Heidel, D. W. Bartlett, M. E. Davis and T. J. Triche, *Cancer Res.*, **65**, 8984-8992 (2005)

[41] H. Cabral, Y. Matsumoto, K. Mizuno, Q. Chen, M. Murakami, M. Kimura, Y. Terada, M. Kano, K. Miyazono, M. Uesaka, N. Nishiyama and K. Kataoka, *Nature Nanotechnology*, **6**, 815-823 (2011)

[42] S. Hirsjarvi, L. Sancey, S. Dufort, C. Belloche, C. Vanpouille-Box, E. Garcion, J. L. Coll, F. Hindre and J. P. Benoit, *Int. J. Pharm.*, **453**, 594-600 (2013)

[43] R. A. Mukhamadiyarov, E. A. Senokosova, S. S. Krutitsky, D. V. Voevoda, I. A. Pyshnaya, V. V. Ivanov, M. J. Lewis and I. Khaliulin, *J. Cardiovasc. Pharmacol.*, **72**, 143-152 (2018)

[44] H. Ren, Y. He, J. Liang, Z. Cheng, M. Zhang, Y. Zhu, C. Hong, J. Qin, X. Xu and J. Wang, *ACS Appl Mater Interfaces*, **11**, 20304-20315 (2019)

[45] W. Shinoda, R. DeVane and M. L. Klein, *J. Phys. Chem. B*, **114**, 6836-6849 (2010)

[46] W. Shinoda, T. Nakamura and S. O. Nielsen, *Soft Matter*, **7** (2011)

[47] N. Kimura, M. Maeki and M. Tokeshi, Microfabrication and microfluidic devices for drug delivery, *Microfluidics for Pharmaceutical Applications: From Nano/Micro Systems Fabrication to Controlled Drug Delivery,* H. A. Santos, D. Liu and H. Zhang, eds., Elsevier, 123-136, (2019)

[48] A. D. Stroock, S. K. Dertinger, A. Ajdari, I. Mezic, H. A. Stone and G. M. Whitesides, *Science*, **295**, 647-651 (2002)

[49] I. V. Zhigaltsev, N. Belliveau, I. Hafez, A. K. K. Leung, J. Huft, C. Hansen and P. R. Cullis, *Langmuir*, **28**, 3633-3640 (2012)

[50] E. Kastner, R. Kaur, D. Lowry, B. Moghaddam, A. Wilkinson and Y. Perrie, *Int. J. Pharm.*, **477**, 361-368 (2014)

[51] A. K. K. Leung, Y. Y. C. Tam, S. Chen, I. M. Hafez and P. R. Cullis, *The Journal of Physical Chemistry B*, **119**, 8698-8706 (2015)

[52] M. Maeki, T. Saito, Y. Sato, T. Yasui, N. Kaji, A. Ishida, H. Tani, Y. Baba, H. Harashima and M. Tokeshi, *RSC Advances*, **5**, 46181-46185 (2015)

[53] M. Maeki, Y. Fujishima, Y. Sato, T. Yasui, N. Kaji, A. Ishida, H. Tani, Y. Baba, H. Harashima and M. Tokeshi, *PLoS One*, **12**, e0187962 (2017)

[54] Y. Li, R. J. Lee, X. Huang, Y. Li, B. Lv, T. Wang, Y. Qi, F. Hao, J. Lu, Q. Meng, L. Teng, Y. Zhou, J. Xie and L. Teng, *Nanomed. Nanotechnol. Biol. Med.*, **13**, 371-381 (2017)

[55] Q. Cheng, T. Wei, L. Farbiak, L. T. Johnson, S. A. Dilliard and D. J. Siegwart, *Nat Nanotechnol*, **15**, 313-320 (2020)

[56] D. Chen, K. T. Love, Y. Chen, A. A. Eltoukhy, C. Kastrup, G. Sahay, A. Jeon, Y. Dong, K. A. Whitehead and D. G. Anderson, *J. Am. Chem. Soc.*, **134**, 6948-6951 (2012)

CHAPTER 2 Development of the iLiNP Device for Precise Size Control of Lipid Nanoparticles

2.1 Introduction

In this chapter, microfluidic devices equipped baffle structures are developed for production of size controlled LNPs with various sizes. The developed microfluidic device enables producing size-controlled LNPs by rapid and controlled ethanol dilution.

Development of nanometer-sized drug carriers for nanodrug delivery systems (DDSs) is expected to improve the biodistribution and delivery efficiency of drugs and mitigate side effects. Nano-DDS technology makes it possible to overcome the problems of current DDS-based medications and provides a breakthrough for next-generation chemo- and gene therapies including tailor-made medicines [1]. Although several types of nano-DDS carriers [2-6] have been developed and showed excellent performance for in vivo and in vitro experiments, lipid nanoparticles (LNPs) are the most widely used nanocarriers for cancer treatment [7].

The size of the nanocarriers including LNPs affects the DNA and RNA delivery efficiency to target organs because large-sized nanocarriers have low permeability to stromal-rich tumors [8-12]. In contrast, small-sized nanocarriers show good permeability to stromal-rich tumors. In other words, stromal cells surrounding the tumor tissues are a barrier to the delivery of nanomedicines, and the interval between the stromal cells depends on the kinds of tumors. Therefore, precisely size-controlled LNPs, such as 10 nm size tuned LNPs, could provide size-selective targeting to various tumors. The LNP size tuning at 10 nm intervals is one of the most significant challenges in the development of next generation LNP-based nano-DDS carriers; however, it has not been achieved in any LNP preparation methods. Microfluidic devices enable rapid LNP preparation and have the potential to satisfy requirements for both a small amount of sample consumption and control of the LNP size [13-15]. In particular, the production of LNPs ranging from 20 to 100 nm, which show high penetration efficiency to the target tumors, was easily achieved by feeding the mixture of a lipid/alcohol solution and a DNA or RNA/buffer solution into a microfluidic device [11, 16-24]. Generally, LNP size is controlled by the flow conditions: flow rate of samples and flow rate ratio (FRR) of buffer to lipid solution. According to the literature, the chaotic mixer device is widely employed for LNP production to enhance the LNP size controllability [21-23, 25]. The chaotic mixer device has complicated three-dimensional grooved mixer

structures that make the rapid mixing of solutions possible [26]. However, LNPs easily clog the grooves of the chaotic mixers, and that leads to stagnation of sample flow. This is the major disadvantage of the chaotic mixer device for LNP production. Although the chaotic mixer device shows good LNP size controllability, its mixer design has low flexibility and robustness, especially regarding the microchannel aspect ratio, compared with two-dimensional mixer structures. This drawback affects the LNP size controllability and LNP productivity [27]. Moreover, the LNP size tuning at 10 nm intervals has not been achieved, even if the chaotic mixer device was to be used for LNP preparation. For these reasons, development of the novel LNP production platform is strongly desired for production of next-generation LNP-based nano-DDS carriers, which realize the LNP size-selective tumor targeting.

In this chapter, I developed the two-dimensional baffle device based on the LNP formation mechanism [23, 25, 28] and a fluid dynamics simulation. I have named the baffle device the invasive lipid nanoparticle production (iLiNP) device. It enabled the LNP size tuning at 10 nm intervals in the size range from 20 to 100 nm, whereas the chaotic mixer could not achieve the LNP size control. To my knowledge, this is the first report on the methodology for LNP size tuning at 10 nm intervals. Ten-nanometer tuned LNPs formed in the iLiNP device make LNP size-selective tumor targeting possible, and DNA and RNA can be delivered to target tumor tissues effectively by passing through the interval between the stromal cells. Furthermore, the iLiNP device had more flexibility and robustness of device design than the chaotic mixer devices. I also evaluated the utility of the iLiNP device for production of LNP-based nano-DDS carriers by an in vivo experiment. Eighty-nanometer-sized LNPs with encapsulated siRNA, which consisted of a pH-sensitive cationic lipid, PEGylated lipid, and cholesterol, were prepared with a narrower standard deviation of size than that of the conventional LNP production method. The siRNA-loaded LNPs were effectively delivered to hepatocytes of the extravascular region and showed good FVII gene-silencing activity.

2.2 Experimental

2.2.1 Materials

1-Palmitoyl-2-oleoyl-sn-glycero-3-phosphocholine (POPC), 1,2-diolleoyl-sn-glycero-3-phosphocholine (DOPC), 1,2-dimirystoyl-sn-glycero, and methoxylene glycol 2000 ether (PEG-DMG) were purchased from the NOF Corporation (Tokyo, Japan). Cholesterol (Chol) was purchased from Sigma-Aldrich (St. Louis, MO, USA). 1,2- Dioleoyl-sn-glycero-3-phosphoethanolamine-N-(lissamine rhodamine B sulfonyl) (Rho-PE) was purchased from Avanti Polar Lipids, Inc. (810150C, Alabaster, AL, USA). Ethanol, sodium chloride, chloroform, acetic acid, 2-morpholinoethane- sulfonic acid, monohydrate (MES), potassium chloride, and disodium hydrogen phosphate 12-water were purchased from Wako Pure Chemical Industries, Ltd. (Osaka, Japan). Sodium acetate and potassium dihydrogen phosphate were purchased from Kanto Chemical Co., Inc. (Tokyo, Japan). A pH-sensitive cationic lipid, YSK05, was synthesized as described previously [29]. RiboGreen and 1,1′ -dioctadecyl-3,3,3′ ,3′ -tetramethylindocarbocyanine perchlate (DiI) were purchased from Molecular Probes (Eugene, OR, USA). FITC-conjugated Isolectin B4 was purchased from Vector Laboratories (Burlingame, CA, USA). All siRNA samples were purchased from Hokkaido System Science Co., Ltd. (Sapporo, Japan). The siFVII sense and antisense strand sequences are 5′ -GGAucAucucAAGucuuAcTsT-3′ and 5′ -GuAAGAcuuGAGAuGAuccTsT-3′ , respectively. The Alexa Fluor-647 (AF647)-labeled siGL4 sense and antisense strand sequences are 5′ -AF647-CCGUCGUAUUCGUGAGCAATsT-3′ and 5′ -UUGCUCACGAAUACGACGGTsT-3′ , respectively. 2′ -Fluoro- modified nucleotides are represented in lower case, and the phosphorothioate linkage is represented as s.

2.2.2 Experimental Conditions for the CFD simulation

Computational fluid dynamics (CFD) simulation was used to study dilution performance of ethanol in the iLiNP device. Concentration profiles of ethanol were numerically simulated with a three-dimensional model

using COMSOL Multiphysics 5.2 (COMSOL, Inc., Burlington, MA). Physical properties of both ethanol and water were selected from the material library (database) in COMSOL. The dimensions of the geometric model for the basic structure iLiNP device were: 3 mm length, 0.2 mm width, and 0.1 mm height. The device design in the geometric model had ten sets of the baffle structures. Mesh elements were created by Free-Quad 2D followed by sweeping the mesh elements (2D plane) to create the 3D model, and the size was selected as "Fine" from the "Predefined list". The flow model selected incompressible flow Navier-Stokes equations. The laminar-flow model (no slip condition) and transport of the diluted species (ethanol) were used for simulation of the ethanol dilution process in the iLiNP device. The flow rate ranged from 50 to 500 μL/min, and the flow rate ratio (FRR; water flow rate to ethanol flow rate) was from 3 to 9.

For the fluid visualization experiment, I prepared 10 mg/ mL of DOPC containing 0.1 mol % Rho-PE ethanol solution and saline. The solutions were introduced into the iLiNP device at the flow rate of 500 μL/min and FRR of 3. A laser scanning confocal microscope (A1R, Nikon, Tokyo, Japan) was used for the microscopic observation. The mixing efficiency was calculated by image analysis using ImageJ (NIH). Fluid visualization in the iLiNP device was carried out at the same experimental conditions as previously studied [23].

2.2.3 iLiNP Device Fabrication

The master molds of the iLiNP devices were fabricated by the standard photolithography [30]. The master molds were made from SU-8 3050 (Nippon Kayaku Co., Ltd., Tokyo, Japan). In brief, SU-8 was spin-coated onto a 3 in. silicon wafer using a spin coater (MS-A100, Mikasa Shoji, Co., Ltd., Tokyo, Japan) to obtain a 100 μm thick SU-8 layer on the wafer. This was followed by baking at 95 °C to evaporate the solvent for SU-8. The silicon wafer was aligned with a photomask and exposed to UV light using a mask aligner (M-1S, Mikasa Shoji). After baking to get a cross-linking reaction of SU-8, the wafer was soaked in an SU-8 developer. The replica and molding process for making the PDMS microfluidic devices (iLiNP devices) was described previously [23].

2.2.4 Synthesis of LNPs

I employed two types of LNP systems, POPC LNPs and YSK-LNPs. For preparation of POPC LNPs, I prepared a 10 mg/mL POPC/ethanol solution and saline. For preparation of YSK-LNPs, a YSK05- based lipid/ethanol solution and 25 mM acetate buffer (pH 4.0) containing siRNA of 0.071 mg/mL were introduced into the iLiNP device. YSK05, chol, and PEG-DMG were dissolved in ethanol at a molar ratio of 50/50/1, and the total lipid concentration was adjusted to 8 mM. To make a comparison of the sizes of YSK-LNPs (Figure 6(A)) formed by the conventional vortex method and two microfluidic methods (one using a flat microchannel and the other using the iLiNP device), I used 25 mM acetate buffer not containing siRNA as the aqueous phase. These solutions were injected from separate syringes (GASTIGHT 1002, Hamilton Inc., Reno, NV, USA) into the iLiNP device by using syringe pumps (model 100, BAS Inc., Tokyo, Japan). The LNP-containing solutions were collected from the outlet in the microtubes. In the case of the YSK-LNPs, the collected YSK-LNPs were dialyzed for 2 h against 20 mM MES buffer (pH 6.0) followed by an overnight dialysis against phosphate-buffered saline (PBS) (pH 7.4) using a Spectra/Por 2 dialysis membrane standard RC tubing (molecular weight cutoff 12000−14000 Da; Spectrum Labo- ratories, Rancho Dominguez, CA). After dialysis, LNP solutions were stored in a refrigerator at 4 °C until the size measurement was carried out by dynamic light scattering (DLS) using a Zetasizer Nano ZS ZEN3600 instrument (Malvern Instru- ments, Worcestershire, UK).

2.2.5 In Vivo Experiments Using YSK-LNPs

I determined the encapsulation efficiency of siRNA using RiboGreen fluorescence assay. For the siRNA standard curve, 2 mg/mL of siRNA was diluted with 10 mM HEPES buffer (pH 7.4) to 500 ng/mL. LNP solutions were also diluted with 10 mM HEPES buffer to appropriate concentrations lower than 500 ng/mL. The diluted LNP solutions were applied to a 96-well microplate at a volume of 100 μL/well. I prepared two types of 10 mM HEPES buffer containing RiboGreen solutions in the presence or absence of 0.1 w/v % Triton X-

100. Then, the solutions were added to each microwell applied to diluted LNP solutions at a volume of 100 μL/well. Fluorescence was measured with an Enspire 2300 Multilabel Reader (PerkinElm- er, Aichi, Japan) with λ_{Ex} = 500 nm and λ_{Em} = 525 nm after incubation at room temperature (700 rpm, 30 s). siRNA encapsulation efficiency was calculated from the following equation.

$$\text{siRNA encapsulation efficiency [\%]} = \frac{\text{siRNA concentration of Triton (+)} - \text{siRNA concentration of Triton (-)}}{\text{siRNA concentration of Triton (+)}} \times 100$$

Triton(+) means the presence of TritonX-100, and Triton(−) means the absence of TritonX-100.

2.2.6 Measurement of Plasma Coagulation Factor VII (FVII)

Four female ICR mice (4 weeks of age) were purchased from Japan SLC (Shizuoka, Japan) and intravenously injected with the siFVII/LNPs. Plasma FVII activity was measured using a Biophen FVII kit (Hyphen BioMed, Oise, France).

2.2.7 Observation of Intrahepatic siRNA Distribution

ICR mice were intravenously injected with DiI-labeled AF647- siGL4/LNPs at a dose of 0.5 mg of siRNA/kg. DiI-labeled LNPs were prepared by adding 1 mM DiI/ethanol solution to the LNP solution at a concentration of 40 μM DiI. Fifty minutes after injection of the LNPs, the mice were administered FITC-conjugated Isolectin B4 (40 μg/mouse), and liver tissues were collected after a 10 min incubation. Intrahepatic distribution of siRNA was observed using a Nikon A1 (Nikon Co. Ltd., Tokyo, Japan), and images were captured by a 40×objectivelens.

2.3 Results and Discussion

2.3.1 Optimization of the Baffle Design and Its Fluid Dynamics Study

Figure 2.1 (A) shows three-dimensional and top views of the basic structure iLiNP device. I defined the standard dimensions of the baffle structure as the width (a) of 150 μm, the depth (b) of 100 μm, and the interval (c) of 100 μm. When there were 20 sets of the mixer structure, I called this the basic structure. The width and height of the microchannel were 200 and 100 μm. The baffle design is similar to a zigzag-shaped microchannel [31, 32] and a meander microchannel [33]. However, I found that the optimized baffle structures (width (a), depth (b), and intervals (c)) only enabled generation of secondary flow under the high flow rate conditions (>100 μL/min), and this leads to rapid dilution of ethanol to produce the small and uniform sized LNPs. Unlike the chaotic mixer device (Figure 2.1 (B)), the iLiNP device has a simple two-dimensional microchannel and mixer structure. In addition, the iLiNP device is expected to provide more effective mixing and dilution performance at the high flow rate condition compared with the chaotic mixer device from the viewpoint of fluid dynamics [32].

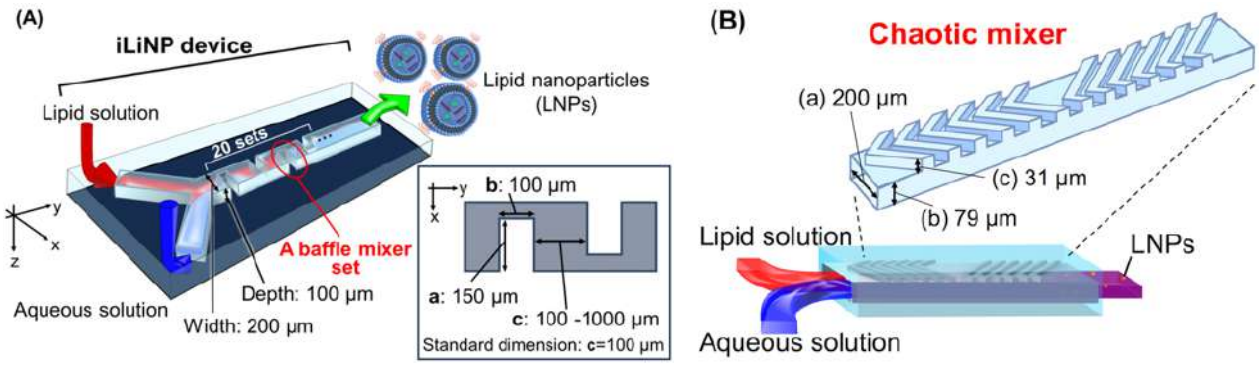

Figure 2.1 (A) Three-dimensional and top views of the iLiNP device with the basic structure of 20 baffle structure sets. Standard dimensions of the baffle structure were width (a) of 150 μm, depth (b) of 100 μm, and the interval (c) of 100 μm. The width and height of the microchannel were 200 and 100 μm. (B) Schematic illustration of the chaotic mixer device. The dimensions of microchannel and height of chaotic mixer structure were width (a) of 200 μm, flat channel height (b) of 79 μm, and mixer height (c) of 31 μm.

To confirm the dilution performance of the iLiNP device, I carried out computational fluid dynamics (CFD) simulation and fluid visualization experiments. Figure 2.2 shows the CFD simulation results of ethanol dilution in the iLiNP device at different flow rate conditions. I evaluated the dilution performance at the cross sections of the narrowed microchannel as shown in Figure 2.2 (A). Figure 2.2 (B) compares CFD analysis results between the flow rates of 50 and 500 μL/min at the FRR of 3. The dilution performance was dramatically accelerated at 500 μL/min, and ethanol was completely diluted within 3 ms. The rapid ethanol dilution was enabled by the generation of the secondary flow at the baffle structure, as shown in Figure 2.2 (C). The secondary flow was only generated at the high flow rate condition, and there was no dependency on FRR. Controlling fluid characteristics is essential for the small-sized LNP production. According to the literature, small-sized LNPs were formed under the high flow rate condition and high FRR condition in microfluidic devices, regardless of the presence or absence of the chaotic mixers [25]. However, I reported that the dilution performance of the chaotic mixer was deteriorated at the flow rate of 500 μL/min due to the mechanism of chaotic advection formation [23]. I assumed that the iLiNP device achieved sufficient ethanol dilution within about 30 ms for producing the small-sized LNPs, regardless of the flow rate after passing through the 10th baffle structure (Figure 2.2 (B)), because rapid dilution of ethanol was more important than complete mixing of ethanol and saline [25].

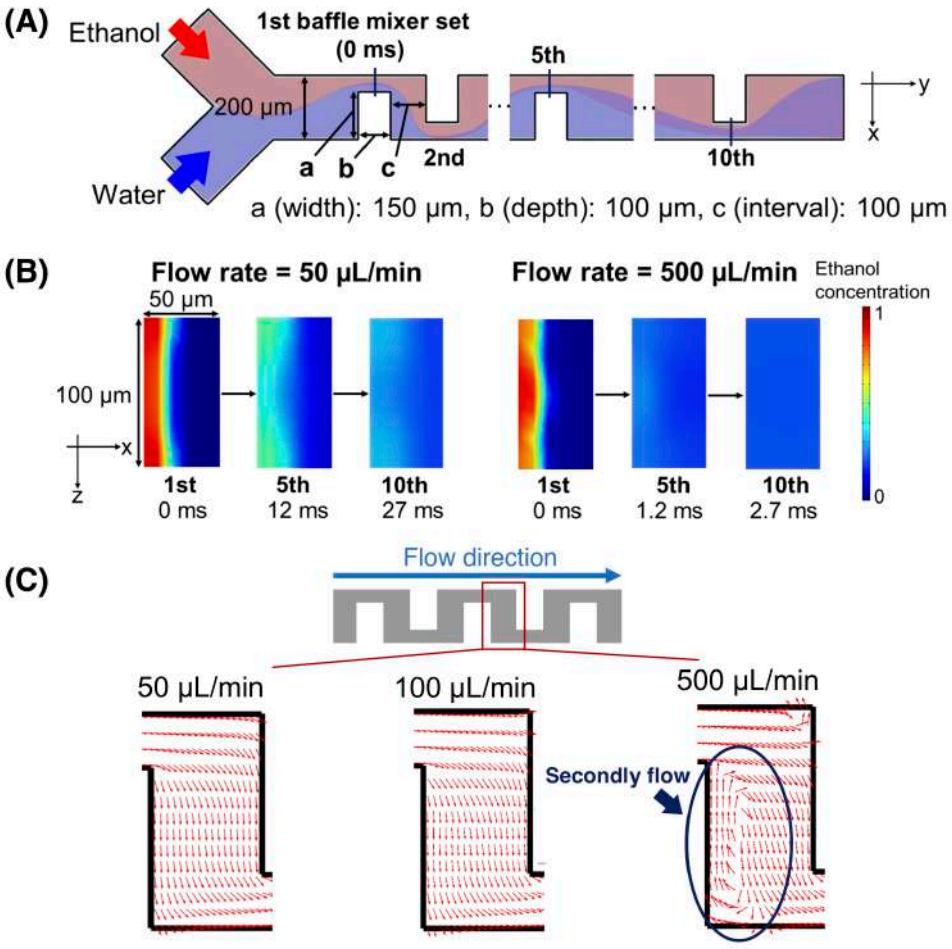

Figure 2.2 (A) Schematic illustration of the iLiNP device and part of the observation position for dilution performance. (B) Comparison of CFD simulation results for the flow rates of 50 μL/min (left) and 500 μL/min (right); flow rate ratio (FRR) of water to ethanol was 3 for both comparisons. The observation positions were the iLiNP device at the first, fifth, and tenth sets. Red and blue colors represent ethanol and water, respectively. (C) Top views of the baffle structure region. The flow rate was varied from 50 to 500 μL/min, and FRR was 3. The arrows represent the streamlines.

Figure 2.3 shows the effects of dimensions of the baffle structures where the width was (a), the depth was (b), and the interval was (c). At the flow rate of 500 μL/min and FRR of 3, the structures with shorter width (a) and shallower depth (b) dimensions had lower ethanol dilution efficiency than the baffle structure with the standard dimensions, even though the solutions were fed at high flow rate. Figure 2.3 (C) shows the effect of baffle structure interval on the ethanol dilution performance. Increasing the baffle structure interval also deteriorated the ethanol dilution performance; however, the width and depth dimensions of baffle structures had a bigger effect on the ethanol dilution performance, more than the interval of the baffle structure.

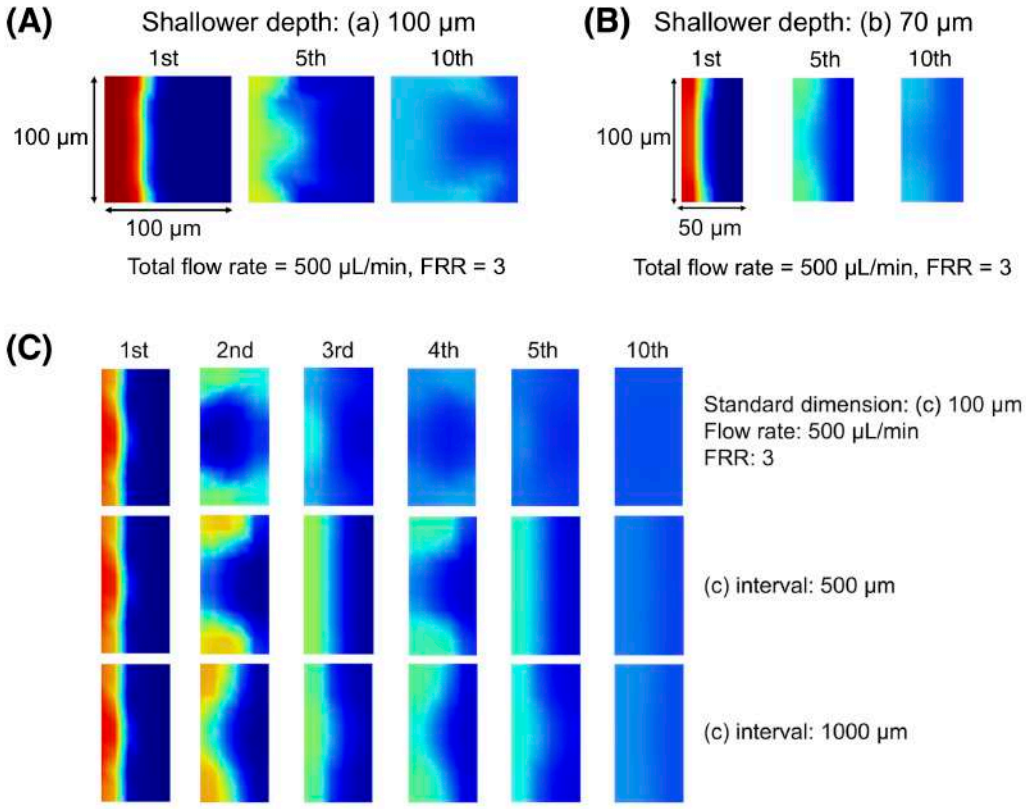

Figure 2.3 CFD results for modified dimensions of the baffle structure at 500 μL/min and FRR of 3: (A) (a) of 100 μm width, (B) (b) of 70 μm depth, and (C) (c) of 500 and 1000 μm intervals. Red and blue colors represent ethanol and water, respectively.

Then, I also performed a visualization experiment [23] using a laser scanning confocal microscope for the basic structure iLiNP device. I prepared the 10 mg/mL DOPC containing 0.1 mol % Rho-PE ethanol solution and saline and confirmed that both solutions were completely mixed within 3 ms at the flow rate of 500 μL/min (Figure 2.4, inset). Figure 2.3 compares the mixing performance between the iLiNP device and the chaotic mixer device. I used the reported chaotic mixer device [23], and the flow rate was 500 μL/min and FRR 9. The results suggested that the iLiNP device was able to dilute ethanol more effectively than the chaotic mixer device at the high flow rate condition. I considered that the rapid dilution of ethanol using the iLiNP device made it possible to control the LNP size precisely and produce the small-sized LNPs.

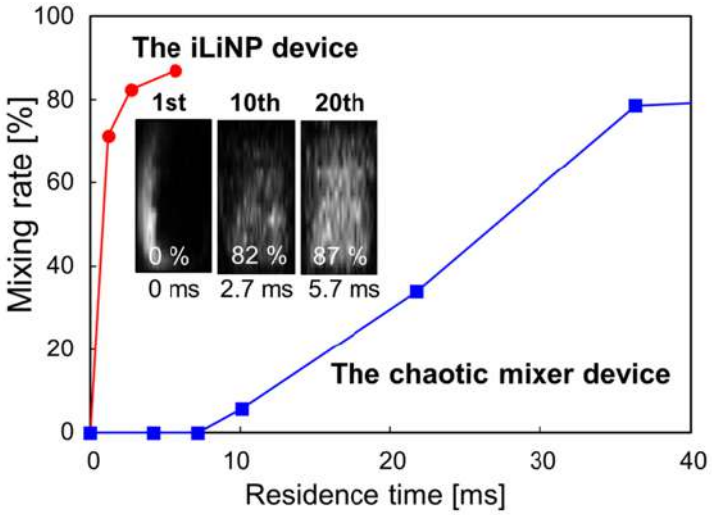

Figure 2.4 Comparison of the mixing performance for the iLiNP device and the chaotic mixer device (Figure 2.1 (B), right). These images were observed at the 1st, 10th, and 20th mixer set positions of the iLiNP device. The flow rate was 500 µL/min, and FRR was 9 (n = 1).

2.3.2 LNP Size Controllability of the iLiNP Devices

First, I attempted to demonstrate the possibility of the LNP size tuning at 10 nm intervals using the basic structure iLiNP device. I used 10 mg/mL of POPC solution and saline for the LNP production. The flow rate was varied from 50 to 500 µL/min, and FRR was from 3 to 9. Figure 2.5 (A) shows the LNP size distributions, and the average LNP sizes ranged from 20 to 100 nm. The iLiNP device was able to precisely control the LNP size, and it achieved 10 nm size tuning of LNPs by changing the flow conditions and slightly modifying the microchannel design. This result indicated that the iLiNP device would offer good LNP size controllability in a wide LNP size range and very limited flow rate range. In fact, the iLiNP device produced LNPs in the size range of 20-40 nm at the flow rates of 50, 100, and 500 µL/min and FRR of 9, as shown in Figure 2.5 (B). Twenty-nanometer-sized LNPs are theoretically the smallest particle size in the lipid system, and these small sized LNPs would penetrate the target tissues and organs effectively. On the other hand, the chaotic mixer device produced the narrow range of LNPs sized from 30 to 40 nm, in spite of the same flow rate conditions.

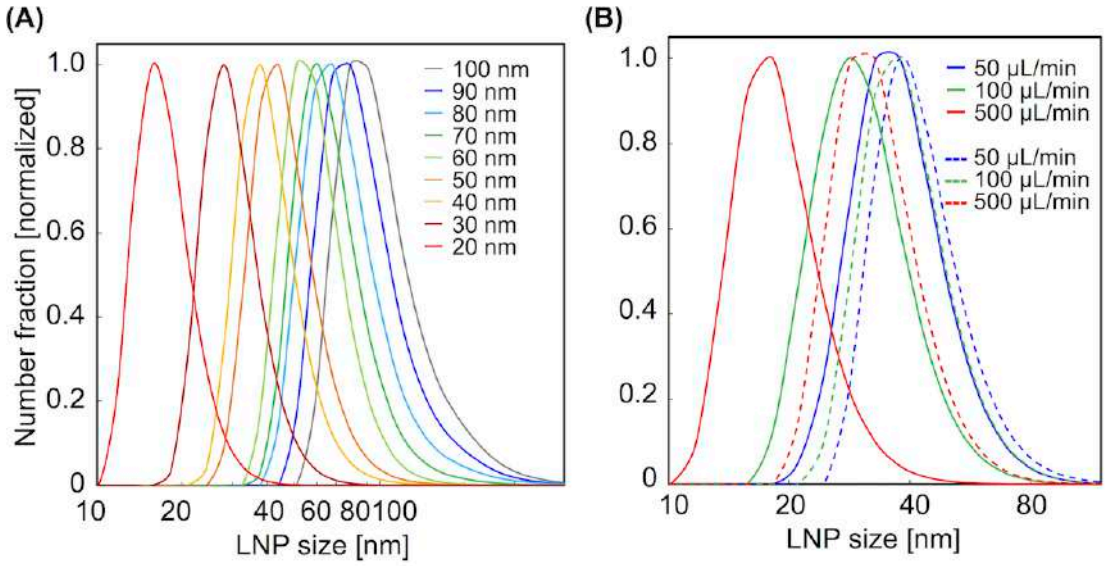

Figure 2.5 (A) Size distribution ranged from 20 to 100 nm for LNPs formed in the iLiNP device. The flow rate was varied from 50 to 500 µL/min, and FRRs were from 3 to 9. The sizes ranged from 60 to 80 nm for the LNPs formed in the sheath flow-type iLiNP device. (B) Comparison of the size distributions of LNPs formed in the iLiNP device (solid lines) and the chaotic mixer device (dashed lines). The flow rates were 50 to 500 µL/min and FRR was 9. The Y-axis was normalized with the maximum intensities of each value as 1.

Figure 2.6 (A) shows the effect of the flow rate and FRR on the LNP size. Increasing flow rate and FRR led to small-sized LNP formation, the same as was observed for the chaotic mixer device [23]. The basic structure iLiNP device was able to produce the LNPs except in the size range from 60 to 80 nm by simply controlling the flow rate and FRR. The standard deviations of LNP sizes produced at the low flow rate and FRR of 3 were slightly larger than that of the high flow rate and high FRR. The particle size polydispersity index (PDI) values were smaller than 0.1 without the LNPs produced at the 50 and 100 µL/min flow rates and FRR of 3. I assumed that the effect of secondary flow was deteriorated at the low flow rate condition and it reduced the dilution performance of ethanol. For this reason, the LNP size controllability was decreased at the low flow rate condition. To enhance the LNP size controllability at the flow rate of 50 µL/min and FRR of 3, I modified the design of the flow system from the Y-shaped flow to sheath flow as shown in Figure 2.6 (right). The sheath flow system leads to the rapid consumption of lipid molecules dissolved in ethanol because of the increased liquid–liquid interface area. I previously reported the effect of lipid concentration on the LNP size [23]. The LNP size was decreased with decreasing lipid concentration in ethanol. I observed similar LNP formation

behavior by changing the flow system (sheath flow system) with low concentration of lipid, and I considered that increasing the liquid-liquid interface area allowed to achieve the rapid dilution of ethanol and consumption of lipid molecules. The improved iLiNP device enabled the production of 60 to 80 nm sized LNPs with a narrow particle size distribution, and the size standard deviations also became small compared with those of the Y-shaped flow system, as shown in Figure 2.6. Remarkably, the iLiNP device was able to control the LNP size range from 20 to 100 nm, whereas the chaotic mixer device produced LNPs in the size range from 30 to 80 nm at the same flow rate conditions. These results suggested that the LNP production performance, that is, the LNP size controllability and productivity of small-sized LNPs, of the iLiNP device and flexibility of the device design were higher than those of the chaotic mixer device due to the two-dimensional simple device geometries.

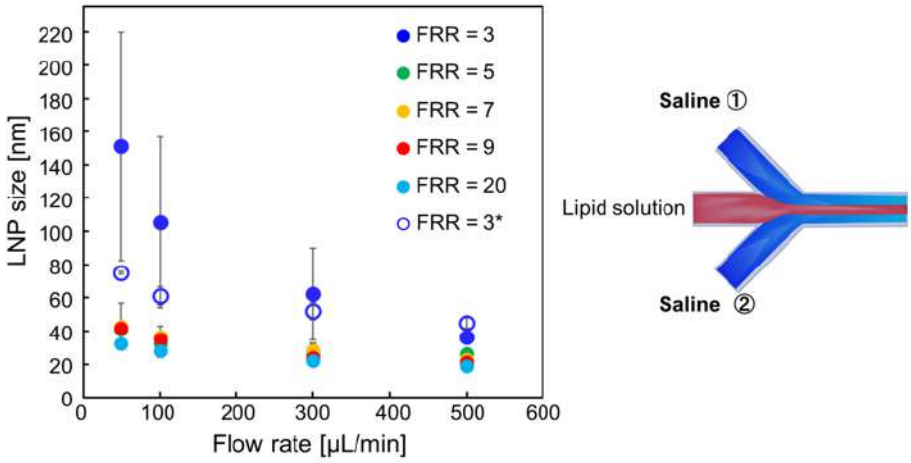

Figure 2.6 Effect of the flow rate and FRR on the LNP size using the iLiNP device. The flow rate is varied from 50 to 500 μL/min, and FRR range is from 3 to 20. For FRR = 3*, the LNP sizes formed in the sheath flow system are described on the right side. The error bars represent the standard deviation calculated from repeating each LNP formation experiment at least three times.

2.3.3 Effects of the Number of Baffle Structure Sets and Intervals on LNP Size

I fabricated other types of iLiNP devices: (A) the iLiNP device equipped with different numbers of the baffle structure sets (0, 6, 10, 20 (designated as the basic structure)) arranged at the interval of 100 μm and (B) the iLiNP device with 20 baffle structure sets arranged at intervals of 100, 500, and 1000 μm. Figure 2.7 (A) shows

the effect of the number of baffle structure sets on the LNP size. The LNP size was decreased on increasing the flow rate the same as for the chaotic mixer device and microfluidic devices without the mixer structure. The iLiNP device showed good LNP size controllability at flow rates of 300-500 μL/min, regardless of the number of sets. In spite of the smaller number of sets, 20 nm sized LNPs formed at 500 μL/min. On the other hand, the microfluidic device with 6 baffle structure sets produced the large-sized LNPs at the low flow rate condition due to the short dilution time of ethanol within the mixer region.

Figure 2.7 (B) shows the relationship between the baffle structure intervals and LNP size at different flow rate conditions. Controlling the LNP size was enabled by changing arrangement intervals of 20 sets of baffle structures. I confirmed that the iLiNP device was able to produce the LNP sizes from 20 to 60 nm with narrow standard deviations at the flow rate of 300–500 μL/min and FRR of 9. This result indicated that the LNP formation process was controllable by passing through the baffle structure rapidly, and the baffle structure was more suitable for rapid dilution under the high flow rate condition than the chaotic mixer device was. I considered that the baffle structure arranged at a wide interval would also be useful for controlling the LNP size for other lipid systems including cationic lipid-PEGylated lipid mixtures at the high flow rate condition because the formation or aggregation kinetics are different from those of the simple POPC lipid system. Generally, the aggregation kinetics of the lipid system are faster than that of the POPC lipid system due to the electrostatic interaction between RNAs and cationic lipids, the small area of the lipid headgroup, and the addition of PEGylated lipids. Therefore, the iLiNP device provided the desired ethanol dilution rate for controlling the LNP size in a wide range at the constant flow rate condition by simply changing the baffle structure intervals. Consequently, I found that the minimum number of baffle structure sets was 10, and they should be arranged at an interval of 100 μm to satisfy both the precise LNP size controllability and production of 20 nm sized LNPs.

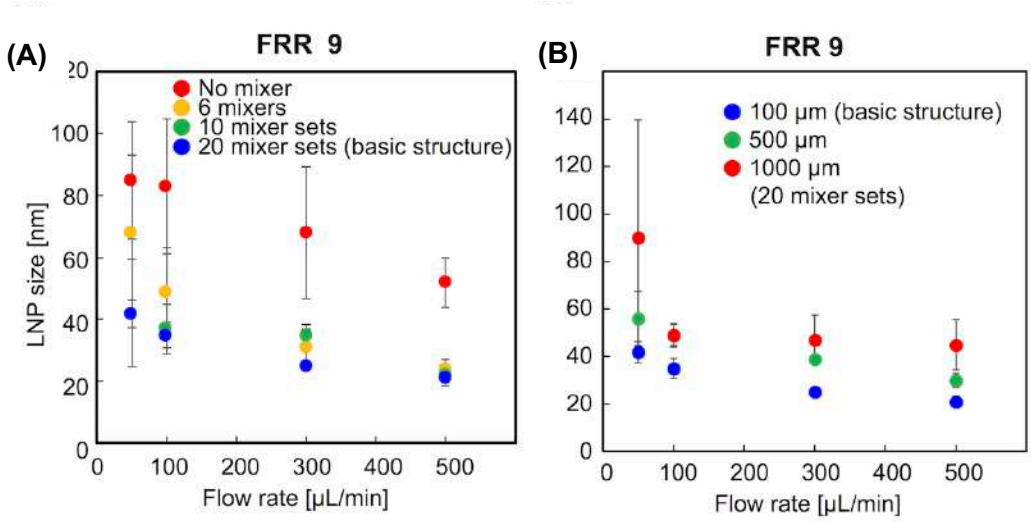

Figure 2.7 (A) The effect of number of sets of the baffle structure on the LNP size. The numbers of the sets were 0 (no mixer), 6, 10, and 20. Flow rates were 50, 100, 300, and 500 μL/min, and FRR was 9. (B) Relationship between the baffle structure intervals and LNP size at different flow rate conditions. Twenty sets of the baffle structures with different intervals were used for the experiments.

2.3.4 Scale-Up Performance of the iLiNP Device for Mass Production

I demonstrated the scale-up performance of the iLiNP device for LNP-based nanomedicine mass production (Figure 2.8). Differing from the chaotic mixer device, the iLiNP device has the two-dimensional simple microchannel geometry. I confirmed that the dimensions of the baffle structure, such as width, depth, and interval, played important roles for the LNP size control. I assumed the height of the microchannel and baffle structure had good robustness for ethanol dilution performance. Then, I fabricated the iLiNP device with a 200 μm height microchannel and baffle structures. The aspect ratio (height/width of the microchannel) of the device was calculated to be 1. As I expected from the viewpoint of fluid dynamics, the LNP size controllability did not change from the basic structure iLiNP device (aspect ratio: 0.5), and 20 nm sized LNPs formed at the flow velocity of 417 mm/s. Hood et al. [27] reported the effect of the aspect ratio of the microchannel on the LNP size using the microfluidic device without mixer structures. Although the high aspect ratio microchannel showed similar LNP formation behavior to that of the low aspect ratio microchannel, the microchannels required

a high flow rate of the aqueous phase, namely, FRR of 50 to 100, to produce 80 nm sized LNPs. For the DDS applications of the LNPs, the content of lipids to DNA or RNA must be adjusted to the optimal molar ratio to get the best therapeutic performance. Moreover, DNA and RNA, which are expensive materials for encapsulation into the LNPs, are dissolved into an aqueous phase. Thus, the LNP production should be performed at the low and constant FRR conditions to control the LNP composition and size range from 20 to 100 nm. In contrast, the iLiNP devices can produce a wide size range of LNPs at low FRR by changing the flow rate.

In the case of the chaotic mixer device, the deeper grooved mixer structure can accelerate the mixing performance [34]. However, the LNPs clog the grooves of the chaotic mixers, regardless of the height of the grooved mixer structure. This is the major disadvantage of the chaotic mixer device for LNP production. Conversely, I did not observe any clogging of the LNPs, and there was no deterioration of ethanol dilution performance in the iLiNP device because of the two-dimensional microchannel, mixer dimensions, and effective generation of secondary flow. From these results, I believed that the iLiNP device would be an ideal apparatus for LNP-based nanomedicine production.

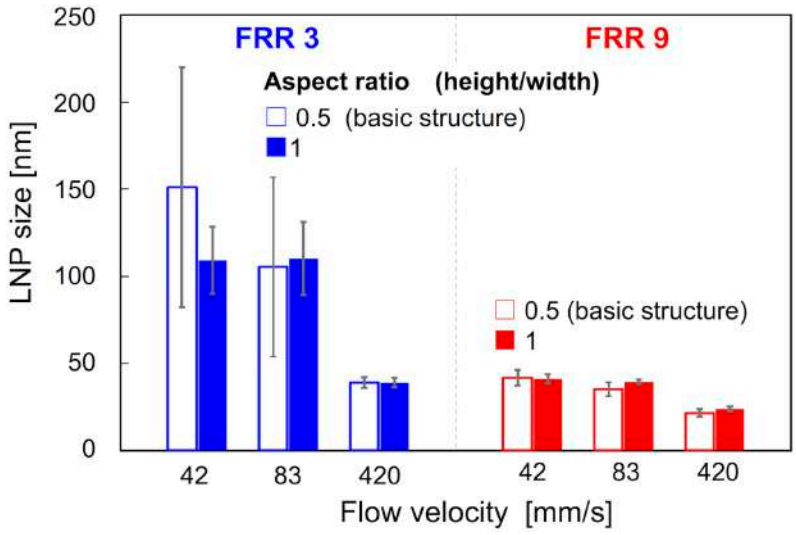

Figure 2.8 Effect of microchannel aspect ratio on LNP size controllability. FRRs were 3 (blue) and 9 (red). The error bars represent the standard deviation calculated from repeating each LNP formation experiment at least three times.

2.3.5 Applicability of the iLiNP Device for DDS

Finally, I demonstrated the applicability of the iLiNP device for DDS uses. I used a pH-sensitive cationic lipid (YSK05), cholesterol (chol), 1,2-dimirystoyl-sn-glycero, and methoxylene glycol 2000 ether (PEG-DMG) lipid system for production of LNPs encapsulating siRNA (siFVII) [11]. The YSK-LNP performance was evaluated by FVII gene silencing activity and intrahepatic distribution of the siRNA via an in vivo experiment. I produced the YSK-LNPs by introducing the solution of ethanol containing YSK05, chol, and PEG-DMG and the solution of 25 mM acetate buffer (pH 4.0) containing siRNA, into the iLiNP device. The concentration of total lipids was 8 mM, and the molar ratios of lipids were 50, 50, and 1 for YSK05, chol, and PEG-DMG, respectively. Figure 2.9 compares LNP sizes produced by the conventional vortex method, the microfluidic device without mixer structures, and the iLiNP device. In this experiment, I used the acetate buffer solution without siRNA as the aqueous phase. The iLiNP device was able to produce the 40 nm sized LNPs with smaller standard deviation of size compared with the other production methods. I previously reported the 40 nm sized LNPs formed in the chaotic mixer device at the flow rate of 1.5 mL/min and FRR of 3. However, 40 nm sized LNPs were produced at the flow rate of 500 μL/min and FRR of 3 using the iLiNP device. Thus, the iLiNP device achieved one-third sample consumption compared to the chaotic mixer device [11]. This result indicated that the iLiNP device had sufficient performance to produce the small-sized LNPs, which can deliver siRNA to hepatocytes.

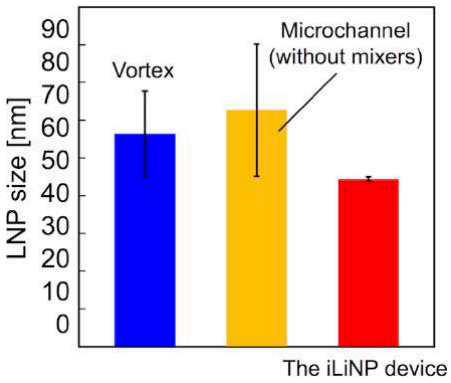

Figure 2.9 Comparison of the YSK-LNP sizes produced by the conventional vortex method, the microfluidic device without mixer structures, and the iLiNP device. The error bars represent the standard deviation calculated from repeating each YSK-LNP formation experiment at least three times.

Then, I prepared 80 nm sized siRNA-loaded YSK-LNPs using the iLiNP device and confirmed the encapsulation efficiency of siRNA was higher than 90%. I selected the LNP size as 80 nm because 80 nm sized LNPs can show both high gene-silencing activity and penetration efficiency [15]. Figures 2.10 (A) and (B) show FVII gene-silencing activity of the 80 nm sized YSK-LNPs in vivo and the intrahepatic distribution of siRNA delivered by 80 nm sized YSK-LNPs. YSK-LNPs showed high FVII gene-silencing activity with no dependency on dose. Furthermore, I confirmed the 80 nm sized YSK-LNPs showed good siRNA delivery efficiency to hepatocytes by a confocal laser scanning microscopic observation of ICR mouse liver tissues. The confocal images indicated that the YSK-LNPs showed low accumulation in blood vessels, and siRNAs were specifically localized to the extravascular region where the hepatocytes were present. From these results, I demonstrated the utility of the iLiNP device for production of LNP-based nano-DDS applications.

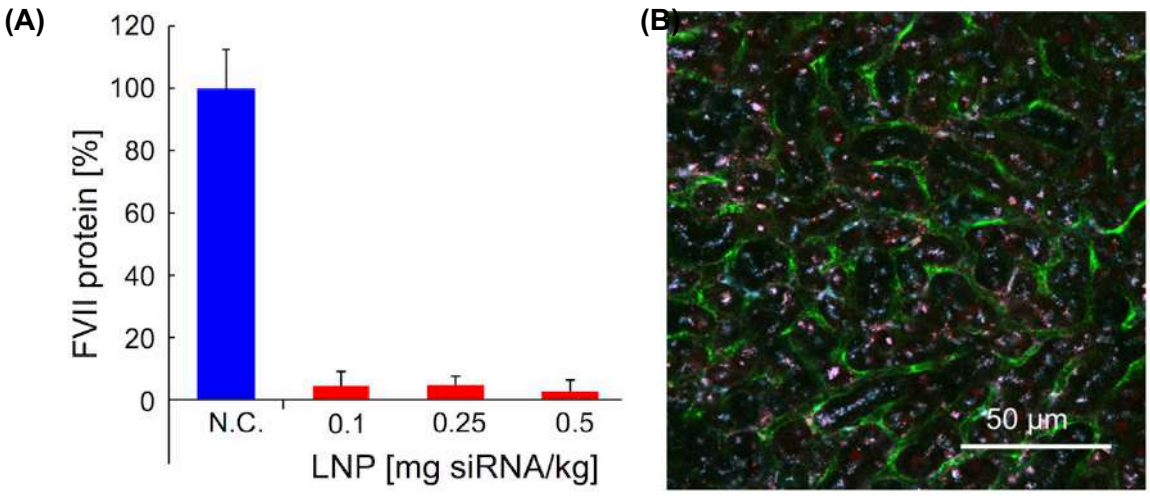

Figure 2.10 Results of YSK-LNPs formed in the iLiNP device and *in vivo* experiments. (A) FVII gene-silencing activity of siFVII-loaded YSK-LNPs at different doses to mice. N.C.: negative control. (B) Confocal microscopic images of the mice liver tissues. Blood vessels, LNPs, and siRNAs were visualized as green, cyan, and red, respectively.

2.4 Conclusion

In summary, I developed the iLiNP device for producing LNPs in the size range from 20 to 100 nm based on the LNP formation mechanism and the CFD simulation. The iLiNP device gave precise LNP size control at 10 nm intervals by changing not only the flow conditions but also the baffle structure dimensions. I found that generation of the secondary flow in the iLiNP device was indispensable for controlling the LNP size and producing the small-sized LNPs. Twenty-nanometer-sized POPC LNPs, which are considered as the theoretically smallest particle size, were formed in the iLiNP device at 500 μL/min flow rate and FRR of 9, whereas the chaotic mixer device could not produce the 20 nm sized POPC LNPs at the same flow conditions. I demonstrated the scale-up performance and robustness of the baffle structure and microchannel designs. I also evaluated the utility of the iLiNP device for production of the LNP-based nano-DDS carriers via the in vivo experiment. The siRNA-loaded LNPs prepared by the iLiNP device effectively delivered the siRNA to hepatocytes and showed good FVII gene-silencing activity. Differing from the chaotic mixer device, the iLiNP device showed high flexibility for the LNP production apparatus, because of the two-dimensional structure, and I could optimize the mixer dimensions depending on the lipid system. I believe that the iLiNP device is more useful than the chaotic mixer device to produce small-sized and size-controlled nanocarriers, not only LNPs but also polymeric micelles, nanogels, and dendrimers, and I expect the iLiNP device can be applied as a novel nano-DDS carrier production apparatus.

References

[1] M. Tibbitt, J. Dahlman and R. Langer, *J. Am. Chem. Soc.*, **138**, 704-717 (2016)

[2] D. Peer, J. Karp, S. Hong, O. FaroKHzad, R. Margalit and R. Langer, *Nature Nanotechnology*, **2**, 751-760 (2007)

[3] J. Kraft, J. Freeling, Z. Wang and R. Ho, *J. Pharm. Sci.*, **103**, 29-52 (2014)

[4] K. Miyata, R. Christie and K. Kataoka, *Reactive & Functional Polymers*, **71**, 227-234 (2011)

[5] R. Duncan and M. Vicent, *Adv. Drug Deliv. Rev.*, **65**, 60-70 (2013)

[6] H. Zhang, Y. Zhai, J. Wang and G. Zhai, *Materials Science & Engineering C-Materials For Biological Applications*, **60**, 560-568 (2016)

[7] T. Pearce, K. Shroff and E. Kokkoli, *Adv. Mater.*, **24**, 3803-3822 (2012)

[8] Q. Lin, J. Chen, Z. Zhang and G. Zheng, *Nanomedicine*, **9**, 105-120 (2014)

[9] Y. MATSUMURA and H. MAEDA, *Cancer Res.*, **46**, 6387-6392 (1986)

[10] H. Cabral, Y. Matsumoto, K. Mizuno, Q. Chen, M. Murakami, M. Kimura, Y. Terada, M. R. Kano, K. Miyazono, M. Uesaka, N. Nishiyama and K. Kataoka, *Nat Nanotechnol*, **6**, 815-823 (2011)

[11] Y. Sato, Y. Note, M. Maeki, N. Kaji, Y. Baba, M. Tokeshi and H. Harashima, *J. Control. Release*, **229**, 48-57 (2016)

[12] S. Chen, Y. Y. Tam, P. J. Lin, A. K. Leung, Y. K. Tam and P. R. Cullis, *J. Control. Release*, **196**, 106-112 (2014)

[13] J. H. Tsui, W. Lee, S. H. Pun, J. Kim and D. H. Kim, *Adv Drug Deliv Rev*, **65**, 1575-1588 (2013)

[14] R. Ran, Q. Sun, T. Baby, D. Wibowo, A. P. J. Middelberg and C.-X. Zhao, *Chem. Eng. Sci.*, **169**, 78-96 (2017)

[15] A. Ozcelikkale, H. R. Moon, M. Linnes and B. Han, *Wiley Interdiscip Rev Nanomed Nanobiotechnol*, **9** (2017)

[16] D. Liu, H. Zhang, F. Fontana, J. T. Hirvonen and H. A. Santos, *Lab Chip*, **17**, 1856-1883 (2017)

[17] A. Jahn, S. M. Stavis, J. S. Hong, W. N. Vreeland, D. L. DeVoe and M. Gaitan, *ACS Nano*, **4**, 2077-2087 (2010)

[18] A. Jahn, J. E. Reiner, W. N. Vreeland, D. L. DeVoe, L. E. Locascio and M. Gaitan, *J. Nanopart. Res.*, **10**, 925-934 (2008)

[19] D. Carugo, E. Bottaro, J. Owen, E. Stride and C. Nastruzzi, *Sci. Rep.*, **6**, 25876 (2016)

[20] M. Maeki, N. Kimura, Y. Sato, H. Harashima and M. Tokeshi, *Adv Drug Deliv Rev*, **128**, 84-100 (2018)

[21] N. M. Belliveau, J. Huft, P. J. Lin, S. Chen, A. K. Leung, T. J. Leaver, A. W. Wild, J. B. Lee, R. J. Taylor, Y. K. Tam, C. L. Hansen and P. R. Cullis, *Mol Ther Nucleic Acids*, **1**, e37 (2012)

[22] I. V. Zhigaltsev, N. Belliveau, I. Hafez, A. K. K. Leung, J. Huft, C. Hansen and P. R. Cullis, *Langmuir*, **28**, 3633-3640 (2012)

[23] M. Maeki, Y. Fujishima, Y. Sato, T. Yasui, N. Kaji, A. Ishida, H. Tani, Y. Baba, H. Harashima and M. Tokeshi, *PLoS One*, **12**, e0187962 (2017)

[24] D. Chen, K. T. Love, Y. Chen, A. A. Eltoukhy, C. Kastrup, G. Sahay, A. Jeon, Y. Dong, K. A. Whitehead and D. G. Anderson, *J. Am. Chem. Soc.*, **134**, 6948-6951 (2012)

[25] M. Maeki, T. Saito, Y. Sato, T. Yasui, N. Kaji, A. Ishida, H. Tani, Y. Baba, H. Harashima and M. Tokeshi, *RSC Advances*, **5**, 46181-46185 (2015)

[26] A. D. Stroock, S. K. Dertinger, A. Ajdari, I. Mezic, H. A. Stone and G. M. Whitesides, *Science*, **295**, 647-651 (2002)

[27] R. R. Hood and D. L. DeVoe, *Small*, **11**, 5790-5799 (2015)

[28] W. Shinoda, R. DeVane and M. L. Klein, *J. Phys. Chem. B*, **114**, 6836-6849 (2010)

[29] Y. Sato, H. Hatakeyama, Y. Sakurai, M. Hyodo, H. Akita and H. Harashima, *J. Control. Release*, **163**, 267-276 (2012)

[30] J. C. McDonald and G. M. Whitesides, *Acc. Chem. Res.*, **35**, 491-499 (2002)

[31] V. Mengeaud, J. Josserand and H. H. Girault, *Anal. Chem.*, **74**, 4279-4286 (2002)

[32] N.-T. Nguyen and Z. Wu, *Journal of Micromechanics and Microengineering*, **15**, R1-R16 (2005)

[33] H. Song, J. D. Tice and R. F. Ismagilov, *Angew. Chem. Int. Ed. Engl.*, **42**, 768-772 (2003)

[34] J. T. Yang, K. J. Huang and Y. C. Lin, *Lab Chip*, **5**, 1140-1147 (2005)

CHAPTER 3 Development of Three-Dimensional, Symmetrically Assembled Microfluidic Devices for Lipid Nanoparticle Production

3.1 Introduction

Lipid nanoparticle (LNP)-based drug delivery systems (DDSs) are among the most advanced nanomedicine systems. The size of LNPs plays important role in both the LNP biodistribution and LNP performance, such as antitumor effect and gene silencing activity [1-7]. Generally, small-sized LNPs are desirable for stromal rich tumor tissues, such as pancreatic cancer. On the other hand, 100 nm-sized LNPs can deliver drugs or RNA into the hepatocytes of liver tissues passing through the fenestrae (with an approximate diameter of 100–150 nm) [8]. Recently, the relationship between the LNP size and DDS performance has been investigated widely (Table 3.1). In previous studies, this relationship was investigated with LNPs with a size of 10–50 nm. However, LNPs are produced with size distribution in spite of size tuning such as extrusion using a polycarbonate filter and ultra-sonication [1, 9]. Therefore, a precise LNP size control method is indispensable for understanding the effect of the LNP size on the DDS performance.

Solvent injection using microfluidic devices can control the LNP size more precisely compared to conventional batch scale production and size tuning methods [10-13]. In the microfluidic-based LNP production method, the LNP size was controlled by the ethanol dilution rate. Therefore, the flow conditions, such as the total flow rate and flow rate ratio (FRR) of aqueous phase to lipid phase, and the microchannel geometry are key parameters for controlling the LNP size [13-16]. To control the LNP size, the LNP formation behavior has been investigated using several types of microfluidic devices (Table 3.2). The microfluidic hydrodynamic focusing device [17] and the chaotic micromixer device [15] are typical microfluidic devices for the production of LNPs with sizes of 50–60 and 30–60 nm, respectively. Although these LNPs are smaller than those produced with conventional methods, they do not cover the size range summarized in Table 3.1. To address the LNP size controllability, I developed a microfluidic device named iLiNP^{TM} (Figure 3.1, 2D-iLiNP device) [14] The iLiNP device was equipped with baffle structures and induced a generation of secondary flow at high total flow rate conditions. As a result, the iLiNP device achieved the production of LNPs in the average size range from 20 to 150 nm. However, the size distribution of large-sized LNPs needs to be improved to understand the influence of the LNP size on the DDS performance in detail.

Table 3.1. Relationship between the LNP size and DDS in vivo according to different studies

Reference		Year	LNP system	Size and DDS in vivo
[1]	Mukhamadiyarov, R. A. *et al.*	2018	EPC/cholesterol	70 nm > 100 nm accumulation at rats' ischemic myocardium
[2]	Cabral, H. *et al.*	2011	(PEG-*b*-P(Glu)) copolymer	30 nm > 50 nm antitumor activity in pancreatic tumors
[3]	Sato, Y. *et al.*	2016	YSK05/cholesterol/DMG-PEG 2K	30 nm > 50 nm siRNA delivery to mice's liver tissues
[4]	Hirsjarvi, S. *et al.*	2013	Solutol®/Lipoid®/Labrafac®	25 nm > 50 nm rapid distribution to peripherical capillaries in mice's tissues
[5]	Ren, H. *et al.*	2019	EPC/cholesterol/DSPE-PEG 2K	100 nm > 70 nm rheumatoid arthritis targeting in mice
[6]	Chen, S. *et al.*	2016	DMAP-BLP/DSPC/cholesterol/DMG-PEG 2K	80 nm > 30 nm FVII gene-silencing in mice
[7]	Yanez Arteta, M. *et al.*	2018	DLin-MC3-DMA/DSPC/cholesterol/DMPE-PEG 2K	65 nm > 50 nm mRNA delivery to mice's hepatocytes and protein expression

PEG-*b*-P(Glu): poly(ethylene glycol)-*b*-poly(glutamic acid), EPC: ethyl phosphatidylcholine, DMG-PEG 2K: 1,2-dimyristoyl-rac-glycero-3-[methoxy(polyethyleneglycol)-2000], DSPE-PEG 2K: distearoyl phosphatidylethanolamine-[methoxy(polyethyleneglycol)-2000], DSPC: 1,2-distearoyl-sn-glycero-3-phosphocholine, DMAP-BLP: 3- (dimethylamino)propyl(12Z,15Z)-3-[(9Z,12Z)-octadeca-9,12-dien-1-yl]henicosa-12,15-dienoate, DMPE-PEG 2K: 1,2-dimyristoyl-sn-glycero-3- phosphoethanolamine-N-[methoxy(polyethylene glycol)-2000]

Table 3.2. Sizes of POPC LNPs prepared by using the several microfluidic devices

Reference		Year	Microfluidic device	Average size	FRR	Total flow rate
[12]	Mijajlovic, M. *et al.*	2013	MHF-device	50-60 nm	20-40	126-246 µL/min
[13]	Maeki, M. *et al.*	2017	CM device	30-60 nm	3-9	50-500 µL/min
[14]	Kimura, N. *et al.*	2018	iLiNP device	20-150 nm	3-9	50-500 µL/min

MHF: microfluidic hydrodynamic focusing, CM: chaotic micromixer, iLiNP: invasive lipid nanoparticle production

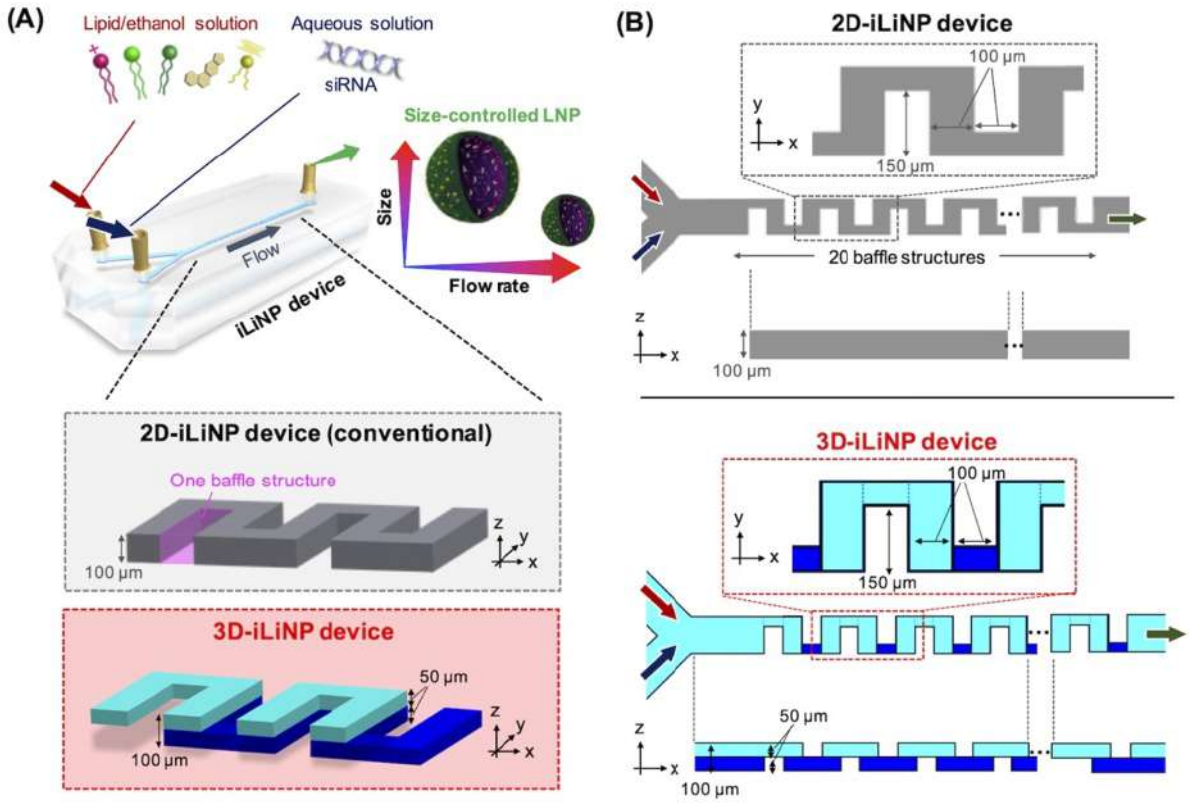

Figure 3.1 (A) Schematic and (B) top and cross-sectional views of the 2D- and 3D-iLiNP devices.

Theoretically, the dilution rate and mixing homogeneity affect the LNP size and size distribution, respectively. Therefore, the chaotic micromixer device, which induces chaotic advection in the microchannel,

allows the production of homogeneous-sized LNPs. In contrast, the 2D-iLiNP device allows the production of small- and large-size LNPs in the high and low flow rate conditions, respectively; the large-sized LNPs are formed through diffusion-based ethanol dilution. However, although fluid control is crucial for the improvement of the LNP size distribution, in particular for large-sized LNPs, the homogeneous and slow rate dilution is still challenging. From the viewpoint of fluid dynamics and mass transportation, the homogeneous and slow rate dilution is a competitive phenomenon to diffusion. To the best of my knowledge, the microfluidic device to achieve homogeneous and slow rate dilution for the improvement of the LNP size distribution has not been reported.

In this chapter, I report a three-dimensional (3D), symmetrically assembled microchannel, named the 3D-iLiNP device, based on the 2D-iLiNP device. I designed the 3D baffle structures using computational fluid dynamics (CFD) simulations. I demonstrated the homogeneous and slow rate ethanol dilution by the generation of 3D secondary flows at the low flow rate condition. Finally, I investigated the effect of the LNP size distribution on the gene silencing activity via in vitro and *in vivo* experiments using siRNA-loaded LNPs.

3.2 Experimental

3.2.1 Materials

1-Palmitoyl-2-oleoyl-sn-glycero-3-phosphocholine (POPC), 1,2-distearoyl-sn-glycero-3-phosphocholine (DSPC), 1,2-dioleoyl-sn-glycero-3-phosphoethanolamine (DOPE), 1,2-dioleoyl-3-dimethylammonium-propane (DODAP), and 1,2-dimyristoyl-rac-glycero-3-methoxypolyethylene glycol-2000 (DMG-PEG2K) were purchased from the NOF Corporation (Tokyo, Japan). Cholesterol was purchased from Sigma-Aldrich (St. Louis, MO, USA). A pH-sensitive cationic lipid, CL4H6, was synthesized in the laboratory as previously described [18]. Ethanol, sodium chloride, citric acid, 2-morpholinoethanesulfonic acid (MES), monohydrate, and phosphate-buffered saline (PBS) were purchased from FUJIFILM Wako Pure Chemical Corporation (Osaka, Japan). The siFVII and Cy-5-labeled siGL4 were purchased from Hokkaido System Science Co. Ltd. (Sapporo,

Japan). Table 3.3 shows the sense and antisense strand sequences of siFVII and Cy5-siGL4. Quant-iT™ Ribogreen™ RNA Reagent and 1,1'-Dioctadecyl-3,3,3',3'-Tetramethylindocarbocyanine Perchlorate (DiI) were obtained from Thermo Fisher Scientific (Waltman, MA, USA). SU-8 3050 was obtained from Nippon Kayaku Co., Ltd. (Tokyo, Japan).

Table 3.3 Sequences of siRNAs

siRNA		**Sequence**
siFVII	sense	5′-GGAucAucucAAGucuuAcTsT-3′
	antisense	5′-GuAAGAcuuGAGAuGAuccTsT-3′
Cy5-siGL4	sense	Cy5-CCGUCGUAUUCGUGAGCAATsT-3′
	antisense	5′-UUGCUCACGAAUACGACGGTsT-3′

3.2.2 Computational fluid dynamics study

COMSOL Multiphysics 5.2 (COMSOL, Inc., Burlington, MA) was used for a CFD study. The experimental conditions were the same as those reported in a previous study [14]. The profiles of the ethanol concentration were numerically simulated using 3D models under both the laminar-flow model (no slip) and transport of diluted species (ethanol) condition. The flow was modeled as an incompressible flow using the Navier–Stokes equation. The total flow rate and FRR (water/ethanol) were set to 50 μL/min and 3, respectively. For the calculation of the ethanol dilution efficiency, I counted a number of mesh with 20% ethanol concentration at each cross-section and each residence time [19]. Then, the ethanol dilution efficiency was calculated from the following equation.

Ethanol dilution efficiency [%]

= Number of meshes with 20% ethanol concentration / Total number of meshes × 100

3.2.3 Fabrication of iLiNP devices

I made poly(dimethylsiloxane) (PDMS) replicas for the 2D- and 3D-iLiNP devices using the standard photolithography method [20]. For the alignment of the 3D-iLiNP device, I employed amino silane coupling with minor modifications (Figure 3.2) [21]. I modified a concentration of 3-aminopropyltriethoxysilane (APTES, Tokyo Chemical Industry, Japan) solution form 1% v/v to 3% v/v. Replicated PDMS pieces were treated with oxygen plasma (CUTE-1MP/R, Femto Science, Gwangju, Korea) and soaked in 3%v/v APTES aqueous solution for 20 min at room temperature. Then, the silanized replicas were washed with DI water and aligned with each replica using an optical microscope. After bonding the replicas, the amino groups remaining on the surface of the microchannel were acetylated by introducing 20%v/v acetic anhydride (Tokyo Chemical Industry, Japan) containing dimethylformamide solution.

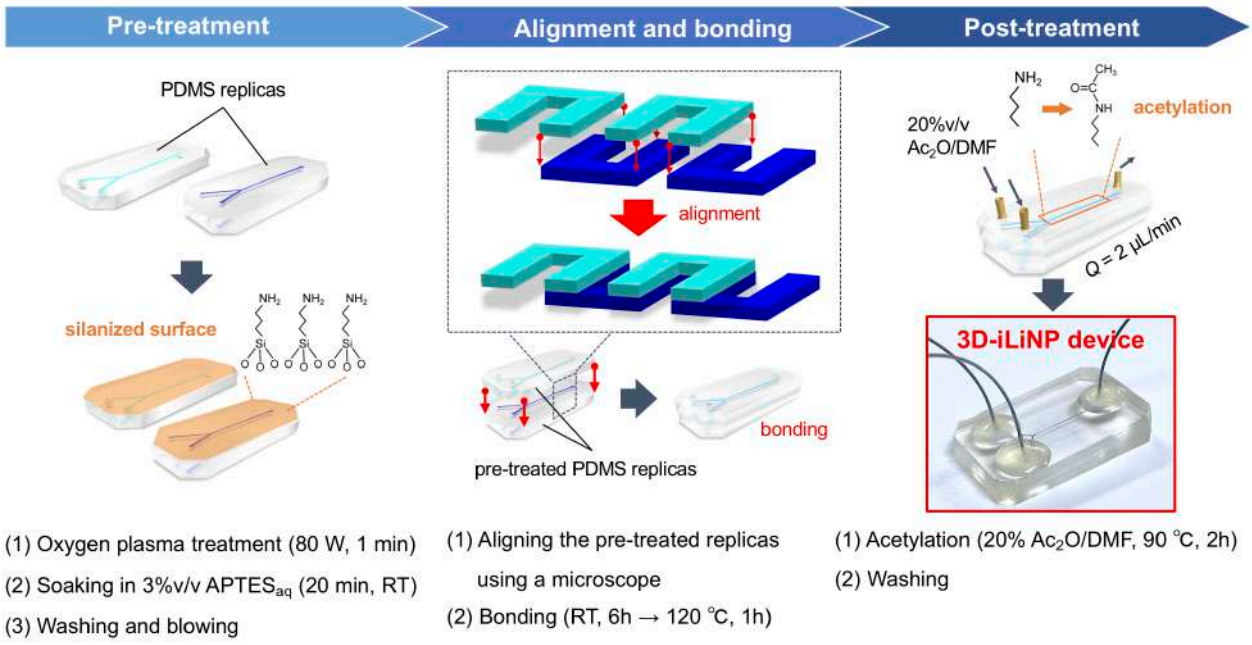

Figure 3.2 Schematic of the 3D-iLiNP device fabrication process

3.2.4 Preparation of LNPs using the 3D-iLiNP device

POPC was used as a model LNP to investigate the size controllability of the 3D-iLiNP device. POPC LNPs were prepared using a 13.4 mM POPC/ethanol solution and saline. The collected LNP suspensions were dialyzed against saline overnight.

To validate the applicability of the 3D-iLiNP device for the production of siRNA-loaded LNPs, I investigated DODAP- and CL4H6-based LNP systems. The lipid amine-to-oligonucleotide phosphate (N/P) ratio was fixed to 4 overnight. The siRNA-loaded DODAP LNPs were prepared by mixing an 8 mM lipid/ethanol solution composed of DODAP/DOPE/cholesterol/DMG-PEG 2K (30/25/40/5 mol%) with a 10 mM citrate buffered solution (pH3.0) containing siRNAs at a concentration of 47.5 μg/mL. The siRNA-loaded CL4H6 LNPs were prepared by mixing a 10 mM lipid/ethanol solution composed of CL4H6/DSPC/cholesterol/DMG-PEG 2K (50/10/38.5/1.5 mol%)[22] with a 10 mM citrate buffered solution containing siRNAs at a concentration of 132 μg/mL. The lipid solution and siRNA in the buffer solution were separately introduced into the iLiNP devices at a total flow rates of 50 or 500 μL/min and FRR of 3. The collected LNP suspensions were dialyzed against 20 mM MES buffer solution (pH6.0) for 2 h followed by an overnight dialysis against PBS. The siRNA encapsulation efficiency was measured using a Ribogreen assay [3]. For in vivo experiments, the CL4H6-LNP suspensions were concentrated using Amicon Ultra filters (100K, Merck, Darmstadt, Germany).

The size and polydispersity index (PDI) of the LNPs were measured by dynamic light scattering (DLS) measurements obtained with a Zetasizer Nano ZEN3600 (Malvern Instruments, Worcestershire, U.K.).

3.2.5 In vitro assay

HeLa cells stably expressing Firefly and Renilla luciferase (HeLa-dluc) were cultured in the same conditions as described previously [18]. Cells were seeded at a concentration of 3×10^3 and 6×10^3 cells/well in a 96 well-microplate for 24 h prior to the LNP treatment for the cell viability assay and gene expression assay. Then, the cells were treated with LNPs and incubated for 24 h. After the incubation, the cell viability was measured using

a Cell Counting Kit-8 (Dojindo, Kumamoto, Japan) according to the manufacture's protocol. For gene expression assay, firefly and renilla luciferase activities were measured using a Dual-Glo assay and a GloMax®Explorer System (Promega), according to the manufacture's protocol.

3.2.6 In vivo experiment

The gene knockdown activity of coagulation factor VII (FVII) and the confocal microscope images of the mice's hepatocytes were analyzed following previously described protocols [14] with minor modifications. For the observation of the intrahepatic siRNA distributions, I prepared DiI- and (Cy5)-labeled siGL4 encapsulated CL4H6 LNPs by mixing a 10 mM lipid/ethanol solution containing 0.5 mol% DiI with a 10 mM citrate buffered solution containing Cy5-labeled siGL4.

3.2.7 Evaluation of scale-up performance of the 3D-iLiNP device

The 3D-iLiNP device used for the investigation of the mass-produced LNPs was made from cycloolefin polymer plates fabricated by a micromachining process (Zeon Corporation, Tokyo, Japan).

3.2.8 Statistical analysis

The results were analyzed with Microsoft® Excel and an unpaired Student's t-test was used to compare the average values of two groups.

3.3 Results and Discussion

3.3.1 Design of the 3D-iLiNP device through computational fluid dynamics (CFD) simulations

Figure 3.1 shows a schematic of the 3D-iLiNP device equipped with 20 baffle structures based on the 2D-iLiNP device [14]. With the 3D-iLiNP device, I predicted a secondary flow in the x–z direction in addition to that in the y-z direction at the 3D-baffle structures; this secondary flow would allow the acceleration of the ethanol dilution of the lipid solution. Figure 3.3 (A) shows the 3D views, cross-sectional views, and CFD results of the 2D- and 3D-iLiNP devices. As a proof of the concept experiment, I preliminary designed the three-types of the 3D-iLiNP devices. The 3D-iLiNP devices consisted of top and bottom layers with different channel thickness; (a) 50–50 μm, (b) 80–20 μm, and (c) 20–80 μm. The total flow rate and the FRR (water to ethanol) was set to 50 μL/min and 3, respectively. The total flow rate and the FRR (water to ethanol) were set to 50 μL/min and 3, respectively. I focused on the generation of the secondary flow in the 3D-baffle structures. As expected, the secondary circulation flow was generated at the baffle structures of the 3D-iLiNP devices, whereas no secondary flow was observed in the 2D-iLiNP device. Figure 3.3 (B) and (C) shows a comparison of the ethanol dilution process and ethanol dilution efficiency of the of the 2D- and 3D-iLiNP devices. The time differences to reach the solutions to cross-sections were shorter than 0.6 ms. In this FRR condition, the final ethanol concentration was 25%. The 2D-iLiNP device retained a high concentration of ethanol at the corner of the microchannel 16 ms after injection. The 3D-iLiNP devices diluted ethanol homogeneously compared with the 2D-iLiNP device. The 3D-iLiNP devices showed complete ethanol dilution within 20 ms, regardless of the device design (Figure 3.3 (C)). The design of the basic-type, –80-20 μm, and –20-80 μm 3D-iLiNP devices did not significantly affect the dilution performance of ethanol in the CFD simulation. The results of the CFD simulation confirm that the 3D-iLiNP device at a low total flow rate is a more suitable structure for homogeneous and slow rate ethanol dilution compared with the 2D-iLiNP device [14, 15]. This fluid dynamics is significant to control the LNP size at the low flow rate condition. Therefore, I carried out the evaluation of the LNP size controllability of the 3D-iLiNP devices.

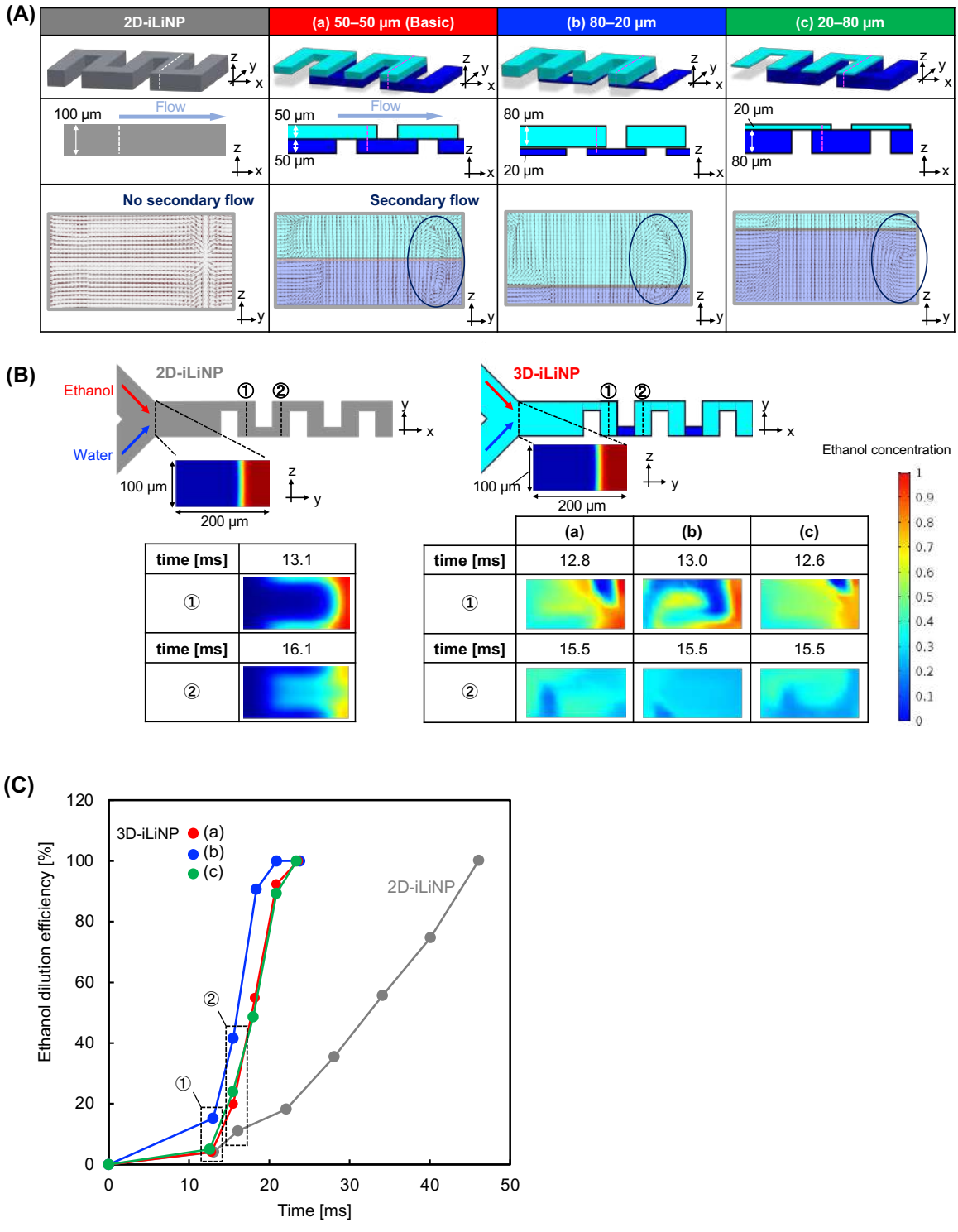

Figure 3.3 CFD simulation of ethanol dilution in the 2D- and 3D-iLiNP devices. The total flow rate was 50 μL/min and the FRR was 3. (A) Streamlines at the cross-section of the 2D- and 3D-iLiNP devices. The dashed line region in the 3D views represent the cross-section of the CFD results. The 3D-iLiNP devices consisted of top and bottom layers with different channel thickness; (a) 50–50 μm, (b) 80–20 μm, and (c) 20–80 μm. (B) Comparison of ethanol dilution process of the 2D- and 3D-iLiNP devices. (C) Ethanol dilution efficiency of the 2D-and 3D-iLiNP devices.

3.3.2 Evaluation of the LNP size controllability of the 3D-iLiNP devices

I determined the 3D-iLiNP device design with the highest LNP size controllability. Figure 3.4 (A) shows the size distribution of 1-Palmitoyl-2-oleoyl-sn-glycero-3-phosphocholine (POPC) LNPs produced using the 2D and 3D-iLiNP devices, the basic-type, –80-20 μm, and –20-80 μm, at a total flow rate and FRR of 50 μL/min and 3, respectively. The basic-type 3D-iLiNP device showed the narrowest LNP size distribution among the four devices, the 2D and three types of 3D-iLiNP devices. Figure 3.4 (B) shows the average LNP size and coefficient variation (CV) value and Figure 3.4 (C) shows the polydispersity index (PDI) of the LNPs produced with the four devices. The average sizes of the POPC LNPs produced with the basic-type, –80-20 μm, and –20-80 μm 3D-iLiNP devices were 101, 78, and 141 nm, respectively. The CV values and PDI were approximately 7%–12% and 0.17–0.23, respectively. In comparison with the 2D-iLiNP device, the basic-type 3D-iLiNP device showed small CV value and PDI even with a large particle size of approximately 100 nm. I assume the sharp change of the device geometry affects the fluid stability and LNP size controllability. From the viewpoint of microfluidics, two solutions introduce into a narrow microchannel is unstable compared with that of a wide microchannel due to the backpressure and the pressure balance of two solutions. As a result, the basic-type 3D-iLiNP device showed small CV value and PDI value. The relationship between the flow condition and the average LNP size is summarized in Figure 3.5 (A). I also measured the concentrations of LNPs using a nanoparticle tracking analyzer (NS300, NanoSight, Malvern Instruments, Worcestershire, UK) (Figure 3.5 (B)). The basic-type 3D-iLiNP device clearly improved the LNP size distribution. From these results, I decided to use the basic-type 3D-iLiNP device in this study.

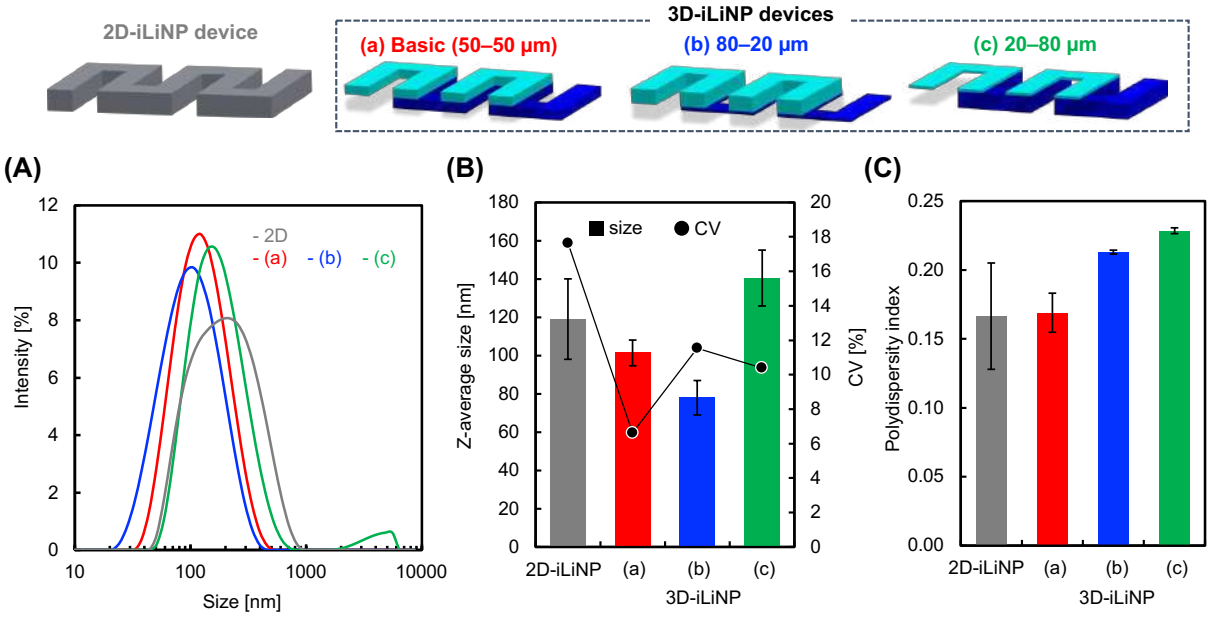

Figure 3.4 (A) Size distributions of the POPC LNPs prepared with the 2D- (gray) and 3D-iLiNP devices. The total flow rate was 50 µL/min and the FRR was 3. Red, blue, and green represent the (a) basic, (b) 80–20 µm, and (c) 20–80 µm devices, respectively. (B) Average sizes and coefficient variation (CV) values of the POPC LNPs. (C) Average values of the polydispersity index (PDI) of the POPC LNPs.

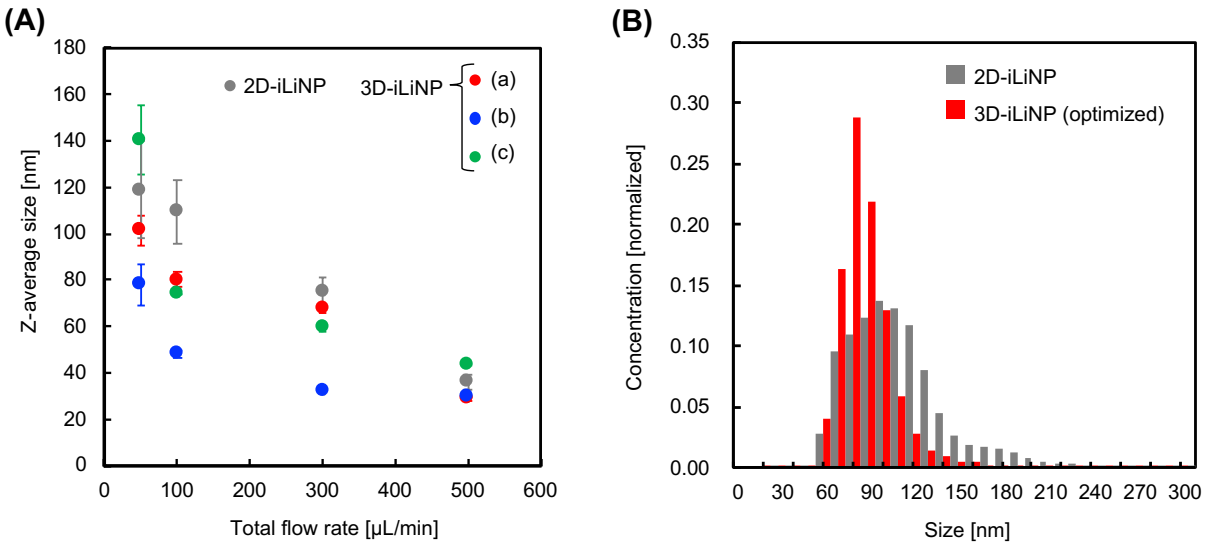

Figure 3.5 Relationship between the flow condition and the average LNP size. The LNP size was measured by (A) a Zetasizer Nano ZEN3600 and (B) a nanoparticle tracking analyzer. The LNPs measured by the nanoparticle tracking analyzer were prepared using the 2D-iLiNP (gray) and the 3D-iLiNP devices (red) at total flow rate of 50 µL/min and an FRR of 3.

Figure 3.6 shows the size distributions of the LNPs produced with the 2D- and 3D-iLiNP devices at total flow rates of 50 or 500 µL/min and FRRs of 3 and 9. In a previous study, it was reported that the increase in the total flow rate and FRR induces the production of small-sized LNPs [14]. From Figure 3.6, it can be seen that the size distribution of the LNPs produced using the 3D-iLiNP device in all flow conditions was significantly more homogeneous than that of the LNP produced with the 2D-iLiNP device. In particular, a single narrow peak can be observed in the size distribution of the LNPs produced with the 3D-iLiNP device at the flow rate of 50 µL/min and FRR of 3.

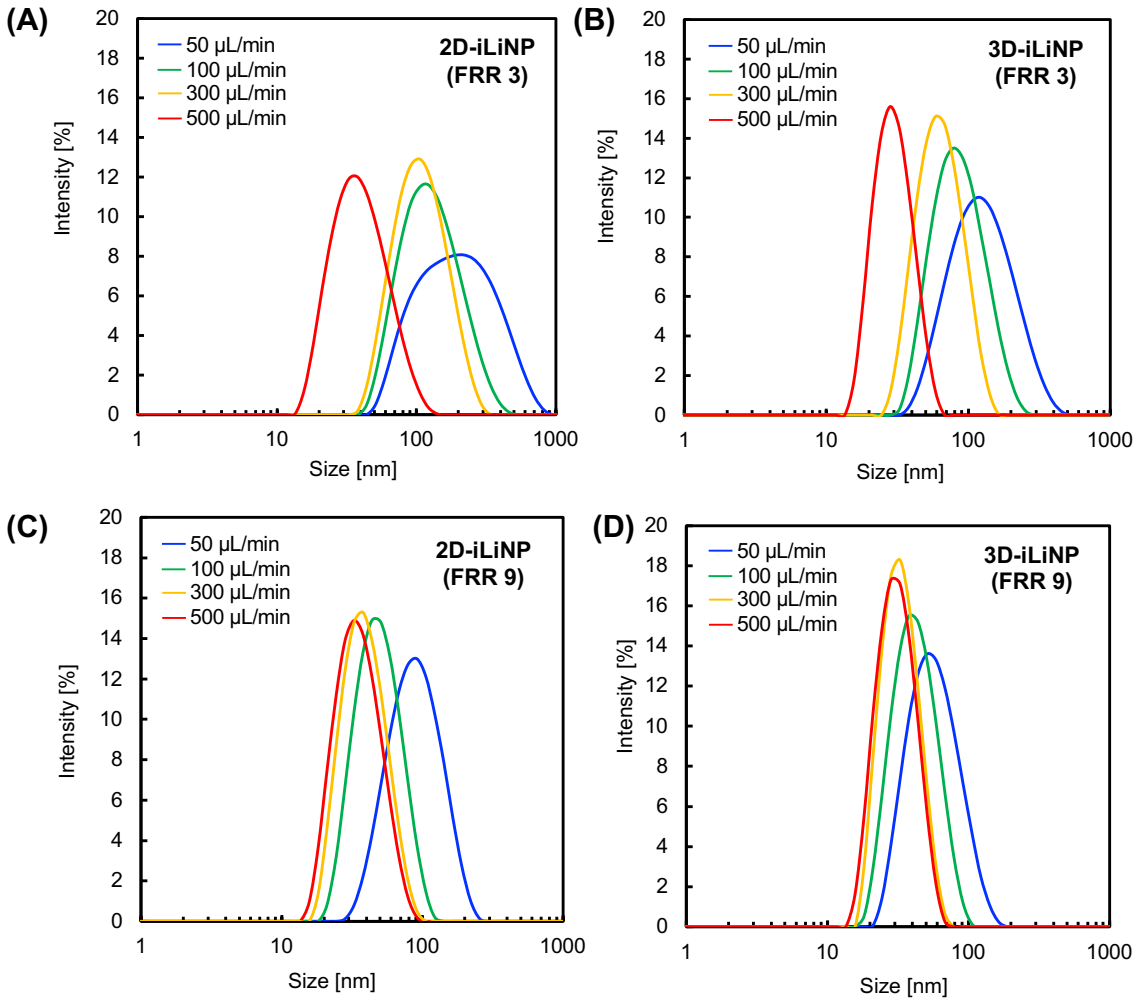

Figure 3.6 Size distributions of the POPC LNPs prepared at FRRs of (A–B) 3 and (C–D) 9. (A) and (C) 2D-iLiNP device; (B) and (D) 3D-iLiNP device.

Figure 3.7 (A) and (B) show a summary of the size of the LNPs produced with the 2D- and 3D-iLiNP devices with an FRR of 3 and 9, respectively. With an FRR of 3, the LNP size range of the iLiNP devices was approximately 30–100 nm, and the LNPs produced with the 3D-iLiNP device were slightly smaller than those produced with the 2D-iLiNP device. With an FRR of 9, the LNP size had a similar trend to that observed at an FRR of 3, and the size range of the LNPs produced with 3D-iLiNP device was 20–50 nm. By controlling the fluid flow, the size of the LNPs produced with the 3D-iLiNP device could be controlled with 10 nm precision (Figure 3.8), even when the device design was modified for mass production (Figure 3.9). Both the 2D- and 3D-iLiNP devices allowed the control of the LNP size through the control of the flow conditions; however, the 3D-iLiNP device led to LNPs with lower CV value in the low flow condition (Figure 3.7 (C) and (D)). In this study, I decide to 10% value of CV (For example, 20 nm ± 2 nm and 100 nm ± 10 nm) is a benchmark to evaluate the LNP size controllability [16]. At all total flow values, the CV value of the LNPs produced with the 3D-iLiNP device was at least 7% smaller than that of the LNPs produced with the 2D-iLiNP device.

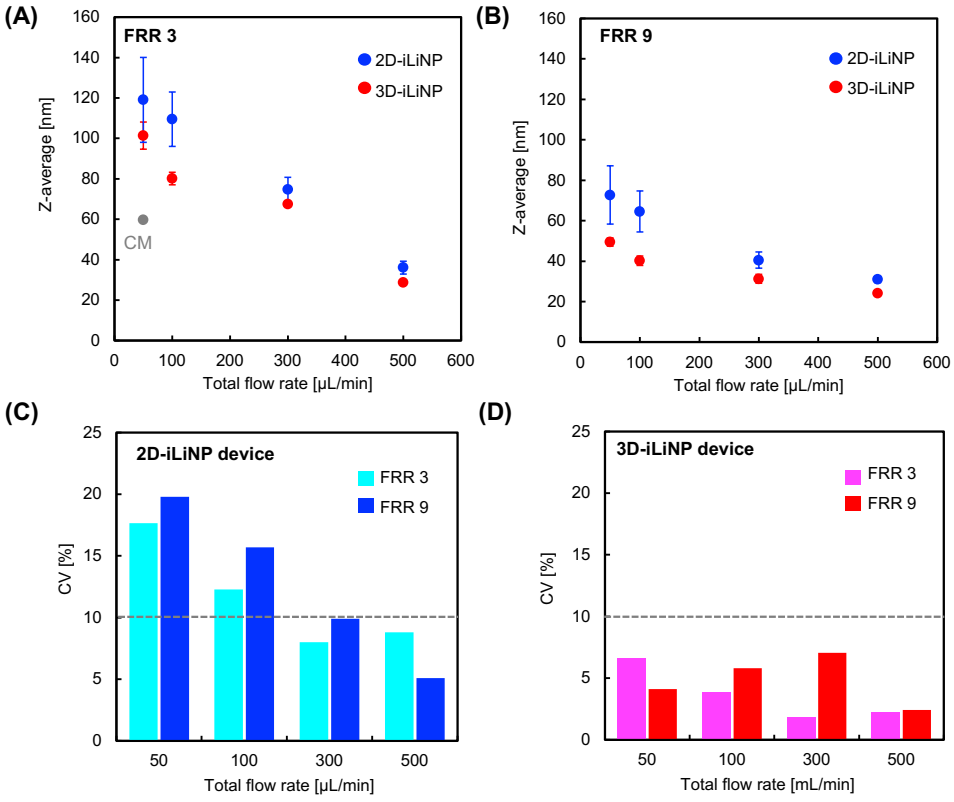

Figure 3.7 Average LNP size as a function of the total flow rate with an FRR of (A) 3 and (B) 9. (C, D) CV values of the LNPs prepared with the 2D- and 3D-iLiNP devices, respectively.

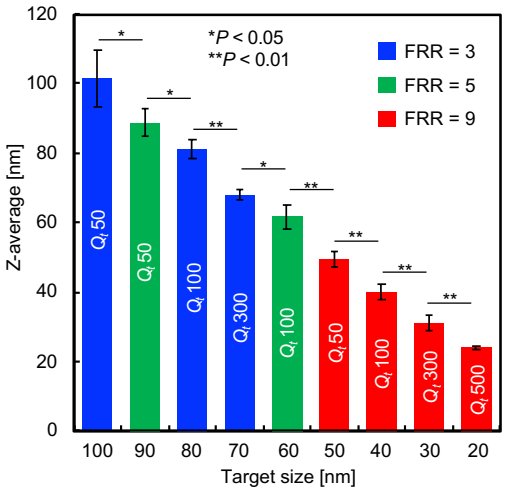

Figure 3.8 Control of the POPC LNP size with 10 nm intervals using the 3D-iLiNP device. The total flow rate was 50–500 µL/min and the FRR was 3–9. *P < 0.05, **P < 0.01, Student's t-test, n = 3–4.

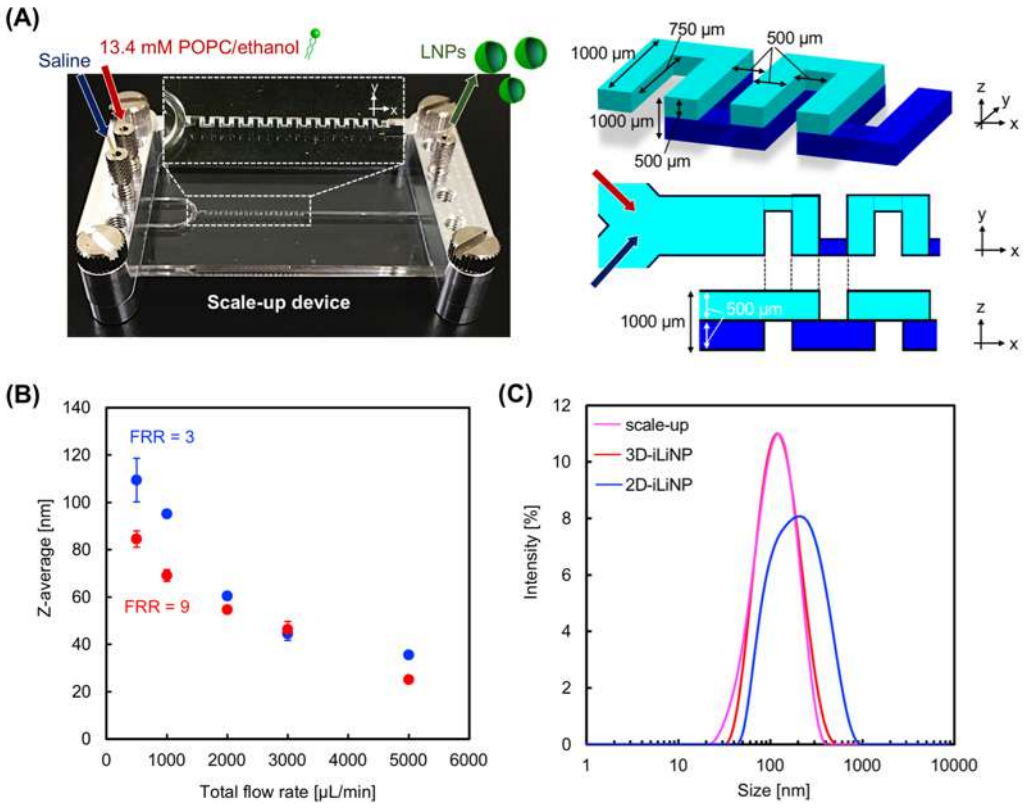

Figure 3.9 (A) Photograph of the 3D-iLiNP device for the scale-up of the LNP production. (B) Relationship between the POPC LNP sizes and total flow rate. (C) Size distributions of 100 nm-sized POPC LNPs prepared using the 3D- (scale-up: magenta; basic: red) and 2D-iLiNP devices (blue). The total flow rate was 50 µL/min and the FRR was 3.

In the microfluidic-based LNP preparation method, the dilution rate affects the LNP size and the mixing homogeneity affects the LNP size distribution [15]. From the viewpoint of fluid dynamics and mass transportation, it is difficult to achieve a homogeneous distribution and slow dilution rate because the homogeneous and slow rate dilution is a competitive phenomenon to diffusion. The concentration gradient induced by diffusion is the major reason for the formation of heterogeneous-sized LNPs because ethanol dilution is a trigger for LNP formation. Therefore, a microfluidic device suitable for low flow rate conditions is indispensable for producing homogeneous- and large-sized LNPs. On the other hand, a homogeneous size distribution and rapid dilution can be achieved with several types of microfluidic devices, such as the chaotic micromixer and 2D-iLiNP devices. The chaotic micromixer device allows homogeneous mixing under low flow rates;[23] however, it could not produce the large-sized LNPs (Table 3.2) [15]. In the case of the 2D-iLiNP device, the formation of the secondary flow plays an important role in the LNP size controllability and depends on the total flow rate [14]. The 2D-iLiNP device allows the control of the LNP Z-average size in the wide range of 20–120 nm through the flow condition. However, the formation of the secondary flow at the low flow rate condition in the 2D-iLiNP was not sufficient to produce homogeneous- and large-sized LNPs. In this study, I revealed that the homogeneous and slow rate dilution was compatible with the rapid dilution by the 3D-iLiNP device, which allowed the production of LNPs in the size range of 20–100 nm with low CV values.

3.3.3 Application for siRNA-loaded lipid nanoparticles

I applied the 3D-iLiNP device for siRNA-encapsulated LNP production to investigate the effect of the LNP size distribution on the gene silencing activity in in vitro and in vivo experiments. The original synthesized pH-sensitive cationic lipid, named CL4H6,[18] and 1,2-dioleoyl-3-dimethylammonium-propane (DODAP), a commercially available lipid, were used as the main components of the lipid systems. Figure 3.10 (A) shows a schematic of the CL4H6-based LNP preparation process and in vivo experimental design. At total flow rates of 50 or 500 μL/min, the 3D-iLiNP device produced 99 and 59 nm LNPs (Figure 3.10 (B)). At the same total flow rates, the average size of the CL4H6 LNPs produced with the 2D-iLiNP device were 102 and 69 nm,

respectively. The siRNA encapsulation efficiency of the LNPs was higher than 97% (Table 3.4). The CV values of the LNPs produced with the 3D-iLiNP device were lower than 10%, while the PDI was almost the same among the four types of LNPs. I did not observe a statistically significant difference on the average size of the 99 and 102 nm-sized LNPs. To investigate the effect of the LNP size distribution on the gene silencing activity, I classified the LNP size into five size ranges based on the LNP size distribution (Figure 3.10 (C) and Figure 3.11): < 40, 40–60, 60–90, 90–120, and > 120 nm. From the LNP size distribution, I confirmed that the 40–60 and 90–120 nm LNPs were the main size ranges of the 59 and 99 nm sized LNPs prepared with the 3D-iLiNP device, respectively. The intensity of the main peaks of both LNPs at the two size ranges were higher than 50%. In contrast, 40–60 and > 120 nm were the main size ranges of the 69 and 102 nm LNPs, respectively; however, the intensity of the main peaks of both particles at the two size ranges were lower than 50%. In particular, the intensity of the 99 nm LNPs in the 90–120 nm size range was twice as high as that of the 102 nm LNPs.

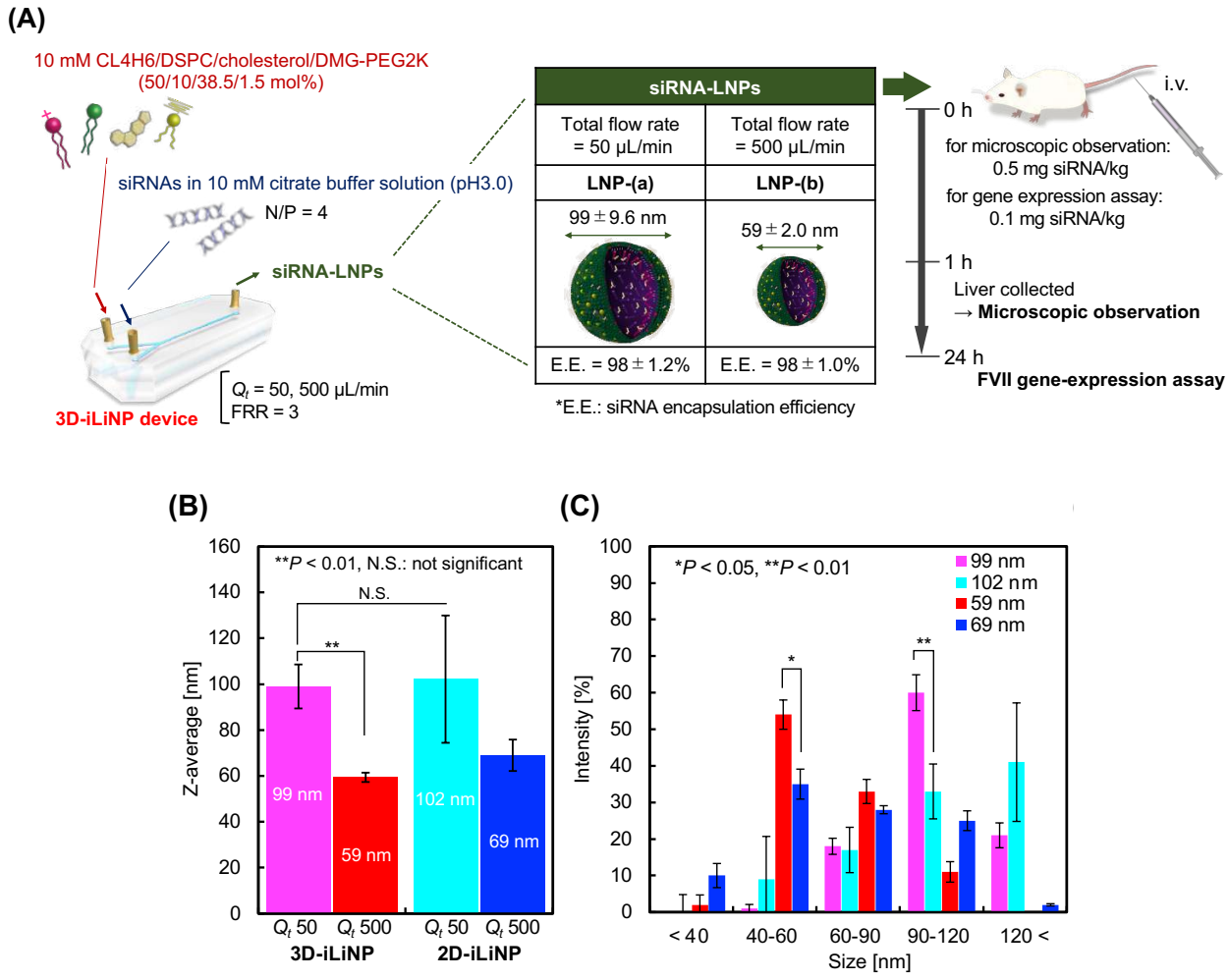

Figure 3.10 (A) Schematic of the CL4H6-based LNP preparation and in vivo experimental design. (B) Average size of the CL4H6 LNPs prepared with the 3D and 2D-iLiNP devices. $^{**}P < 0.01$, N.S.: not significant ($P > 0.05$), $n = 3$, Student's *t-test*. (C) Size distributions of the CL4H6 LNPs. $^{*}P < 0.05$, $^{**}P < 0.01$, $n = 3$, Student's *t-test*.

Table 3.4 Summary of siRNA LNPs characters

pH-sensitive cationic lipid	Device	Total flow rate [μL/min]	Z-average [nm]	CV [%]	PDI	E.E.[a] [%]
DODAP	3D	50	73±5.6	8	0.15±0.012	98±1.0
		500	37±1.9	5	0.22±0.040	97±1.5
	2D	50	81±21.5	27	0.16±0.015	98±1.0
		500	56±8.2	15	0.30±0.093	98±1.0
CL4H6	3D	50 (LNP-(a))	99±9.6	10	0.09±0.010	98±1.2
		500 (LNP-(b))	59±2.0	3	0.07±0.037	98±1.0
	2D	50	102±27.7	27	0.13±0.039	97±2.5
		500	69±6.8	10	0.16±0.086	98±1.8

[a]E.E.: Encapsulation efficiency

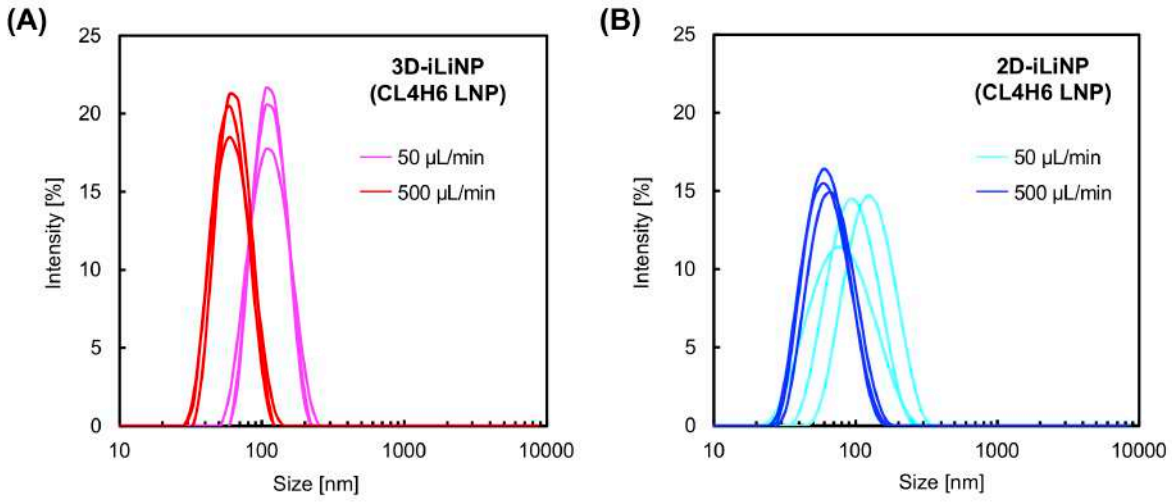

Figure 3.11 Size distributions of siRNA-encapsulated CL4H6 LNPs prepared with the (A) 3D- and (B) 2D-iLiNP devices. The total flow rate was 50 or 500 μL/min and the FRR was 3.

Next, I carried out an in vitro experiment to evaluate the gene silencing activity of the LNPs with four sizes (Figure 3.12). The 99 nm LNPs showed the best gene silencing activity among the four LNP sizes and suppressed almost 40% of the luciferase expression at a dose of 0.1 nM siRNA. Interestingly, the 102 and 69 nm LNPs prepared with the 2D-iLiNP device suppressed luciferase expression by 30 %, whereas the 59 nm LNPs prepared with the 3D-iLiNP device did not induce gene silencing. It was found that gene silencing activity depends on the amount of LNPs with size ranging from 90 to 120 nm. The DODAP LNPs showed a similar trend to that of the CL4H6 LNPs (Figure 3.13). This result indicates that the LNP size distribution plays a crucial role on the gene silencing activity, and 3D-iLiNP allows the production of LNPs highly efficient for siRNA delivery.

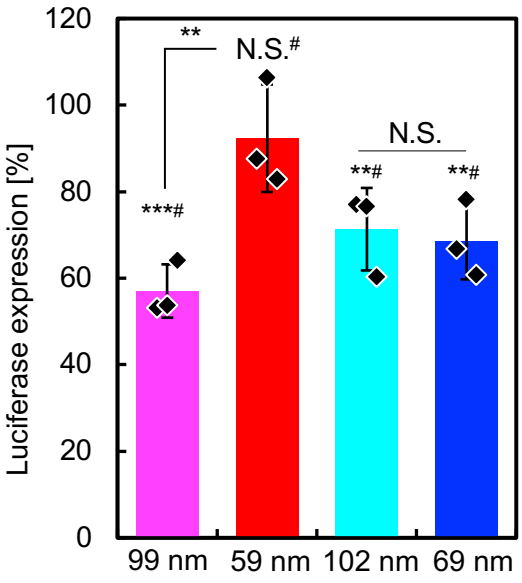

Figure 3.12 Gene-silencing activity of the 99 and 59 nm LNPs in HeLa-dluc cells at a dose of 0.1 nM siGL4. $^{**}P < 0.01$, $^{***}P < 0.001$ (#: vs. N.C.), N.S.: not significant (#: vs. N.C., $P > 0.01$), $n = 3$, Student's *t-test*.

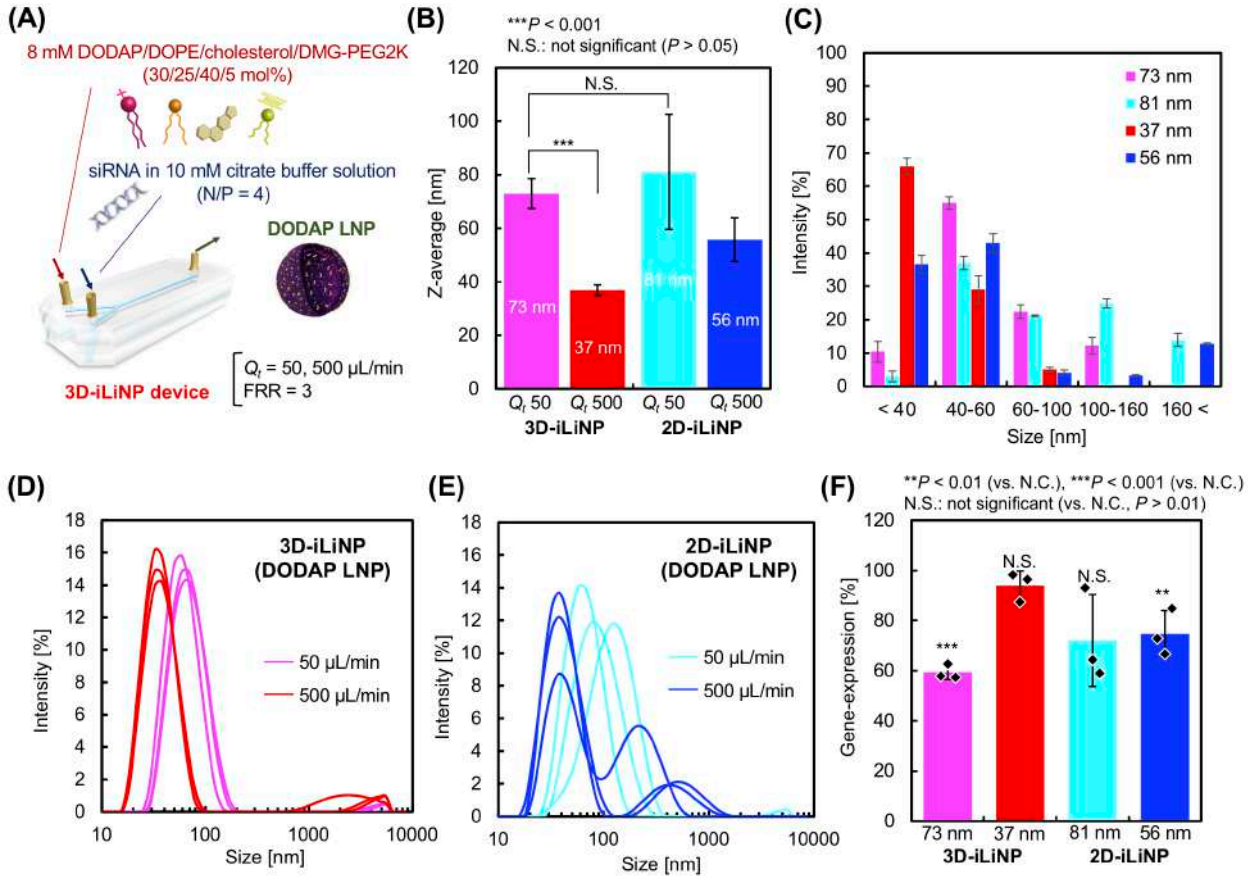

Figure 3.13 (A) Schematic of the DODAP-based LNP preparation. (B) Z-average sizes and (C) size distributions of the DODAP LNPs. The LNP sizes were classified into five size ranges (< 40, 40–60, 60–100, 100–160, and >160) based on the size distributions of the LNPs produced with the (D) 3D- and (E) 2D-iLiNP devices. The total flow rate was 50 or 500 µL/min and the FRR was 3. ***P < 0.001, N.S.: not significant (P > 0.05), Student's t-test, n = 3. (F) Gene-silencing activity of the LNPs at a dose of 50 nM siGL4. **P < 0.01, ***P < 0.001, N.S.: not significant (P > 0.01), Student's t-test, n = 3.

Figure 3.14 (A) shows the gene silencing activity observed in the in vivo experiment. The lipid system was optimized for the in vivo experiment;[18] therefore, both the 99 and 59 nm LNPs suppressed plasma coagulation factor VII (FVII) expression in mice at a dose of 0.1 mg siRNA/kg. The 99 nm LNPs showed 75% gene silencing activity, while the 59 nm LNPs suppressed 50% of the FVII expression. Figure 3.14 (B) shows the intrahepatic LNP distributions of the 99 and 59 nm LNPs. I observed a size-specific intrahepatic LNP distribution consistent with previous reports [3]. From the results of the gene silencing activity experiments, intrahepatic distribution,

and size of fenestrae (approximately 100–150 nm), the LNPs with a size range of 90–120 nm exhibited the highest RNA delivery performance in vivo using this lipid system. Therefore, the 3D-iLiNP device will be a key technology for the production of size-controlled LNPs for RNA delivery applications.

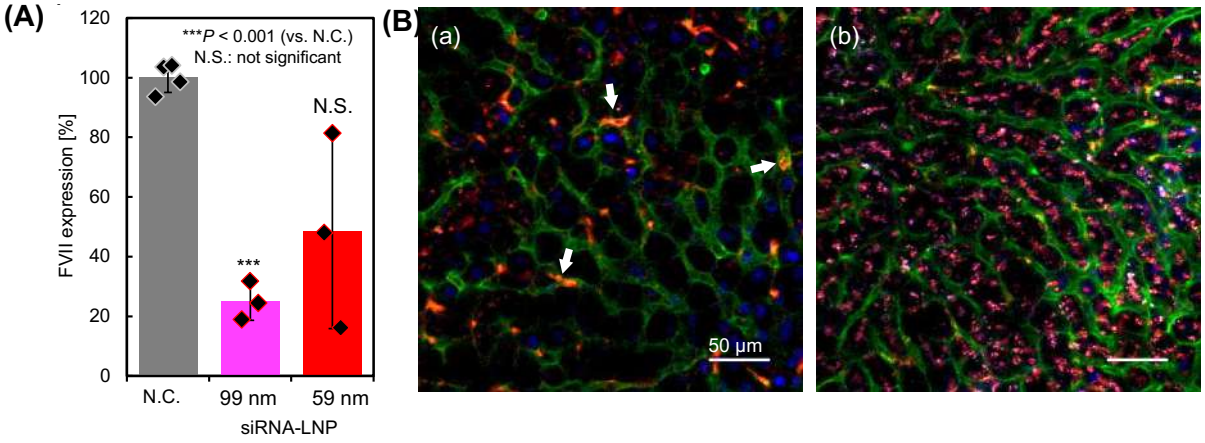

Figure 3.14 (A) FVII expression of the ICR mice treated with CL4H6 LNPs at a dose of 0.1 mg siRNA/kg. ***$P < 0.001$ (vs. N.C.), N.S. not significant ($P > 0.01$), n = 3-4, Student's *t-test*. (B) Confocal microscope images of the mice liver tissues treated with (a) 99 and (b) 59 nm LNPs at a dose of 0.5 mg siRNA/kg. Blue, green, red, and cyan represent nuclei, blood vessel, LNP, and siRNA, respectively. The arrows indicate the accumulation of LNPs in the blood vessels.

3.4 Conclusion

I developed a 3D, symmetrically assembled microfluidic device named 3D-iLiNP with the aim of improving the size distribution of large-sized LNPs produced at low flow rate conditions. The 3D-iLiNP device allowed the production of LNPs with a narrow size distribution owing to the 3D secondary flow. I demonstrated that the 3D-iLiNP device could produce POPC LNPs in the size range of 20 to 100 nm depending on the flow conditions with CV values smaller than 10%. I employed the 3D-iLiNP device for the production of siRNA-loaded LNPs to investigate the effect of the LNP size distribution on the gene silencing activity. The 3D-iLiNP device allowed the production of siRNA-loaded LNPs with a size distribution more homogenous than that of the LNPs produced

with the 2D-iLiNP device. I clearly distinguished the main LNP size ranges produced by the 3D-iLiNP device and found that the 90–120 nm LNPs suppressed the luciferase expression of HeLa cells. For the in vivo experiment, 100 nm LNPs showed a higher gene silencing activity than the small-sized siRNA LNPs. I believe that the 3D-iLiNP device and size-controlled LNPs could improve not only the RNA delivery and gene silencing activity, but also the transfection or genome-editing performance of LNP-DDSs.

References

[1] R. A. Mukhamadiyarov, E. A. Senokosova, S. S. Krutitsky, D. V. Voevoda, I. A. Pyshnaya, V. V. Ivanov, M. J. Lewis and I. Khaliulin, *J. Cardiovasc. Pharmacol.*, **72**, 143-152 (2018)

[2] H. Cabral, Y. Matsumoto, K. Mizuno, Q. Chen, M. Murakami, M. Kimura, Y. Terada, M. R. Kano, K. Miyazono, M. Uesaka, N. Nishiyama and K. Kataoka, *Nat Nanotechnol*, **6**, 815-823 (2011)

[3] Y. Sato, Y. Note, M. Maeki, N. Kaji, Y. Baba, M. Tokeshi and H. Harashima, *J. Control. Release*, **229**, 48-57 (2016)

[4] S. Hirsjarvi, L. Sancey, S. Dufort, C. Belloche, C. Vanpouille-Box, E. Garcion, J. L. Coll, F. Hindre and J. P. Benoit, *Int. J. Pharm.*, **453**, 594-600 (2013)

[5] H. Ren, Y. He, J. Liang, Z. Cheng, M. Zhang, Y. Zhu, C. Hong, J. Qin, X. Xu and J. Wang, *ACS Appl Mater Interfaces*, **11**, 20304-20315 (2019)

[6] S. Chen, Y. Y. C. Tam, P. J. C. Lin, M. M. H. Sung, Y. K. Tam and P. R. Cullis, *J. Control. Release*, **235**, 236-244 (2016)

[7] M. Yanez Arteta, T. Kjellman, S. Bartesaghi, S. Wallin, X. Wu, A. J. Kvist, A. Dabkowska, N. Szekely, A. Radulescu, J. Bergenholtz and L. Lindfors, *Proc Natl Acad Sci U S A*, **115**, E3351-E3360 (2018)

[8] J. Snoeys, J. Lievens, E. Wisse, F. Jacobs, H. Duimel, D. Collen, P. Frederik and B. De Geest, *Gene Ther.*, **14**, 604-612 (2007)

[9] S. G. Ong, M. Chitneni, K. S. Lee, L. C. Ming and K. H. Yuen, *Pharmaceutics*, **8** (2016)

[10] A. Jahn, S. M. Stavis, J. S. Hong, W. N. Vreeland, D. L. DeVoe and M. Gaitan, *ACS Nano*, **4**, 2077-2087 (2010)

[11] E. Kastner, R. Kaur, D. Lowry, B. Moghaddam, A. Wilkinson and Y. Perrie, *Int. J. Pharm.*, **477**, 361-368 (2014)

[12] N. Kimura, M. Maeki and M. Tokeshi, Microfabrication and microfluidic devices for drug delivery, *Microfluidics for Pharmaceutical Applications: From Nano/Micro Systems Fabrication to Controlled Drug Delivery,* H. A. Santos, D. Liu and H. Zhang, eds., Elsevier, 123-136, (2019)

[13] N. Kimura, M. Maeki, Y. Sato, A. Ishida, H. Tani, H. Harashima and M. Tokeshi, *ACS Appl Mater Interfaces*, **12**, 34011-34020 (2020)

[14] N. Kimura, M. Maeki, Y. Sato, Y. Note, A. Ishida, H. Tani, H. Harashima and M. Tokeshi, *ACS Omega*, **3**, 5044-5051 (2018)

[15] M. Maeki, Y. Fujishima, Y. Sato, T. Yasui, N. Kaji, A. Ishida, H. Tani, Y. Baba, H. Harashima and M. Tokeshi, *PLoS One*, **12**, e0187962 (2017)

[16] I. V. Zhigaltsev, N. Belliveau, I. Hafez, A. K. K. Leung, J. Huft, C. Hansen and P. R. Cullis, *Langmuir*, **28**, 3633-3640 (2012)

[17] M. Mijajlovic, D. Wright, V. Zivkovic, J. X. Bi and M. J. Biggs, *Colloids Surf B Biointerfaces*, **104**, 276-281 (2013)

[18] Y. Sato, K. Hashiba, K. Sasaki, M. Maeki, M. Tokeshi and H. Harashima, *J. Control. Release*, **295**, 140-152 (2019)

[19] T. J. Johnson, D. Ross and L. E. Locascio, *Anal Chem*, **74**, 45 (2002)

[20] J. C. McDonald and G. M. Whitesides, *Acc. Chem. Res.*, **35**, 491-499 (2002)

[21] L. Tang and N. Y. Lee, *Lab Chip*, **10** (2010)

[22] M. Jayaraman, S. M. Ansell, B. L. Mui, Y. K. Tam, J. Chen, X. Du, D. Butler, L. Eltepu, S. Matsuda, J. K. Narayanannair, K. G. Rajeev, I. M. Hafez, A. Akinc, M. A. Maier, M. A. Tracy, P. R. Cullis, T. D. Madden, M. Manoharan and M. J. Hope, *Angew. Chem. Int. Ed. Engl.*, **51**, 8529-8533 (2012)

[23] A. D. Stroock, S. K. Dertinger, A. Ajdari, I. Mezic, H. A. Stone and G. M. Whitesides, *Science*, **295**, 647-651 (2002)

CHAPTER 4 Development of a Microfluidic-Based Post-Treatment Process for Size-Controlled Lipid Nanoparticles

4.1 Introduction

Drug delivery system (DDS) technologies using lipid nanoparticles (LNPs) are expected to provide invasive and more effective chemotherapies than present treatments [1-4]. For the LNP-based DDS treatment, the LNP size played an important role in biological distribution, including lymph nodes, and particle function, such as cancer chemotherapy and gene silencing activity [5-9]. Nakamura et al. reported that 30 nm sized LNPs were efficiently translocated to lymph nodes compared with 100 and 200 nm sized LNPs [5]. Cabral et al. reported that small-sized LNPs also showed high penetration efficiency to poorly permeable pancreatic tumors [6]. On the other hand, 60 nm sized small interfering RNA (siRNA)-loaded LNPs led to higher gene silencing in hepatocytes than 30 nm sized siRNA-loaded LNPs [7]. In addition, LNPs of sizes larger than 200 nm were filtered by the spleen [10]. Therefore, LNPs of sizes from 20 to 200 nm are most widely used for nano-DDSs, and size tuning of LNPs depending on the target tissue is strongly desired for practical applications.

To produce size-controlled LNPs, the organic solvent injection method using microfluidic devices is one of the most effective methods [11-13]. For the microfluidic-based organic solvent injection method, ethanol, having relatively low toxicity compared with other solvents, is generally used as the lipid solvent in the microfluidic LNP preparation methods [14]. An ethanol solution containing lipids and an aqueous solution are introduced into a microfluidic device and LNPs form by self-assembly of lipid molecules because of the diluting ethanol. The first approved siRNA medicine-encapsulated LNPs have been marketed as Onpattro, which is produced using the microfluidic-based ethanol injection method. Microfluidic devices with herringbone micromixer structures have been widely used for the preparation of size-controlled LNPs [15-18]. Recently, I have developed a microfluidic device equipped with baffle structures for the production of precise size-tuned LNPs [19]. The microfluidic device with baffle structures showed many advantages for LNP production, including its simple structure, a wide range of LNP size controllability from 20 to 100 nm, and realization of an integrated LNP production process. Microfluidic-based LNP production methods are important for achieving practical use of nano-DDSs; however, several post-treatment processes like dilution or dialysis to remove

ethanol from the LNP suspension and for concentration of the LNP suspension are also indispensable for the LNP production.

Conventionally, the removal or dilution of ethanol from the LNP suspension is carried out by bulk scale dialysis or direct dilution with a buffer solution as the post-treatment [20]. These conventional post-treatment processes are labor-intensive and time-consuming. Moreover, the coexistence of LNPs and a high concentration of ethanol, a solvent for lipids, for long-term post-treatment processes lead to instability of the LNPs and leakage of loaded drugs [21-24]. In addition, the difference in ethanol concentration between the inner and outer membranes of the LNPs affects the fusion of lipid membranes [25].

Although structural dynamics of lipid nanocarriers have been reported by several research groups [26, 27], the effects of the post-treatment on the final product size of LNPs have not been investigated in detail. In particular, the LNP production using the microfluidic-based organic solvent injection method is dominated by the kinetics rather than the thermodynamics. From the viewpoint of kinetics, removal of ethanol molecules by hydration from the LNP system including the inner and outer lipid membrane surfaces could induce the fusion of LNPs [28]. In this chapter, I investigated the effects of the post-treatment on the size of the LNPs when using microfluidic devices with baffle structures and I compared these effects to effects when using the conventional methods. I found that the flow conditions at the post-treatment affected the final product size of LNPs. Then, I developed the integrated baffle device composed of the LNP production region and the post-treatment region for the microfluidic-based LNP production system. I also developed the integrated baffle device for scaled-up LNP production and siRNA-loaded LNP production based on the microfluidic-based post-treatment. To ensure the applicability of the integrated microfluidic system for DDS treatment, the siRNA delivery and LNP activity were evaluated by in vivo experiments.

4.2 Experimental

4.2.1 Materials

1-Palmitoyl-2-oleoyl-sn-glycero-3-phosphocholine (POPC), 1,2-dipalmitoyl-sn-glycero-3-phosphocholine (DPPC), 1,2-distearoyl-sn-glycero-3-phosphoethanolamine-N-[amino(poly(ethylene glycol))-2000] (DSPE-PEG2K), and 1,2-dimyristoyl-rac-glycero-3-methoxypolyethylene glycol-2000 (DMG-PEG2K) were purchased from the NOF AMERICA Corporation (White Plains, NY). Cholesterol was purchased from Sigma-Aldrich (St. Louis, MO). The pH-sensitive cationic lipid, YSK05, was synthesized in the laboratory as reported previously [29]. Ethanol, sodium chloride, acetic acid, 2-morpholinoethanesulfonic acid (MES), monohydrate, and phosphate-buffered saline (PBS) were purchased from FUJIFILM Wako Pure Chemical Corporation (Osaka, Japan). The siRNA targeting factor VII (siFVII) was purchased from Hokkaido System Science Co. Ltd. (Sapporo, Japan), and its sense and antisense strand sequences were 5′-GGAucAucucAAGucuuAcTsT-3′ and 5′-GuAAGAcuuGAGAuGAuccTsT-3′, respectively. Ribogreen, 1,1′-dioctadecyl-3,3,3′,3′-tetramethylindodicarbocyanine, and 4-chlorobenzenesulfonate salt (DiD) were purchased from Molecular Probes (Eugene, OR).

4.2.2 Fabrication of Microfluidic Devices

The microfluidic devices with baffle structures (baffle devices) were fabricated using the standard photolithography method [30]. The detailed protocol was described previously [19]. In brief, I made the master molds from SU-8 3050 (Nippon Kayaku Co., Ltd., Tokyo, Japan) for the 100 μm thick layer and from SU-8 3010 for the 20 μm thick layer onto silicon wafers. Finally, replicated poly(dimethylsiloxane) (PDMS) pieces were bonded with glass slides or PDMS replicas by the oxygen plasma treatment (CUTE-1MP/R, Femto Science, Gwangju, Korea).

4.3.3 Preparation of LNPs Using the Microfluidic Devices

For the preparation of the POPC LNPs, 13.4 mM POPC/ethanol solution and saline were introduced into the simple baffle device at a total flow rate of 50 µL/min and a flow rate ratio (FRR) of 3, as shown in Figure 4.1. Therefore, 25% v/v ethanol remained in the collected LNP suspension. For the POPC/cholesterol (50:50 mol %) LNP preparation, 13.4 mM lipid/ethanol solution and saline were also introduced into the simple baffle device at a total flow rate of 50 µL/min and an FRR of 3. After the LNP synthesis step, the LNP suspension was fed into the simple baffle device for the additional ethanol dilution as a microfluidic post-treatment. In the case of the microfluidic-based method, the LNP suspension containing 25% v/v ethanol and saline were separately introduced into the baffle device at a total flow rate ranging from 0.1 to 500 µL/min and an FRR of 24. In post-treatment, ethanol was diluted to 1% concentration. In the previous study, I confirmed the formation of theoretically minimum-sized POPC LNPs at 500 µL/min. For this reason, I decide the flow rate of 500 µL/min as the highest flow rate in this study. To compare the effect of post-treatment, I employed dialysis and dilution with a buffer solution as the conventional processes. In the case of dialysis, the collected LNP suspension was dialyzed overnight against 154 mM NaCl aqueous solution. I used dialysis membrane tubing with 12–14 kDa molecular weight cutoffs purchased from Repligen Corporation (Waltham, MA). In the case of direct dilution, the LNP suspension was dropped into saline using a pipet with vortex mixing and diluted from 25 to 1% ethanol concentration.

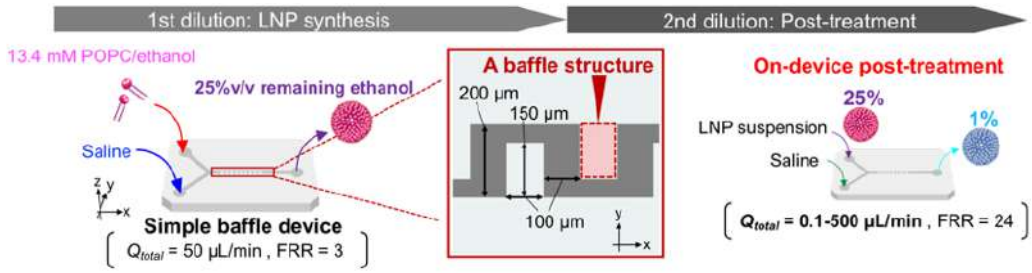

Figure 4.1 Microfluidic rapid ethanol dilution method using baffle devices. Schematic illustration of the LNP preparation using the simple baffle device. In the LNP synthesis step, 13.4 mM POPC/ethanol solution and saline were introduced into this baffle device at a total flow rate of 50 µL/min and a flow rate ratio (FRR) of 3. In the on-device post-treatments, the collected LNP suspension with 25% v/v remaining ethanol was diluted to 1% via the simple baffle device at different total flow rate conditions.

For the preparation of the DPPC LNPs, 1,2-Dipalmitoyl-sn-glycero-3-phosphocholine (DPPC), cholesterol and 1,2-distearoyl- sn-glycero-3-phosphoethanolamine-N-[amino(polyethylene glycol)-2000] (DSPE- PEG2K) were dissolved in ethanol at the molar ratio of 67/33/5, and the total lipid concentration was 15 mM. The lipid solution and PBS were introduced into the baffle device at the total flow rate of 50 μL/min and the flow rate ratio (FFR) of 3. The collected suspension containing 25%v/v ethanol was post-treated by the conventional methods (the dialysis method and the direct dilution with a buffer solution method) and the microfluidic method. For the microfluidic method, the LNP suspension containing 25%v/v ethanol was diluted from 25% to 1 % at 500 μL/min and the FRR of 24. In the direct dilution method, the suspension was also diluted from 25% to 1% ethanol. After the post-treatment, the sizes of LNPs were measured by dynamic light scattering (DLS) measurement.

I measured the size of the LNPs by dynamic light scattering (DLS) measurement with a Zetasizer Nano ZS ZEN3600 instrument (Malvern Instruments, Worcestershire, U.K.) and a nanoparticle tracking analyzer (NTA), NanoSight NS300 (Quantum Design, Tokyo, Japan). The refractive index of the LNP suspension containing ethanol was measured using a refractometer RX-5000i-Plus (ATAGO Co., Ltd., Tokyo, Japan).

POPC LNPs were observed by transmission electron microscopy (TEM, JEM-1400Plus; JEOL Ltd., Tokyo, Japan) at an acceleration voltage of 100 kV. Digital images (3296 × 2472 pixels) were taken with a CCD camera (EM-14830RUBY2; JEOL). The samples were absorbed to carbon-coated copper grids (400 mesh) and stained with 2% phosphotungstic acid solution (pH 7.0) for 20 s.

4.3.4 Evaluation of the size stability of the post-treated POPC LNPs

I prepared the LNP suspension with 13.4 mM POPC/ethanol solution and saline by using the simple baffle device at the total flow rate of 50 μL/min and the FRR of 3. The POPC LNP suspension was treated by the conventional post-treatment methods and the on-device method. In the on-device post-treatment method, the POPC LNP suspension was diluted at the total flow rate of 500 μL/min. After each post-treatment processes,

these treated LNP suspension was incubated at 4°C for 10 days. I measured the size of the LNPs before and after the incubation by DLS.

4.3.5 Evaluation of the Mass Productivity of the LNPs

I prepared the 67 mM POPC/ethanol solution and introduced it into the integrated baffle device, as shown in Figure 4.2. In the first dilution region, LNPs formed at a total flow rate of 100 μL/min and an FRR of 3. LNPs in the first dilution region (red and blue colors) were additionally diluted with saline fed at 2400 μL/min in the second region (green color).

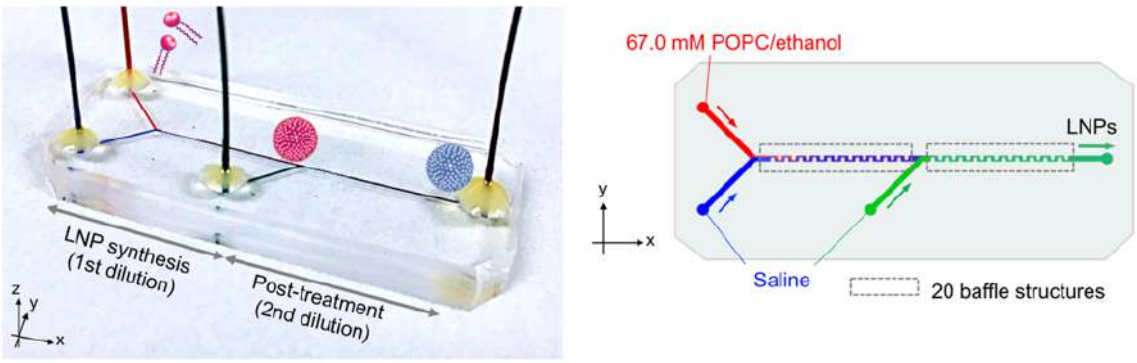

Figure 4.2 Photograph of the integrated baffle device for scaled-up LNP production. The integrated baffle device was composed of the first and second diluting regions; each region had 20 baffle structures. In the first dilution region, the LNPs were produced at a total flow rate of 100 μL/min and an FRR of 3. The produced LNPs were continuously diluted by saline introduced at 2400 μL/min in the second region.

4.3.6 Preparation of siRNA-Encapsulated LNPs

The siRNA-loaded LNPs were prepared using the simple and integrated baffle devices and the physical properties and activities were evaluated, as previously described with slight modifications [19]. Briefly, I used the YSK05-based LNP system composed of a pH-sensitive cationic lipid (YSK05), cholesterol, and PEGylated lipid (DMG-PEG2K). These lipids were dissolved in ethanol at a molar ratio of 50:50:3 and a total lipid concentration of 8 mM. The prepared lipid solution and 25 mM acetate buffer solution (pH 4.0) containing 71

μg/mL siFVII (pH 4.0) were injected into the simple baffle device at a total flow rate of 500 μL/min and an FRR of 3.

In the conventional dialysis method, the LNP suspension containing 25% of ethanol was dialyzed for over 2 h against 20 mM MES buffer solution (pH 6.0). In the direct dilution method, the LNP suspension was diluted in the same manner as the POPC LNPs with 20 mM MES buffer. After the dialysis or dilution, the LNP suspensions were further dialyzed overnight against PBS (pH 7.4). In the microfluidic post-treatment, the LNP suspension with 25% of ethanol was diluted with 20 mM MES buffer (pH 6.0) using the integrated baffle device. The diluted suspension collected from the outlet of the device was dialyzed overnight against PBS. LNP suspensions were concentrated using Amicon Ultra filters (100K, Merck, Darmstadt, Germany) for in vivo experiments.

The siRNA encapsulation efficiency was measured by the RiboGreen assay. FVII gene knockdown activity and the confocal microscopic imaging of the mice liver tissue were carried out as previously described [19].

4.3 Results and Discussion

4.3.1 Effects of the Microfluidic Post-Treatment Process on LNP Size

I investigated the effect of the post-treatment using the microfluidic-based simple and integrated baffle devices and the conventional methods on the size of LNPs. Figure 4.1 shows the schematic illustration of the experimental design. In the first dilution, LNPs were synthesized and their suspension was immediately diluted in the second dilution. Figures 4.3 (A) shows the size distributions of the POPC LNPs prepared by different post-treatment methods. Interestingly, the sizes of the LNPs were changed depending on the total flow rate. The sizes of LNPs post-treated by the simple baffle device at flow rates higher than 10 μL/min were smaller than those by the conventional methods. A similar tendency was observed in another lipid system that consisted of DPPC, cholesterol, and DSPE-PEG2K (Figure 4.4). At a total flow rate of 500 μL/min, the number-weighted

average size of LNPs was 25 nm and the coefficient variation (CV) value was smaller than 1% (Figure 4.3 (B), inset).

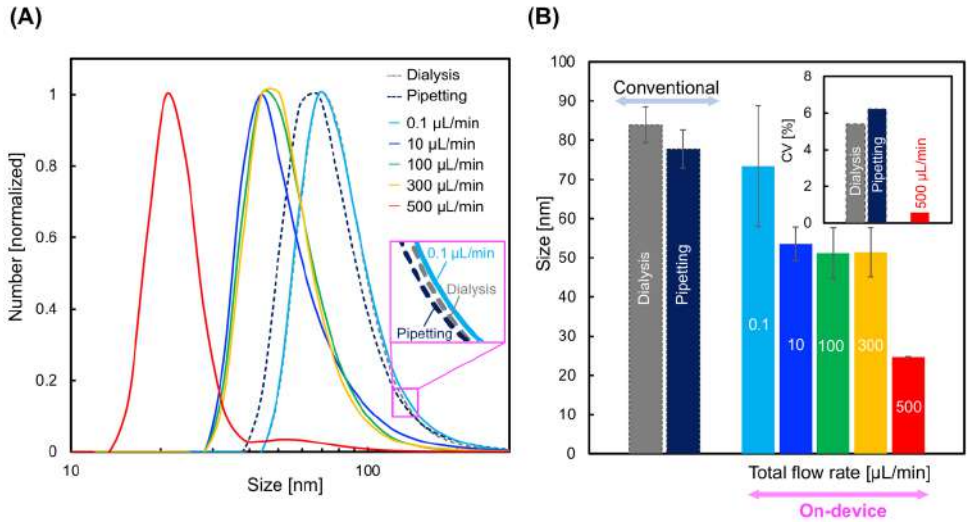

Figure 4.3 (A) Number-weighted size distributions of the LNPs produced at different post-treatment conditions and the conventional methods. These distributions were normalized by the respective maximum intensity value. (B) Number-weighted average size of the LNPs prepared by the different post-treatment methods. The inset graph shows coefficient variation (CV) values of the LNPs. The error bars mean the standard deviation calculated from at least three reproducibility experiments.

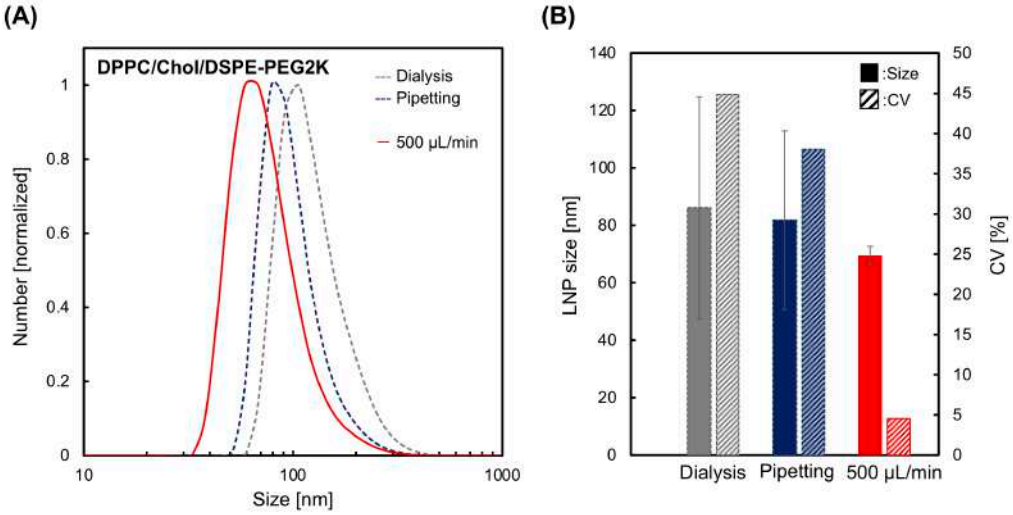

Figure 4.4 Effects of the post-treatment process on the DPPC-LNP size controllability. (A) Number-weighted size distributions of the LNPs prepared by the conventional and microfluidic post-treatment methods. (B) Average sizes of LNPs (number-weighted) and CV values. These error bars were calculated from reproducibility experiments carried out three times.

The size stability of the POPC LNPs treated by the conventional and the on-device post-treatment methods is shown in Figure 4.5. POPC LNPs were observed by TEM, and I found the formation of multilamellar and unilamellar vesicles, regardless of the post-treatment methods. The results of TEM analysis showed good agreement with that of the DLS measurement. From the TEM image, I confirmed the partial fusion phenomenon of the POPC LNPs suspended in 25% ethanol (Figure 4.6 (A)).

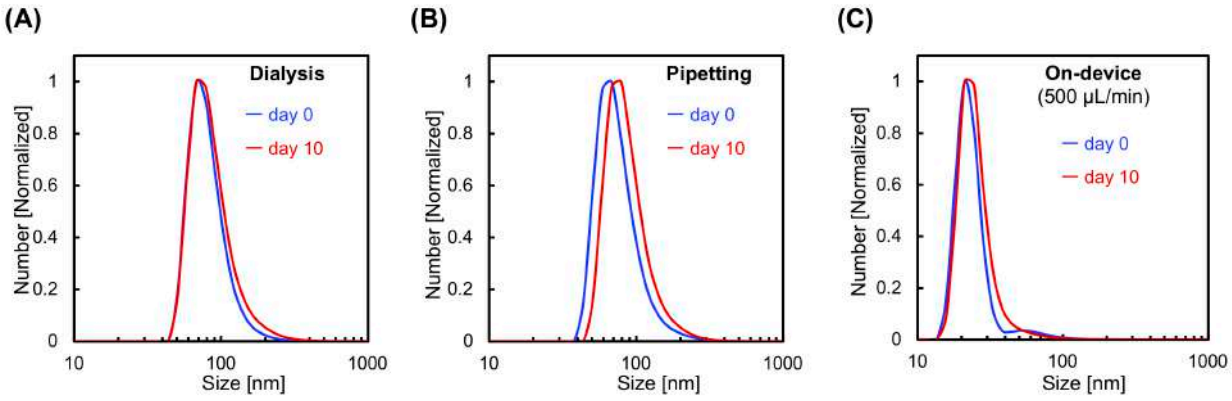

Figure 4.5 Number-weighted size distributions of the LNPs treated by the conventional and the on-device post-treatment methods. The POPC LNP was synthesized at the total flow rate of 50 µL/min and FRR of 3. The total flow rate of the on-device method was 500 µL/min. After the post-treatment method, the LNPs were incubated at 4°C for 10 days (red). These distributions were normalized by the respective maximum intensity value.

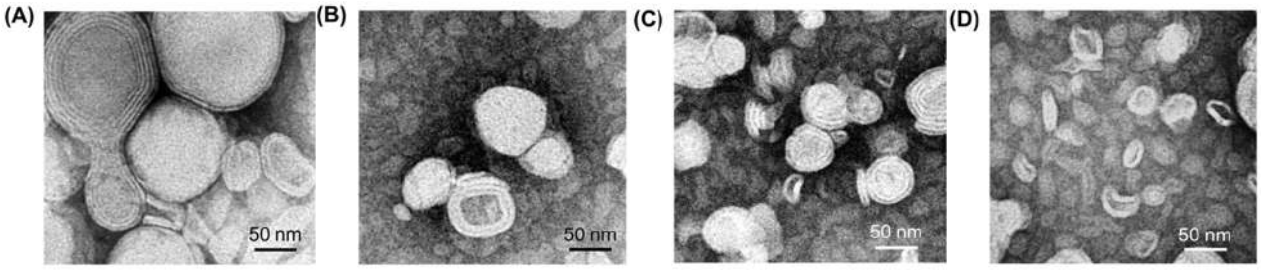

Figure 4.6 TEM images of the POPC LNPs (A) suspended in 25% ethanol, (B) treated by the conventional dialysis post-treatment. (C and D) The POPC LNPs treated by the microfluidic post-treatments at the total flow rate of (C) 10 µL/min and (D) 500 µL/min.

To verify the effect of flow conditions in the post-treatment, the LNP suspension was incubated in a refrigerator at 4 °C before the second dilution at a flow rate of 500 μL/min. The size of LNPs incubated in 25% ethanol for 24 h was 40 nm and did not decrease. The average size of LNPs without incubation was 25 nm, and it did not decrease either after incubating for 24 h (Figure 4.7 (A)). Although the average sizes of incubated LNPs were shifted to 30-40 nm, the LNP sizes were smaller than those of the conventional dialysis and direct dilution (80 nm). Figure 4.7 (B) shows the sizes of LNPs before and after the microfluidic post-treatment process for various incubation times. The LNP suspensions before the post-treatment included 25% v/v ethanol; therefore, the LNP sizes were corrected by the refractive index. The corrected LNP sizes after the microfluidic post-treatment were smaller than those of the LNPs before the post-treatment, regardless of the incubation time. Incubation time in 25% v/v ethanol affected the final product size of LNPs.

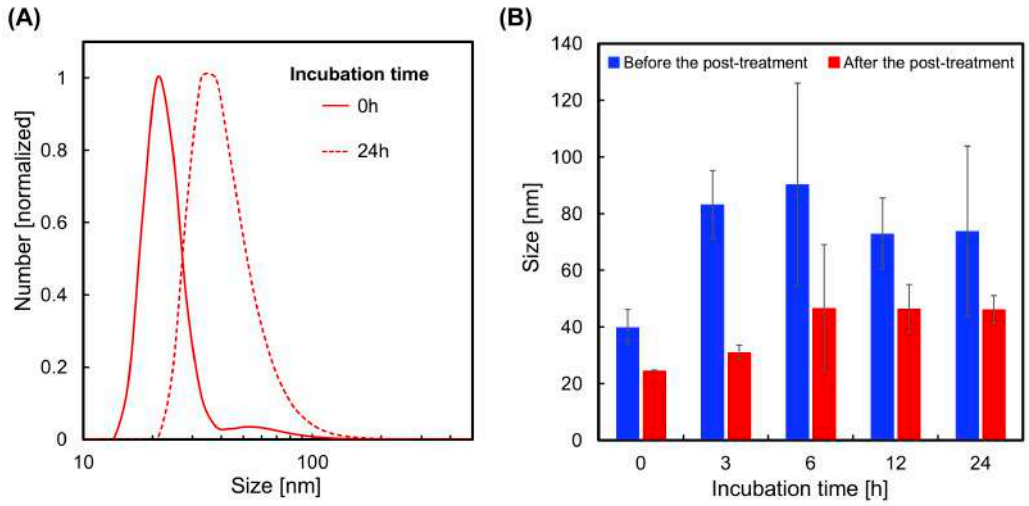

Figure 4.7 (A) Number-weighted size distributions of the POPC LNPs. (B) LNP average sizes before and after the post-treatment. POPC LNP suspensions containing 25% v/v ethanol were incubated at 4 °C for up to 24 h. After the incubation, the suspensions were diluted using the simple baffle device at a total flow rate of 500 μL/min and an FRR of 24 (red). The sizes of LNPs suspended in 25% v/v ethanol were corrected with the appropriate refraction index.

From the viewpoint of thermodynamics, the high concentration of ethanol within the LNP suspension leads to an unstable lipid membrane and enhances the fusion of the LNPs [22, 31]. Many research groups have reported that the LNP size was controlled by the flow conditions at the first dilution: total flow rate and FRR [16-19, 32, 33]. Rapid ethanol dilution using microfluidic devices allows the formation of small-sized LNPs;

on the other hand, slow ethanol dilution at low flow produces large-sized LNPs. Conversely, the findings clearly indicated that the LNP size was not only determined in the first ethanol dilution but also was tunable in the post-treatment.

The difference in size for the microfluidic post-treated LNPs possibly resulted from the shearing force flow-through in the simple baffle device. Therefore, I evaluated the effect of the shearing force on the LNP size. I prepared the LNP suspension with 13.4 mM POPC/ethanol solution and saline by using the simple baffle device at the total flow rate of 50 μL/min and the FRR of 3. The prepared suspension of POPC LNPs (25%v/v remaining ethanol) was introduced into this baffle device at the flow rate of 500 μL/min without additional ethanol dilution. As shown in Figure 4.8, 25% v/v ethanol remaining POPC LNP suspensions (A) and the dialyzed (B) did not show any size-shift after passing through the simple baffle device at the flow rate of 500 μL/min.

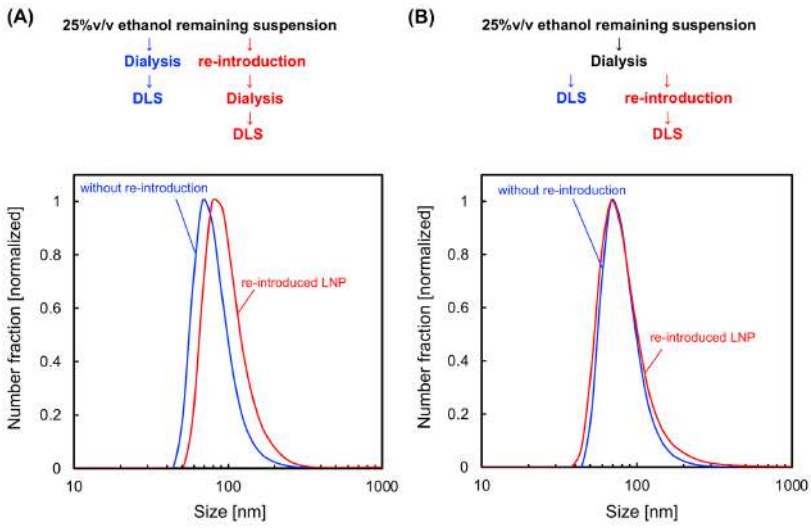

Figure 4.8 LNP size distributions. (A) The collected LNP suspension with 25% v/v remaining ethanol was dialyzed after the preparation (blue) or re-introduced into the simple baffle device (red). (B) The dialyzed LNP suspension was introduced again into the simple baffle device.

These results suggested the shearing force in this baffle device was not a major factor in the LNP size-shift for the microfluidic post-treatment. I also measured the size distributions of the LNPs with the NTA to determine more specific size distributions (Figure 4.9). As a result, small-sized LNPs formed in the LNP suspension containing 25% v/v ethanol before the post-treatment.

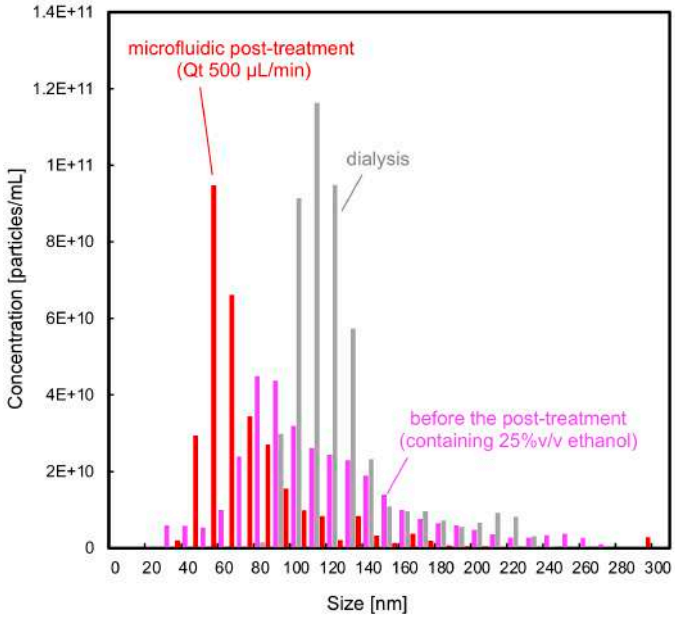

Figure 4.9 The size distributions of the POPC LNPs measured with the NTA (NanoSight NS300; Quantum Design, Tokyo, Japan). LNPs were prepared by introducing 13.4 mM POPC/ethanol solution and saline into the simple baffle device at the total flow rate of 50 µL/min and the FRR of 3. The collected LNP suspension containing 25%v/v ethanol (magenta) was post-treated by the microfluidic method (red) or the dialysis method (grey).

The hypothesis of the effects of the post-treatment on the final product of LNPs is shown in Figure 4.10. The small-sized LNPs form in the first dilution step.

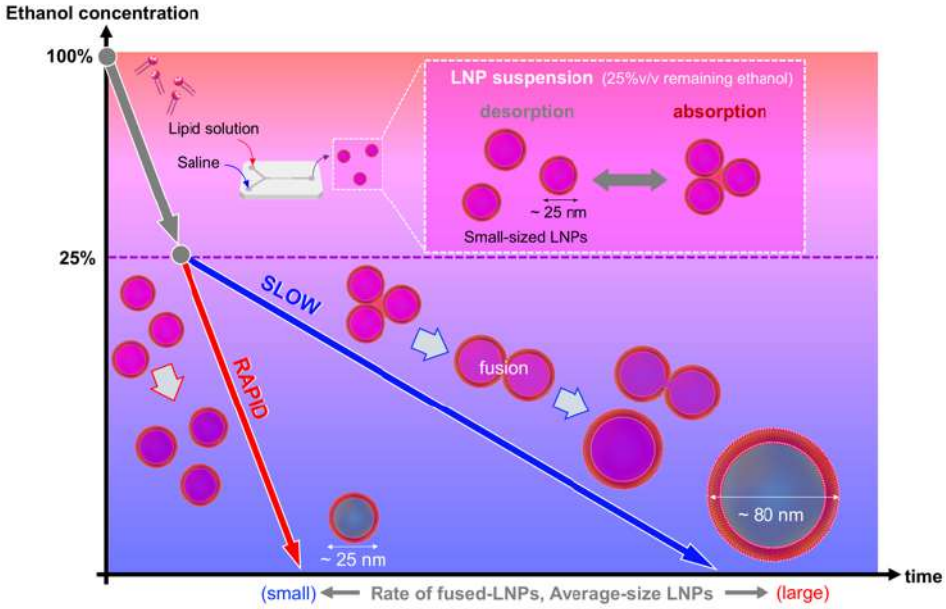

Figure 4.10 Schematic models of the effect of the post-treatment process on the final product of LNPs.

For the size measurement before the post-treatment, the LNPs interacting with each other were observed by both DLS, NTA, and TEM analysis. According to the literature, ethanol induced the fusion of LNPs composed of phosphatidylethanolamines (PEs) [25]. The energy barrier of phosphatidylcholine (PC)-based LNPs used in the present study for membrane fusion is higher than that of the PE-composed LNPs due to the size of the hydrophilic head group. From a thermodynamic viewpoint, the frequency of membrane–membrane attachment and the fusion by the LNP–LNP absorption cause the high concentration of ethanol during long-time incubation.

In the case of the on-device post-treatment, the concentration of ethanol in the LNP suspension immediately decreases to 1% v/v within milliseconds by the microfluidic dilution. The inside and outside of the LNPs are in equilibrium. Therefore, low-polarity small molecules like ethanol are transported passing thought the lipid bilayer based on Fick's law of diffusion. On the other hand, in the case of the conventional post-treatment method, ethanol molecules in a dialysis membrane are diffused to the outer solution (saline). Then, the concentration of ethanol in the LNP suspension decreases depending on the dialysis time. After decreasing the ethanol concentration in the LNP suspension, ethanol molecules are transported from the inner to outer of LNPs by Fick's law of diffusion.

A part of the diffused ethanol is replaced by water on the LNP surface and the bound ethanol at the lipid head group could induce the interdigital structure of the lipid membrane [28]. The formation of the interdigital structure is a trigger for membrane fusion because it has a larger surface area of hydrophobic groups compared with the typical lipid bilayer structure. I prepared POPC/cholesterol (50:50 mol %) LNPs and evaluated the effect of the on-device post-treatment on the final product size of LNPs to examine the hypothesis. Cholesterol plays two roles in this lipid system: increase the particle size and suppress the formation of the interdigital structure [28, 34].

Figure 4.11 shows the comparison of the LNP sizes between the POPC LNPs and POPC/cholesterol (50:50 mol %).

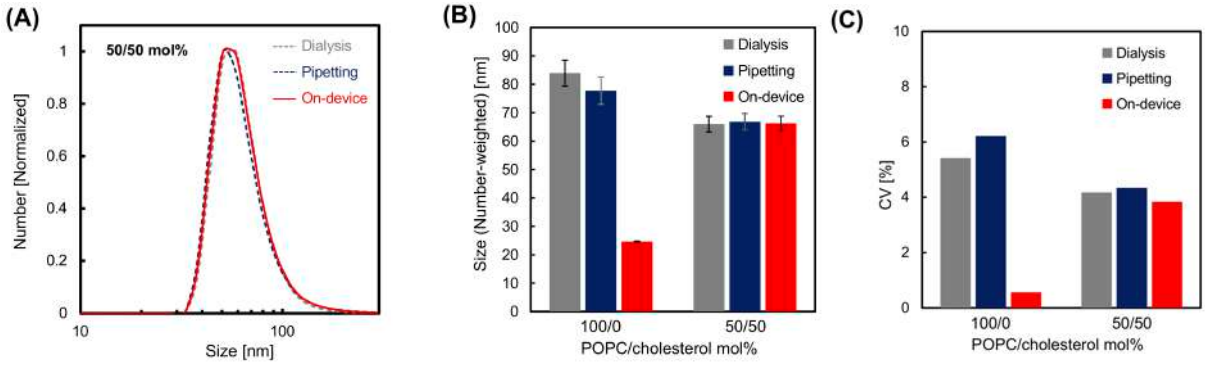

Figure 4.11 (A) Number-weighted size distributions of POPC/cholesterol LNPs prepared by three post-treatment methods. (B) Number-weighted average size and (C) CV values of the POPC/cholesterol LNPs treated by the conventional methods (gray and dark blue) and the on-device post-treatment (red). In the case of the on-device post-treatment, the total flow rate was 500 μL/min.

The sizes and CV values of POPC/cholesterol LNPs were almost the same, regardless of the post-treatment methods. In the case of the on-device post-treatment, I confirmed the increase of the POPC/cholesterol LNP size from 25 to 65 nm. In contrast, the LNP sizes prepared by the conventional methods decreased compared with the POPC LNP sizes. These results support the hypothesis regarding the formation of the interdigital structure and membrane fusion. Based on these results and the hypothesis, I consider that the conventional post-treatment method might induce the fusion of small-sized LNPs.

On the other hand, in the microfluidic post-treatment, ethanol molecules present outside the LNPs are rapidly diluted and the ethanol concentration in the LNP suspension decreases to 1% within milliseconds. For this reason, the formation of the interdigital structure and the fusion of LNPs are prevented by rapid dilution. Therefore, the post-treatment dilution rate affects the final product size of the LNPs and that is why I saw different average sizes ranging from 25 to 80 nm. Consequently, I confirmed rapid ethanol dilution by the microfluidic post-treatment was one significant process, just as it was for the LNP synthesis process.

4.3.2 Design of the Integrated Baffle Device for Mass Production of LNPs

Mass production performance of the size-controlled LNPs in a short time is important for the quality control of practical applications, and it is considered as a major challenge for realizing the microfluidic-based LNP preparation method. Increasing the initial lipid concentration in the lipid/ethanol solution is one of the simple approaches for overcoming this limitation. However, the initial lipid concentration affects the LNP size controllability and the homogeneity. The high concentration of lipid solution led to increasing LNP size with a wide size distribution because the produced LNPs were easily aggregated or fused [35]. Therefore, I developed a continuous LNP production system based on the simple baffle device. The LNP production system integrated the LNP production and post-treatment regions by putting baffle structures in tandem (Figure 4.2). In detail, the LNP production system consisted of the first dilution region for LNP production and the second dilution region for the post-treatment. I prepared 67.0 mM POPC solution, which had five times higher concentration than the standard condition, for the proof-of-concept experiment. In the first dilution region, LNPs formed at a total flow rate of 100 μL/min and an FRR of 3. Under these conditions, 60 nm sized LNPs were formed using the integrated baffle device and 13.4 mM POPC/ethanol solution. The number-weighted average sizes of the LNPs prepared using the integrated device, the pipetting method, and the dialysis method were 60, 75, and 80 nm, respectively (Figure 4.12). The integrated baffle device produced the smallest LNPs among the three and enabled the production of precisely controlled 60 nm sized LNPs in a short time (28 ms) with good reproducibility. In addition, the size distribution of the LNPs produced by the integrated baffle device showed more precise size controllability than the that of the LNPs produced with the single baffle device followed by microfluidic post-treatment (Figure 4.13).

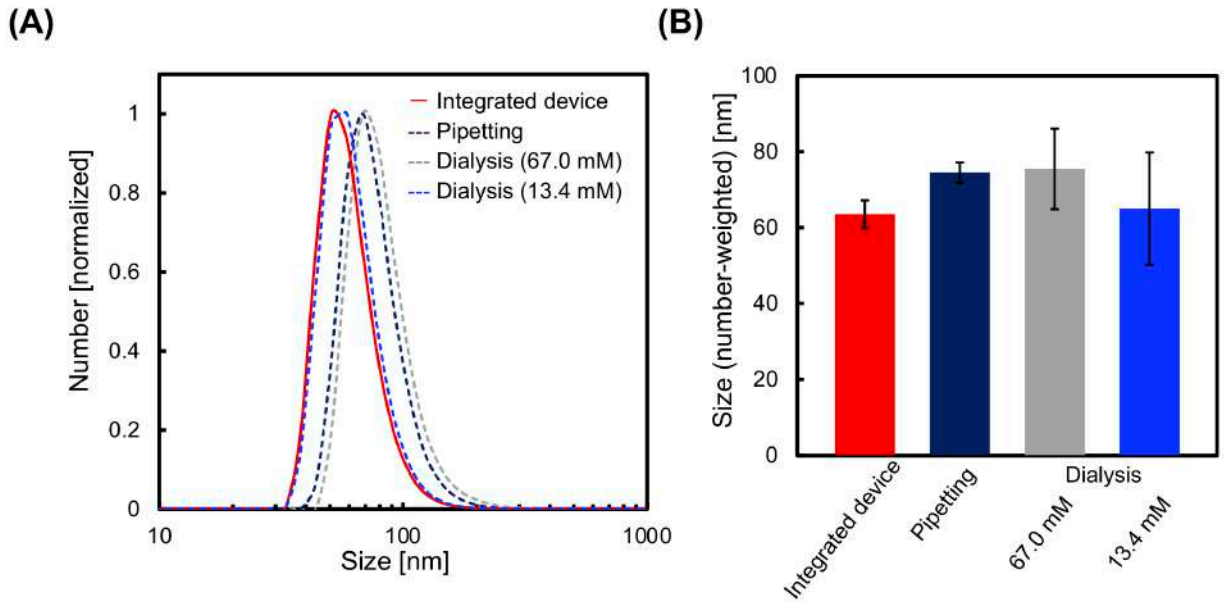

Figure 4.12 (A) Number-weighted size distributions and (B) number-weighted average sizes of the LNPs produced by the conventional methods and the integrated baffle device.

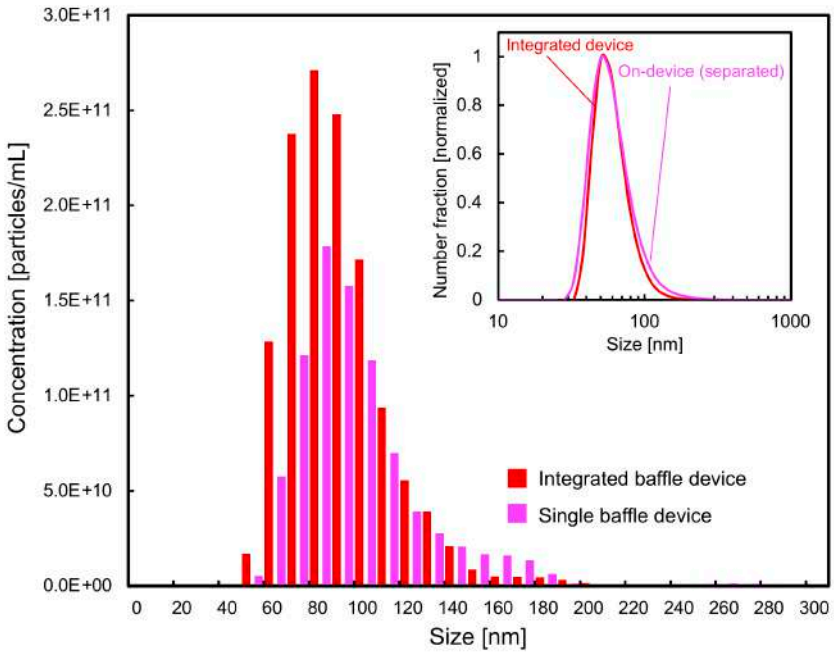

Figure 4.13 The size distributions of the POPC LNPs prepared under the high lipid concentration condition. The LNP sizes were measured with the NTA and using DLS (number-weighted, inset). I prepared 67 mM POPC/ethanol solution and saline. These solutions were injected into the integrated baffle device for the mass production (red). To confirm the features of the integrated baffle device, the LNP suspension collected from the baffle device was re-introduced and post-treated using the same baffle device at the total flow rate of 500 μL/min (magenta).

I confirmed that this integrated baffle device was useful for the mass production of precisely size-controlled LNPs. For the additional post-treatment process, namely, the concentration of the LNP suspension, the integrated baffle device can be connected with the commercially available tangential flow system without any complicated equipment. The continuous size-controlled LNP mass production system including formation of LNPs, dilution of remaining ethanol, and concentration is expected to be applicable to the production of LNPs for DDS nanomedicines, cosmetics, and functional foods.

4.3.3 Application to Production of siRNA-Loaded LNPs

I demonstrated the applicability of the microfluidic post-treatment method for the siRNA-encapsulated LNP production. I used the pH-sensitive cationic LNP system, YSK05 system [9], for the siRNA-loaded LNP production and investigated the effects of the microfluidic second dilution on the LNP size, siRNA encapsulation efficiency, and target gene knockdown activity using an in vivo experiment. As previously reported, the YSK-based LNPs need stepwise dialysis: the acidic condition (pH 4.0-6.0) near its p*Ka* is followed by the physiological condition of pH 7.4 [7]. The prepared siRNA-loaded LNP suspension underwent a second dilution using the MES buffer solution (Figure 4.14 (A)). Figure 4.14 (B) shows the CV values of the number-weighted size of the siRNA-loaded LNPs produced by the different post-treatment methods. The number-weighted average size of the LNPs was 35 nm, regardless of the post-treatment methods. In contrast to the POPC LNP production, the single-step ethanol dilution from 25 to 1% by the pipetting and on-device methods did not show any effective improvement in the size controllability (Figure 4.14 (B)).

From these results, I assumed that controlling the ratio of the charged and noncharged cationic YSK at the LNP surface was also important just as the rapid ethanol removal was important for the LNP size control [36, 37]. Therefore, I demonstrated a stepwise post-treatment to achieve rapid ethanol dilution with a moderate change in the pH. As shown in Figure 4.14 (B)-b, the LNP stepwise post-treatment using the simple baffle device showed the smallest CV value. I confirmed the siRNA encapsulation efficiencies were higher than 90%,

regardless of the post-treatment processes (Figure 4.14 (C)). In addition, these siRNA-loaded LNPs showed good stability on size and siRNA encapsulation efficiency at least for a week (Figure 4.15).

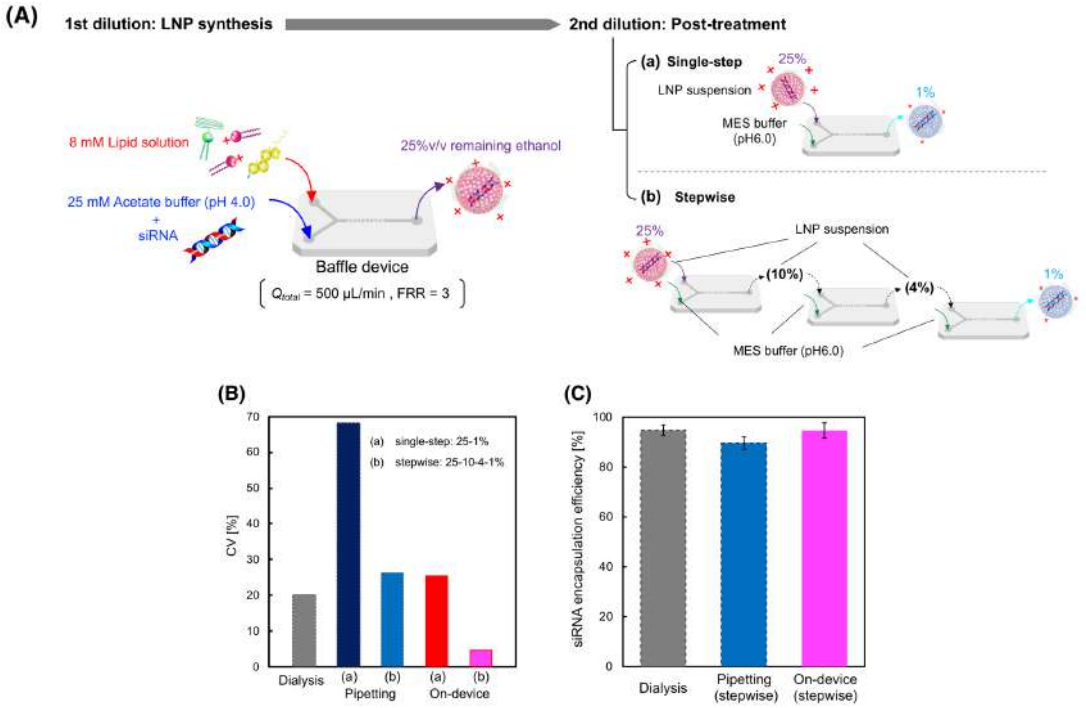

Figure 4.14 (A) Schematic of the production of siRNA-loaded LNPs. At the second ethanol dilution step, single-step dilution (a) and the stepwise dilution (b) were demonstrated. The dilution buffer solution was 20 mM MES buffer solution (pH 6.0). The flow rate of the dilution step was 500 µL/min. (B) Coefficient variation (CV) values of the siRNA-loaded LNPs prepared by different post-treatment methods. (C) siRNA encapsulation efficiencies of the LNPs prepared by the conventional and the on-device post-treatment methods.

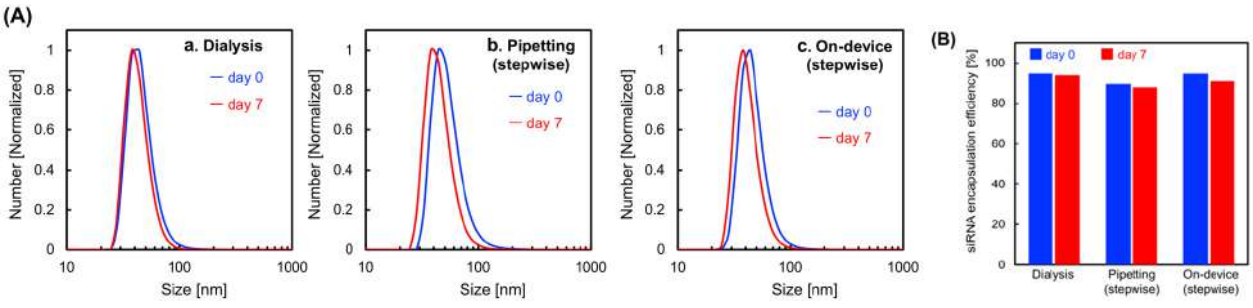

Figure 4.15 (A) Number-weighted size distributions of the siRNA-loaded LNPs treated by the conventional and the on-device post-treatment methods. For the pipetting and on-device post-treatment method, I employed the stepwise dilution. These distributions were normalized by the respective maximum intensity value. (B) siRNA encapsulation efficiency of the prepared LNPs by the different post-treatment methods.

Based on the microfluidic stepwise post-treatment, I designed an integrated baffle device for this LNP system (Figure 4.16 (A)). The integrated baffle device was composed of two PDMS layers (Figure 4.16 (B)). The siRNA-loaded LNPs were synthesized at layer 1 and introduced into layer 2 with 25% v/v ethanol. The siRNA/LNP suspension was step-wisely diluted from 25 to 1% by 20 mM MES buffer, and the siRNA/LNP suspension was collected at the outlet to be dialyzed against PBS. The integrated device produced the 33 nm sized siRNA-loaded LNPs, and the encapsulation efficiency was higher than 90%.

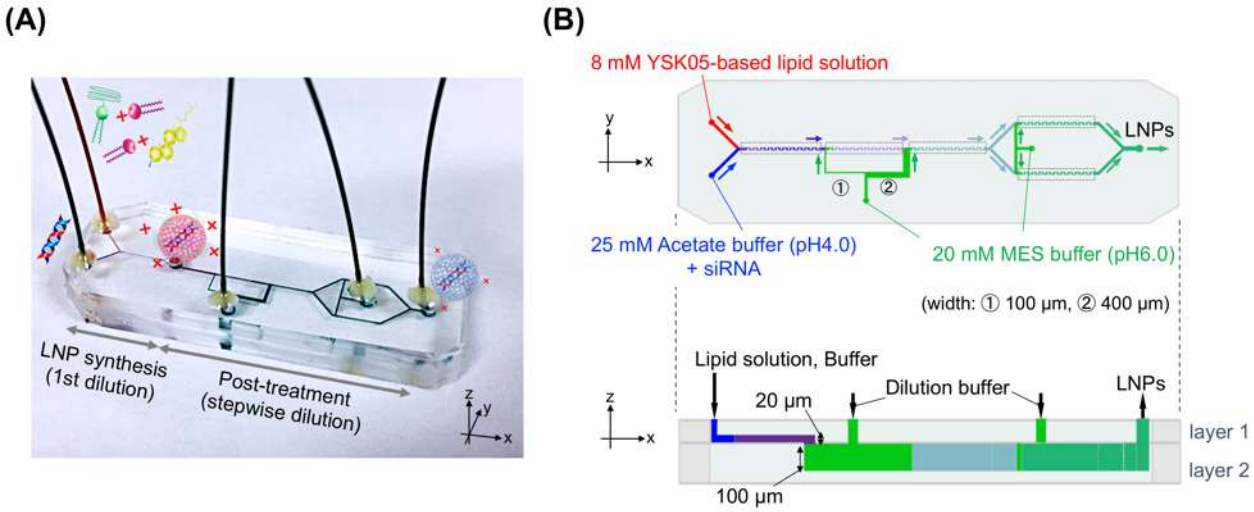

Figure 4.16 (A) Photograph of the integrated baffle device for production of siRNA-loaded LNPs. The device was composed of two PDMS layers for the LNP production and the post-treatment regions. (B) Top and side view illustrations of the integrated baffle device. The prepared lipid-containing ethanol solution and 25 mM acetate buffer solution containing 70 μg/mL siFVII (pH 4.0) were injected into the device at a total flow rate of 100 μL/min and an FRR of 3. After producing the siRNA-loaded LNPs, the LNPs were stepwise diluted with 20 mM MES buffer solution (pH 6.0) and introduced into the device at flow rates of 1000 and 1400 μL/min for the dilution buffer at the left inlet and right inlet, respectively.

Then, I carried out the in vivo experiment to evaluate the gene silencing activity of siRNA-loaded LNPs prepared by the microfluidic stepwise post-treatment method. The siFVII specifically knocks down the plasma coagulation factor VII (FVII). I confirmed that the delivered siRNAs at mice liver tissues effectively knocked down more than 80% of FVII gene activity and the LNPs were specifically delivered to the extravascular region with low accumulation around the blood vessels (Figure 4.17).

I also examined the effect of the post-treatment methods on the siRNA release. siRNA-loaded YSK-05 LNPs were prepared by the conventional dialysis and the stepwise on-device post-treatment. The LNPs were prepared in the same manner as the main text (Preparation of siRNA encapsulated LNPs) except for the lipid composition (YSK05/ cholesterol/DMG-PEG2K: 50/50/1 mol%). Figure 4.18 shows number-weighted average sizes, siRNA-encapsulation efficiency and FVII activity of the siRNA-loaded LNPs treated by the conventional and the on-device post-treatment. The LNP size and siRNA encapsulation efficiency were almost the same values for the conventional dialysis method and the on-device post-treatment method. I confirmed higher gene silencing activity than 90% by both the conventional and the new post-treatment. This result indicates the post-treatment method does not affect the drug release.

These results indicated that the microfluidic stepwise post-treatment method had no significant influence on siRNA delivery efficiency. Therefore, this microfluidic post-treatment system enables realization of fast and simple preparation processes for LNP-based nanomedicines.

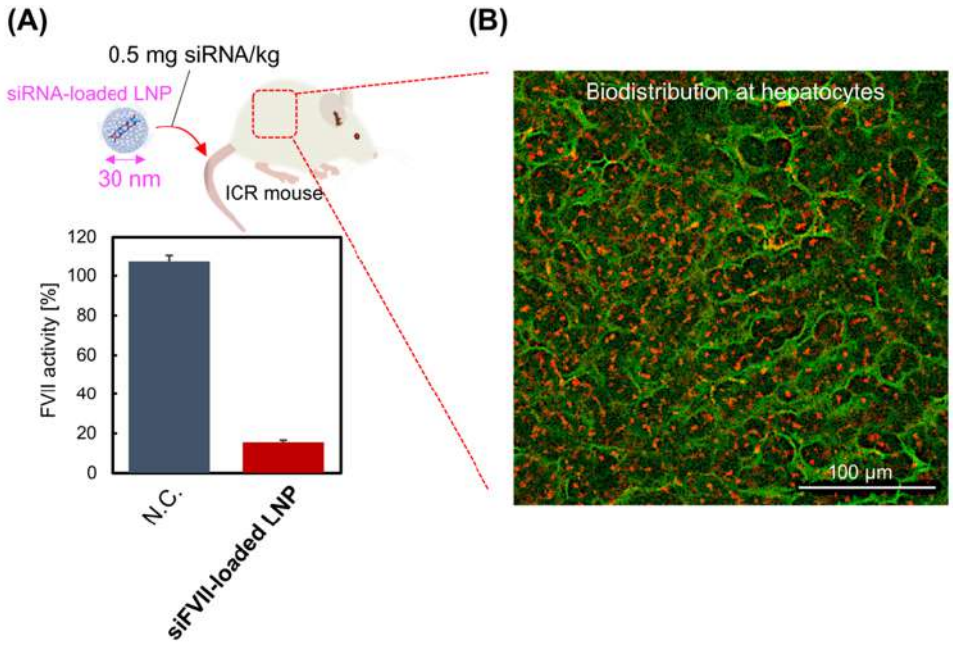

Figure4.17 Results of the in vivo experiment using the siRNA-loaded LNPs prepared by the stepwise on-device ethanol dilution method. (A) FVII knockdown activity of the 30 nm sized siFVII-loaded LNPs. The LNPs were intravenously administered to ICR mice at a dose of 0.5 mg siFVII/kg. The reproducibility experiments were carried out at least three times. (B) Confocal microscopic image of the mice hepatocytes. siRNA-loaded LNPs and blood vessels were visualized as red and green, respectively.

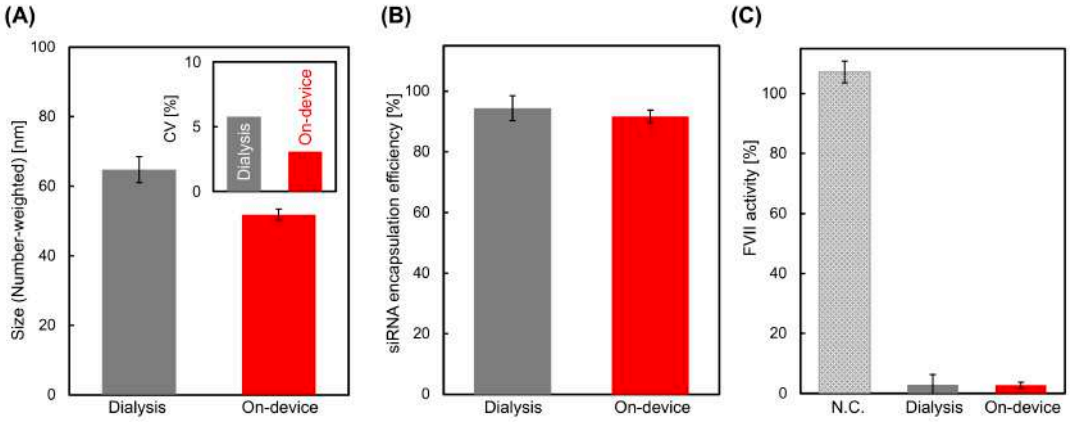

Figure 4.18 (A) average sizes, (B) the siRNA encapsulation efficiencies and (C) FVII activity of the siRNA-loaded YSK-05 LNPs post-treated by the conventional dialysis (gray) and the on-device stepwise dilution (red). The LNPs were intravenously administered to ICR mice at the dose of 0.5 mg siFVII/kg. (C) Used with permission from the American Chemical Society. (Reference: Kimura, N.; Maeki, M.; Sato, Y.; Note, Y.; Ishida, A.; Tani, H.; Harashima, H.; Tokeshi, M. *ACS Omega*, **3**, 5044-5051 (2018))

4.4 Conclusion

I investigated the effect of post-treatment on the final product size of LNPs in detail and found that the LNP size was tunable not only in the LNP synthesis step but also in the post-treatment. The new findings regarding the kinetics at the post-treatment will be useful for the design of a microfluidic system for practical use in microfluidic-based LNP production. Under the high flow rate condition, the baffle structures rapidly diluted the remaining ethanol in the LNP suspension and provided a more precise size control of LNPs. Based on the present study, I designed an integrated baffle device for scaled-up production of LNPs and siRNA-loaded LNPs. The microfluidic stepwise post-treatment system enabled to realize a seamless and simple production line. Finally, I evaluated the delivery efficiency of the siRNA-loaded LNPs prepared by the stepwise post-treatment. The LNPs effectively delivered siRNAs to mice hepatocytes with low accumulation and showed great knockdown activity. I confirmed that the microfluidic post-treatment method had no significant effect on siRNA delivery and LNP activity. Consequently, I demonstrated that the rapid ethanol dilution after the LNP

synthesis allowed more precise size controllability of LNPs compared with the conventional post-treatment methods. I expect that more precise size-controlled LNP-based nanomedicines can be produced by the integrated baffle devices to improve the efficacy of present nanomedicines and to enable high-throughput production under strict hygiene-controlled conditions.

References

[1] T. Sun, Y. S. Zhang, B. Pang, D. C. Hyun, M. Yang and Y. Xia, *Angew. Chem. Int. Ed. Engl.*, **53**, 12320-12364 (2014)

[2] P. Yingchoncharoen, D. S. Kalinowski and D. R. Richardson, *Pharmacol. Rev.*, **68**, 701-787 (2016)

[3] S. T. Sanjay, W. Zhou, M. Dou, H. Tavakoli, L. Ma, F. Xu and X. Li, *Adv Drug Deliv Rev*, **128**, 3-28 (2018)

[4] B. Garcia-Pinel, C. Porras-Alcala, A. Ortega-Rodriguez, F. Sarabia, J. Prados, C. Melguizo and J. M. Lopez-Romero, *Nanomaterials (Basel)*, **9** (2019)

[5] T. Nakamura, M. Kawai, Y. Sato, M. Maeki, M. Tokeshi and H. Harashima, *Mol. Pharm.*, **17**, 944-953 (2020)

[6] H. Cabral, Y. Matsumoto, K. Mizuno, Q. Chen, M. Murakami, M. Kimura, Y. Terada, M. R. Kano, K. Miyazono, M. Uesaka, N. Nishiyama and K. Kataoka, *Nat Nanotechnol*, **6**, 815-823 (2011)

[7] Y. Sato, Y. Note, M. Maeki, N. Kaji, Y. Baba, M. Tokeshi and H. Harashima, *J. Control. Release*, **229**, 48-57 (2016)

[8] A. Puri, K. Loomis, B. Smith, J. H. Lee, A. Yavlovich, E. Heldman and R. Blumenthal, *Crit. Rev. Ther. Drug Carrier Syst.*, **26**, 523-580 (2009)

[9] H. Matsui, Y. Sato, H. Hatakeyama, H. Akita and H. Harashima, *Int. J. Pharm.*, **495**, 171-178 (2015)

[10] D. Liu, A. Mori and L. Huang, *Biochim. Biophys. Acta*, **1104**, 95-101 (1992)

[11] A. Jahn, S. M. Stavis, J. S. Hong, W. N. Vreeland, D. L. DeVoe and M. Gaitan, *ACS Nano*, **4**, 2077-2087 (2010)

[12] D. Liu, H. Zhang, F. Fontana, J. T. Hirvonen and H. A. Santos, *Lab Chip*, **17**, 1856-1883 (2017)

[13] M. Maeki, N. Kimura, Y. Sato, H. Harashima and M. Tokeshi, *Adv Drug Deliv Rev*, **128**, 84-100 (2018)

[14] International Conference Harmonisation of Technical Requirements for registration of Pharmaceuticals for Human Use (ICH) guideline Q3C (R6) on impurities: guideline for residual solvents-step 5, ICH, (2019)

[15] N. Kimura, M. Maeki and M. Tokeshi, Microfabrication and microfluidic devices for drug delivery, *Microfluidics for Pharmaceutical Applications: From Nano/Micro Systems Fabrication to Controlled Drug Delivery,* H. A. Santos, D. Liu and H. Zhang, eds., Elsevier, 123-136, (2019)

[16] I. V. Zhigaltsev, N. Belliveau, I. Hafez, A. K. K. Leung, J. Huft, C. Hansen and P. R. Cullis, *Langmuir*, **28**, 3633-3640 (2012)

[17] D. Chen, K. T. Love, Y. Chen, A. A. Eltoukhy, C. Kastrup, G. Sahay, A. Jeon, Y. Dong, K. A. Whitehead and D. G. Anderson, *J. Am. Chem. Soc.*, **134**, 6948-6951 (2012)

[18] M. Maeki, T. Saito, Y. Sato, T. Yasui, N. Kaji, A. Ishida, H. Tani, Y. Baba, H. Harashima and M. Tokeshi, *RSC Advances*, **5**, 46181-46185 (2015)

[19] N. Kimura, M. Maeki, Y. Sato, Y. Note, A. Ishida, H. Tani, H. Harashima and M. Tokeshi, *ACS Omega*, **3**, 5044-5051 (2018)

[20] A. Laouini, C. Jaafar-Maalej, I. Limayem-Blouza, S. Sfar, C. Charcosset and H. Fessi, *Journal of Colloid Science and Biotechnology*, **1**, 147-168 (2012)

[21] A. A. Gurtovenko and J. Anwar, *J. Phys. Chem. B*, **113**, 1983-1992 (2009)

[22] H. I. Ingolfsson and O. S. Andersen, *Biophys. J.*, **101**, 847-855 (2011)

[23] P. Sakdiset, Y. Kitao, H. Todo and K. Sugibayashi, *J Pharm (Cairo)*, **2017**, 7409420 (2017)

[24] R. Nallamothu, G. C. Wood, C. B. Pattillo, R. C. Scott, M. F. Kiani, B. M. Moore and L. A. Thoma, *AAPS PharmSciTech*, **7**, E32 (2006)

[25] J. Paxman, B. Hunt, D. Hallan, S. R. Zarbock and D. J. Woodbury, *Biophys. J.*, **112**, 121-132 (2017)

[26] B. Angelov, A. Angelova, S. K. Filippov, M. Drechsler, P. Stepanek and S. Lesieur, *ACS Nano*, **8**, 5216-5226 (2014)

[27] B. Angelov, A. Angelova, S. K. Filippov, T. Narayanan, M. Drechsler, P. Stepanek, P. Couvreur and S. Lesieur, *J. Phys. Chem. Lett.*, **4**, 1959-1964 (2013)

[28] H. Komatsu and S. Okada, *Biochimica Et Biophysica Acta-Biomembranes*, **1235**, 270-280 (1995)

[29] Y. Sato, H. Hatakeyama, Y. Sakurai, M. Hyodo, H. Akita and H. Harashima, *J. Control. Release*, **163**, 267-276 (2012)

[30] J. C. McDonald and G. M. Whitesides, *Acc. Chem. Res.*, **35**, 491-499 (2002)

[31] L. Toppozini, C. L. Armstrong, M. A. Barrett, S. Zheng, L. Luo, H. Nanda, V. G. Sakai and M. C. Rheinstädter, *Soft Matter*, **8** (2012)

[32] S. Amrani and M. Tabrizian, *ACS Biomaterials Science & Engineering*, **4**, 502-513 (2018)

[33] Y. Li, R. J. Lee, X. Huang, Y. Li, B. Lv, T. Wang, Y. Qi, F. Hao, J. Lu, Q. Meng, L. Teng, Y. Zhou, J. Xie and L. Teng, *Nanomed. Nanotechnol. Biol. Med.*, **13**, 371-381 (2017)

[34] B. De Kruijff, P. R. Cullis and G. K. Radda, *Biochim. Biophys. Acta*, **436**, 729-740 (1976)

[35] M. Maeki, Y. Fujishima, Y. Sato, T. Yasui, N. Kaji, A. Ishida, H. Tani, Y. Baba, H. Harashima and M. Tokeshi, *PLoS One*, **12**, e0187962 (2017)

[36] J. A. Kulkarni, M. M. Darjuan, J. E. Mercer, S. Chen, R. van der Meel, J. L. Thewalt, Y. Y. C. Tam and P. R. Cullis, *ACS Nano*, **12**, 4787-4795 (2018)

[37] J. A. Kulkarni, D. Witzigmann, J. Leung, R. van der Meel, J. Zaifman, M. M. Darjuan, H. M. Grisch-Chan, B. Thöny, Y. Y. C. Tam and P. R. Cullis, *Nanoscale*, **11**, 9023-9031 (2019)

CHAPTER 5 One-Step iLiNP-Based Production of Size-Controlled Exosome-Like Nanoparticles

5.1 Introduction

Nucleic acid delivery systems using lipid nanoparticles (LNPs) are an ideal nonviral and noninvasive technique for gene therapies [1-3]. Cationic lipids have been widely used for the production of DNA/RNA-loaded LNPs because of the strong electrostatic interactions with the negatively charged nucleic acids [4, 5]. Cationic-lipid-based NPs enable the effective encapsulation of DNA/RNA and its delivery to target tissues [6]. However, the nonspecific adsorption of cationic-LNPs induces cytotoxicity and reduces gene delivery efficiency [7, 8]. In contrast, noncationic NPs allow selective drug delivery by preventing the nonspecific adsorption of proteins [9-11]. Natural-lipid-based NPs, such as exosome-like NPs, show no cell cytotoxicity and enable effective siRNA delivery [12-14]. Exosomes have drawn attention in the life sciences and have played an important role in miRNA delivery to target tissues. Therefore, exosomes are a natural nanocarrier for RNA delivery, and artificial exosomes are expected to have high biocompatibility. However, the encapsulation of RNA into noncationic (neutral or anionic) lipid systems is difficult because of the lack of a driving force, such as electrostatic interactions, for the interaction between cationic lipids and RNA. In particular, electrostatic repulsion is unavoidable in anionic lipid systems, such as those containing phosphatidylserine (PS).

Several groups have reported methods for the production for RNA-loaded noncationic NPs, as well as evaluated the physical properties and cytotoxicities of these NPs [12-14]. Conventionally, RNA-loaded noncationic NPs are produced by the hydration method, which is a conventional liposome preparation method. The NPs are then passed through a polycarbonate filter having 100-nm pores to adjust the NP size. However, this process requires multiple steps to produce the RNA-loaded and size-controlled NPs, including the formation of a lipid film by evaporation, hydration of the lipid film with RNA/buffer solution, and filtration of the NP suspension for size control. Furthermore, although the NP suspension is filtered for size control, the NPs have a broad size distribution because of their flexibility. The size of the LNPs, as well as the lipid components, is a crucial factor for target-selective delivery [15-18]. For these reasons, the development of a simple one-step production method for RNA-loaded noncationic NPs is urgently required.

Microfluidic devices promise the precise size control of LNPs, as well as simple operation [19-24]. In fact, Onpattro®, the first FDA-approved siRNA-loaded LNP-based nanomedicine (containing an ionizable lipid named D-Lin-MC3-DMA), is produced using microfluidic technology [25-27]. However, the production of size-controlled noncationic NPs with high RNA encapsulation efficiency is still challenging.

In this chapter, I report a one-step method using a microfluidic device for the production of size-controlled siRNA-loaded noncationic NPs. I demonstrate that the microfluidic device, which I have called iLiNP™,[28] is able to encapsulate siRNA into the noncationic NPs effectively and control the NP size precisely. The iLiNP device-based method was applied to produce the exosome-like NPs, and I evaluated the physical properties, cytotoxicity, and target gene silencing activity. In addition, the effect of the exosome-like NP size on the gene silencing activity was investigated by in vitro experiments. The one-step production method for size-controlled noncationic exosome-like NPs encapsulated siRNA is expected to enable the production of artificial and functionally modified exosomes for gene and cell therapies.

5.2 Experimental

5.2.1 Materials

1,2-Distearoyl-sn-glycero-3-phosphocholine (DSPC), 1,2-dioleoyl-sn-glycero-3-phosphocholine (DOPC), 1,2-dioleoyl-sn-glycero-3-phosphoethanolamine (DOPE), 1,2-dioleoyl-sn-glycero-3-phospho-l-serine (sodium salt) (DOPS), sphingomyelin (chicken egg) (SM), 1,2-dioleoyloxy-3-trimethylammonium propane (DOTAP), and 1,2-dimyristoyl-*rac*-glycero-3-methylpolyoxyethylene glycol-2000 (DMG-PEG2K) were purchased from the NOF Corporation (Tokyo, Japan). SU-8 3050 was obtained from Nippon Kyaku Co., Ltd. (Tokyo, Japan). Cholesterol, low glucose Dulbecco's modified Eagle medium (DMEM), and paraformaldehyde were purchased from Sigma–Aldrich (St. Louis, MO, USA). Protamine sulfate from salmon, dextran sodium sulfate, sodium acetate, acetic acid, calcium chloride, tris(hydroxymethyl)aminomethane, and phosphate buffered saline (PBS) were purchased from FUJIFILM Wako Pure Chemical corporation (Osaka, JAPAN). Fetal bovine serum (FBS),

penicillin–streptomycin, trypsin (2.5%), Lipofectamine™ RNAiMAX, and Quant-iT™ RiboGreen™ RNA Reagent were obtained from Thermo Fisher Scientific (Waltham, MA, USA). Cell Counting Kit-8, 4′,6-diamidino-2-phenylindole (DAPI), Calcein AM, and ethylenediaminetetraacetic acid (EDTA) were purchased form Dojindo Laboratories (Kumamoto, Japan). G418 was obtained from Nacalai Tesque (Kyoto, Japan). Dual-Glo Luciferase Assay System was obtained from Promega (Madison, WI, USA). Polylysine-coated cover glass was purchased from Matsunami Glass Ind., Ltd. (Osaka, Japan). The siFVII and Cy5-labeled siGL4 were purchased from Hokkaido System Science Co. Ltd. (Sapporo, JAPAN). The sense and antisense strand sequences of siFVII were 5′-GGAucAucucAAGucuuAcTsT-3′ and 5′-GuAAGAcuuGAGAuGAuccTsT-3′, respectively. The sense and antisense strand sequences of (Cy5)-siGL4 were 5'-Cy5-CCGUCGUAUUCGUGAGCAATsT-3' and 5'-UUGCUCACGAAUACGACGGTsT-3', respectively.

5.2.2 Fabrication of the microfluidic devices

The iLiNP and CM devices were fabricated using standard photolithography techniques, as described in a previous paper [29]. Briefly, the master molds were made from SU-8 3050. Replicated polydimethylsiloxane (PDMS) pieces were treated by oxygen plasma and bonded with glass slides using a plasma cleaner (CUTE-1MP/R, Femto Science, Gwangju, Korea).

5.2.3 Preparation of LNPs using the microfluidic devices

LNP encapsulated siRNA was produced using two methods: (1) protamine/siRNA complexation[30] or (2) a Ca^{2+}-mediated method. For the protamine/siRNA complex method, protamine/siRNA complexes with different molar ratios were prepared before LNP production. Protamine sulfate and siRNA were separately dissolved in 25 mM acetate buffer solution at concentrations of 25 μM and 25 mM, respectively. The molar ratios of protamine/siRNA were 1/10, 1/1, 5/1, and 10/1. Then, an appropriate volume of the siRNA/acetate buffer solution was added to the protamine/acetate buffer solution, and the mixture was vortexed for 10 s. The

protamine/siRNA solution was incubated for 20 min at 25 °C. For the Ca^{2+}-mediated method, 10 mM Tris-HCl buffer solutions (pH 8.0) containing calcium chloride and siRNA were used as an aqueous phase. I prepared the siRNA/calcium chloride/Tris-HCl solution with different concentrations of Ca^{2+}: 0, 0.02, 0.2, 0.6, 1, 13, 30, and 130 mM. The concentration of siRNA was fixed at 5.3 μM.

Lipid solutions were prepared by dissolving lipid mixtures in ethanol to a final lipid concentration of 10 mM. Three-types of LNP systems were employed in this study: neutral LNPs composed of DSPC/cholesterol (50/50 mol.%), anionic LNPs composed of DSPC/DOPS/cholesterol, and exosome-like NPs composed of DOPC/SM/cholesterol/DOPE (21/17.5/30/14/17.5 mol.%) [31]. The concentration of siRNA in the buffer solutions and the final molar ratio of lipids/siRNA were fixed at 70 μg/mL and 10 mM/10 μM (1000/1), respectively.

LNPs were produced by both the iLiNP device and a batch method. In the case of the iLiNP device, the aqueous solution (the siRNA/acetate buffer solution or the siRNA/calcium chloride/Tris-HCl solution) and the lipid solution were separately introduced to produce the LNPs. In the case of the batch method, the lipid solution and the aqueous solution were vortex mixed. After the LNP production process, the LNP suspensions were dialyzed against PBS using dialysis membrane tubing (12–14 kDa MW cutoffs, Repligen Corporation (Waltham, MA) overnight to remove the remaining ethanol.

5.2.4 Characterization of siRNA-loaded LNPs

The LNP size, PDI, LNP size distribution, and ζ-potential were measured by DLS using a Zetasizer Nano ZS ZEN3600 instrument (Malvern Instruments, Worcestershire, UK). The siRNA encapsulation efficiency of the calcium chloride-supported LNPs was determined by RiboGreen assay as previously described [17]. For the protamine/siRNA complex-loaded LNPs, I used RiboGreen with dextran sodium sulfate as a detection reagent.

Exosome-like NPs were observed by TEM (JEM-1400Plus; JEOL Ltd., Tokyo, Japan) at an acceleration voltage of 100 kV. Digital images (3296 × 2472 pixels) were taken with a CCD camera (EM-14830RUBY2; JEOL).

The samples were placed on carbon-coated copper grids (400 mesh) and were stained with 2% phosphotungstic acid solution (pH 7.0) for 20 s.

5.2.5 Preparation of LNPs for in vitro assays

For the in vitro assays, I prepared three kinds of siGL4 carrier particles: Lipofectamine™ RNAiMAX, cationic LNPs composed of DOTAP/DOPE/cholesterol/DMG-PEG 2K (30/40/30/3 mol.%), and exosome-like NPs. Lipofectamine™ RNAiMAX was used according to the manufacturer's protocol. DOTAP-LNPs were prepared using 5 mM lipid/ethanol solution and 25 mM acetate buffer solution (pH 4.0) containing 15 μg/mL siGL4 using the iLiNP device at a total flow rate of 500 μL/min and an FRR of 9. Exosome-like NPs were prepared in the same manner as the Ca^{2+}-mediated method. PEGylated exosome-like NPs were also produced in the same way as the exosome-like NPs at a lipid composition of DOPC/SM/cholesterol/DOPS/DOPE/DMG-PEG2K (21/17.5/30/14/17.5/1 mol.%). The collected LNP suspensions were dialyzed against PBS overnight. After dialysis, the LNP suspensions were concentrated by Amicon Ultra filters (100K, Merck, Darmstadt, Germany).

5.2.6 Cell culture and in vitro assays

HeLa cells stably expressing Firefly and Renilla luciferase (HeLa-dluc) were cultured in 12-well cell culture dishes (Eppendorf) containing growth media at 37 °C in 5% CO_2. The growth media contained DMEM, 10% FBS, 100 U/mL penicillin, 100 μg/mL streptomycin, and 400 μg/mL G418. The HeLa-dluc cells were cultured and transfected referring to the previously reported protocols [32].

For the cell viability assay, 100 μL portions of HeLa-dluc cells suspension containing the growth medium were seeded in a 96-well clear plate (Nunc) (3×10^3 cells/well) and incubated for 24 h at 37 °C in 5% CO_2. siGL4-loaded LNPs were suspended in DMEM to achieve siRNA concentrations ranging from 50 to 500 nM, and the same volume of PBS (-) was added as a negative control. Then, the culture medium was exchanged with 100

μL of the LNP suspension and incubated for 4 h at 37 °C in 5% CO_2. After incubation, the LNP suspensions were aspirated from the culture dishes, and new growth media was added, followed by incubation for 24 h at 37 °C in 5% CO_2. Cell viability was measured by using Cell Counting Kit-8 at the wavelength of 450 nm and a microplate reader Sunrise^{TM} (TECAN, JAPAN).

For gene-silencing activity evaluation, HeLa-dluc cells (6×10^3 cells/well) were seeded in a 96-well white clear-bottom plate and incubated for 24 h at 37 °C in 5% CO_2. After incubation, the cells were transfected in the same manner as described above. The gene silencing activities were measured by using the Dual-Glo assay and a GloMax®Explorer System (Promega) according to the manufacturer's protocol.

5.2.7 Microscopic observation of cells

HeLa-dluc cells were cultured in a 12-well cell culture dish set with a poly-l-lysine-coated cover glass on the bottom of the well. After overnight incubation, the growth media was exchanged with the LNP suspension at a dose of 100 nM siGL4 followed by incubation for 1 h at 37 °C in 5% CO_2. The HeLa-dluc cells were washed with PBS at three times and stained with 5 μM Calcein AM for 15 min. After washing HeLa-dluc cells with PBS, the cells were treated with 4% paraformaldehyde solution and stained with and 1 μg/mL DAPI for 1 min. After several washes, the cells were viewed using a BZ-X810 fluorescence microscope (KEYENCE Corporation, Japan).

5.2.8 Statistical analysis

Experimental results were analyzed with Microsoft® Excel. For comparisons between the average values of two groups, I used the unpaired Student's *t*-test.

5.3 Results and Discussion

5.3.1 Protamine/siRNA complex-loaded LNPs

In the development of the process for the production of siRNA-loaded noncationic exosome-like NPs, I predicted that the cancelation of the negative charge of the siRNA would play a crucial role. The negatively-charged siRNA could induce electrostatic repulsion between siRNA strands or between siRNA and negatively-charged lipids such as PS. To cancel the negative charge of the siRNA, I used two different methods: (1) protamine/siRNA complexation and (2) a Ca^{2+}-mediated method. In addition, the effect of the flow conditions on the LNP size and siRNA encapsulation in the siRNA-loaded noncationic NPs were not well understood. As a proof of concept experiment for one-step production of the size-controlled siRNA-loaded noncationic LNPs using the iLiNP device, I used protamine/siRNA complexation to verify the significance of the negative charge cancelation and flow conditions. Protamine consists of 30 to 50 amino acids with 60% of arginine residues and one of the major polypeptides used in the DNA and RNA delivery [30]. I assumed the protamine/siRNA molar ratio of 1/1 could cancel the negative charge of siRNA. Therefore, the molar ratios of protamine/siRNA of 1/10, 1/1, 5/1, and 10/1 were studied to understand the effect of the molar ration and charge balance on the LNP size and the siRNA encapsulation efficiency. I also optimized the flow conditions to achieve both high LNP size controllability and siRNA encapsulation efficiency. Figure 5.1(A) shows the relationship between the molar ratio of the protamine/siRNA complex and the zeta potential. A protamine/siRNA molar ratio of 5/1 was sufficient to cover the siRNA with protamine and form core particles (Figure 5.2(A)). Then, I investigated the effect of the flow conditions and the protamine/siRNA molar ratio on the formation of the neutral LNP system composed of 1,2-distearoyl-sn-glycero-3-phosphocholine (DSPC)/cholesterol (50/50 mol.%). For the neutral LNP formulation, a 10 mM lipid/ethanol solution and the protamine/siRNA complexes were introduced into the iLiNP device (Figure 5.1(B)). Figures 5.1(C) and 5.1(D) shows the Z-average sizes and siRNA encapsulation efficiency of the neutral LNPs prepared at total flow rates of 100 and 500 μL/min.

The neutral LNP size obtained at a flow rate of 100 μL/min increased with increase in the protamine/siRNA molar ratio. In contrast, at a flow rate of 500 μL/min, neutral LNPs of almost 100-nm size were produced

regardless of the protamine/siRNA molar ratio. In addition to the similar LNP sizes, the molar ratios of 5/1 and 10/1 enabled the encapsulation of siRNA with high and similar efficiencies, but, as shown in Figure 5.1(D), to achieve this, the protamine/siRNA molar ratio need to be higher than 5/1 in this study. Thus, I believe that the lipids cannot coat the protamine/siRNA complexes at low molar ratios and, thus, form empty LNPs. In conclusion, I determined that a molar ratio of 5/1 and a flow rate of 500 μL/min were appropriate for achieving siRNA-loaded neutral LNPs with a narrow particle size distribution (Figure 5.2(C)). Figures 5.2(A) and 5.2(C) show the protamine/siRNA complex core particles were coated by neutral lipids, and the slight shift in the particle size distribution under the optimal conditions suggests the formation of siRNA-loaded neutral LNPs.

In the case of microfluidic-based LNP production method, the rapid ethanol dilution condition, namely, the high flow rate and the high FRR conditions are required for the size-controlled LNP production. However, the rapid ethanol dilution for the production of size-controlled LNP is not a preferable condition for the siRNA encapsulation. The rapid ethanol dilution might form empty LNPs before the siRNA encapsulation. In the case of the batch method, a large reaction space compared with the microfluidic device leads to heterogeneity of the LNP formation and siRNA encapsulation process. At the non-optimal condition, siRNAs would be encapsulated into the NPs stochastically and it shows low reproducibility.

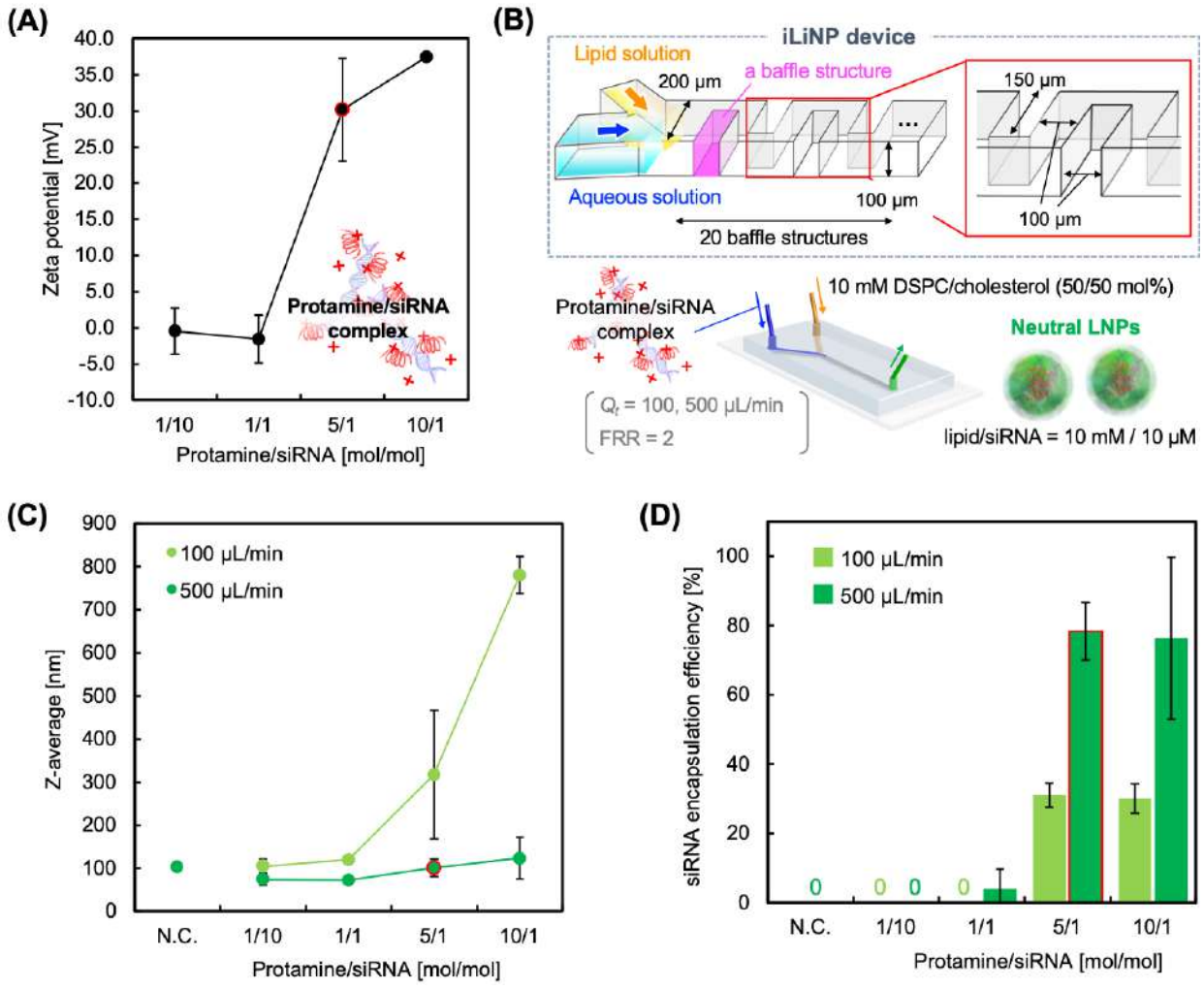

Figure 5.1 (A) Relationship between the molar ratio of protamine/siRNA complex and the zeta potential. (B) Schematic illustration of the iLiNP device and the one-step production of the protamine/siRNA-complex-loaded neutral LNPs. Ten millimolar neutral lipid/ethanol solution and acetate buffer containing protamine/siRNA complex were introduced into the iLiNP device at total flow rates of 100 or 500 μL/min and a ratio of the flow rates of the aqueous and lipid phases of 2. (C) Z-average sizes and (D) siRNA encapsulation efficiency of the neutral LNPs. DSPC: 1,2-distearoyl-sn-glycero-3-phosphocholine.

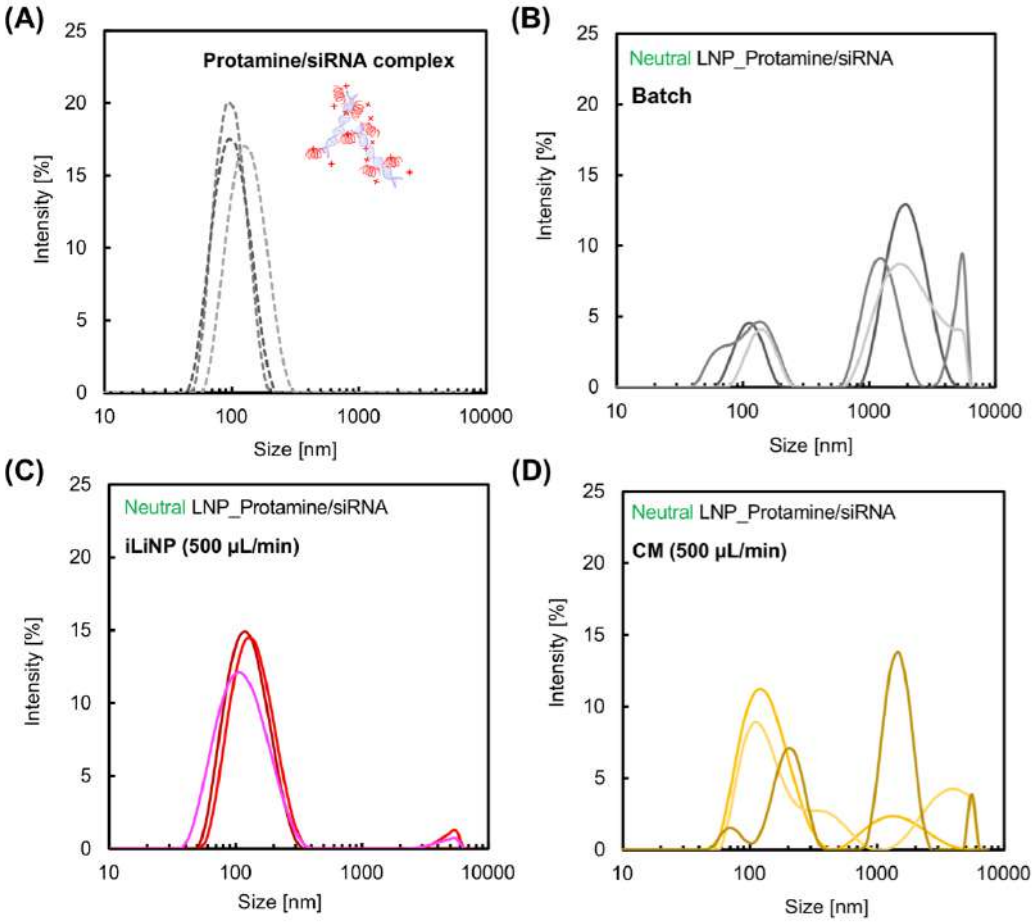

Figure 5.2 Size distributions of (A) protamine/siRNA complexes (5/1 mol/mol) and (B-D) neutral lipid nanoparticles (LNPs) prepared by the batch method and the microfluidic devices. Experiments were repeated three times. CM: chaotic mixing.

Then, I optimized the ratio of the flow rates of the aqueous and lipid phases (FRR). Figures 5.3(A) and 5.3(B) show the effects of the FRR on the LNP size and the siRNA encapsulation efficiency. Only at an FRR of 2 were I able to produce 100-nm-sized LNPs with a narrow polydispersity index (PDI) and standard deviation compared with the FRRs of 3 and 9, and the siRNA encapsulation efficiency was almost 80%. The characteristics of the siRNA-loaded neutral LNPs produced by a chaotic mixer (CM) device and the iLiNP device are summarized in Table 5.1. The CM device, which is used worldwide for LNP preparation,[29, 33, 34] did not yield 100-nm-sized LNPs with high siRNA encapsulation efficiency (Figure 5.3(C)). These results

suggest that the production of size-controlled noncationic siRNA-loaded LNPs is only possible in the iLiNP device at a high flow rate. To validate the applicability of the iLiNP-based approach for the production of exosome-like NPs, I attempted to encapsulate siRNA into anionic LNPs using the microfluidic device under the optimized conditions. In the case of the anionic LNPs, the iLiNP device produced the smallest-sized LNPs with the narrowest particle size distribution (Figures 5.3(D) and 5.3(E), Figure 5.4). The PDI value of the LNPs produced at a flow rate of 500 μL/min using the iLiNP device was below 0.1, and the encapsulation efficiency was above 70% (Figure 5.3(F)). In comparison with the neutral LNPs, the anionic LNPs showed the highest siRNA encapsulation efficiency in all preparation methods. I assume that the electrostatic interaction between the positively charged protamine/siRNA complex (5/1 mol/mol) and 1,2-dioleoyl-sn-glycero-3-phospho-l-serine (DOPS) contributed to the high encapsulation efficiency. However, the iLiNP-based approach was the only method that enabled the encapsulation of siRNA into neutral and anionic LNPs with controlled sizes. Although I used protamine as an additive to aid siRNA encapsulation into the LNPs, the iLiNP device could also be used to prepare noncationic LNPs with high siRNA loadings. Thus, the findings reveal that the iLiNP device is a suitable tool for the preparation of siRNA-loaded exosome-like NPs.

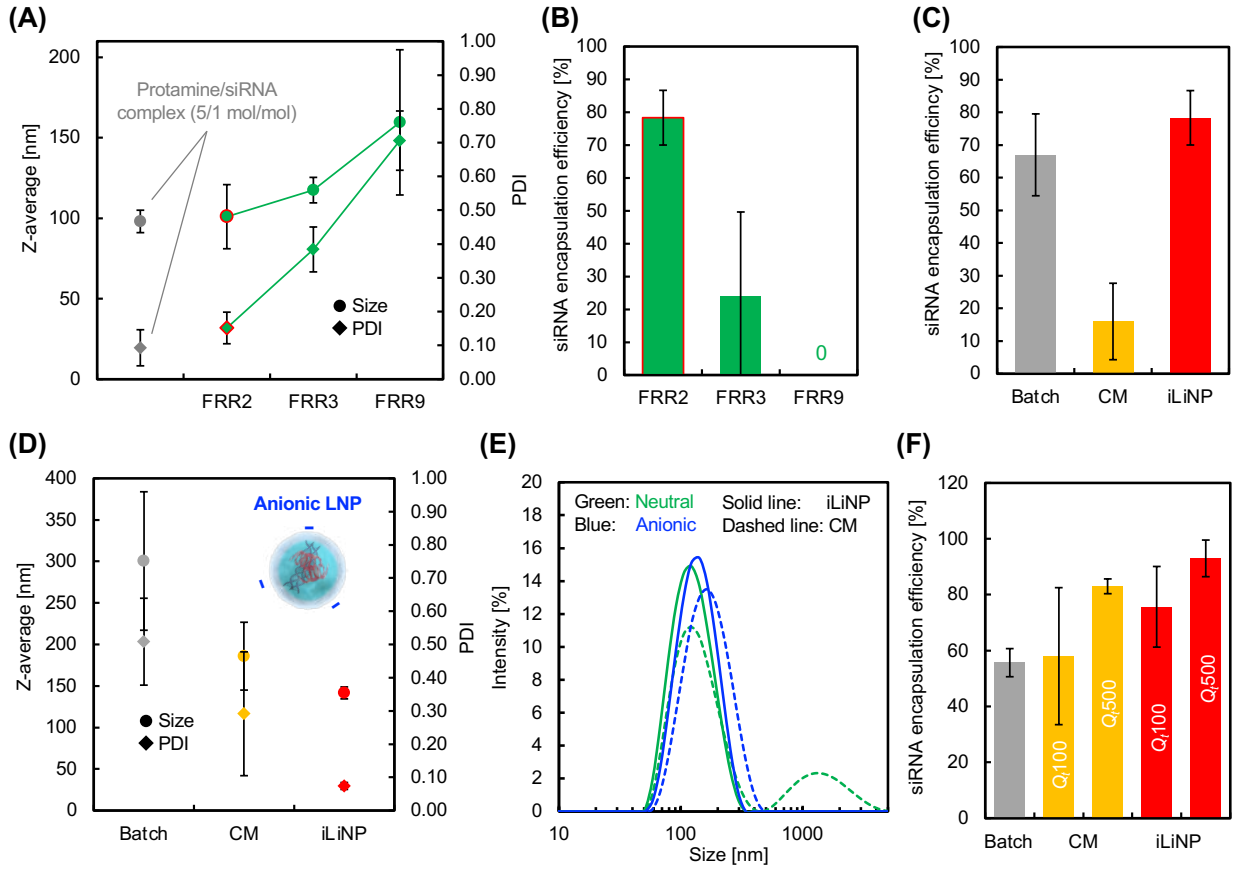

Figure 5.3 Effects of the ratio of the flow rates of the aqueous and lipid phases (FRR) on (A) the LNP size and the polydispersity index and (B) siRNA encapsulation efficiency. (C) Comparison of siRNA encapsulation efficiency of the neutral LNPs prepared by three different methods. For the chaotic mixer (CM) and iLiNP devices, the total flow rate was 500 µL/min and the FRR was 2. (D) Z-average sizes and PDI of the anionic LNPs prepared by the batch method and the microfluidic devices at 500 µL/min and an FRR of 2. (E) Size distributions of the neutral LNP (green) and the anionic LNP (blue) prepared by using the iLiNP (solid line) and the CM (dashed line) devices. (F) siRNA encapsulation efficiency of the anionic LNPs. The total flow rates were 100 and 500 µL/min, and the FRR was 2.

Table 5.1 Characteristics of siRNA-loaded neutral LNPs

Method			Z-average [nm]	PDI	Zeta potential [mV]	E.E.[a] [%]
Batch			491 ± 290.7	0.72 ± 0.479	-8 ± 2.0	67 ± 12.5
CM	Q_t[b]	100	332 ± 159.4	0.59 ± 0.230	-7 ± 2.5	11 ± 4.5
		500	401 ± 169.5	0.41 ± 0.189	-6 ± 2.1	16 ± 11.7
iLiNP	Q_t	100	317 ± 149.2	0.56 ± 0.378	-8 ± 1.7	31 ± 3.5
		500	101 ± 19.9	0.15 ± 0.047	-6 ± 1.9	78 ± 8.3

[a]E.E.: siRNA encapsulation efficiency

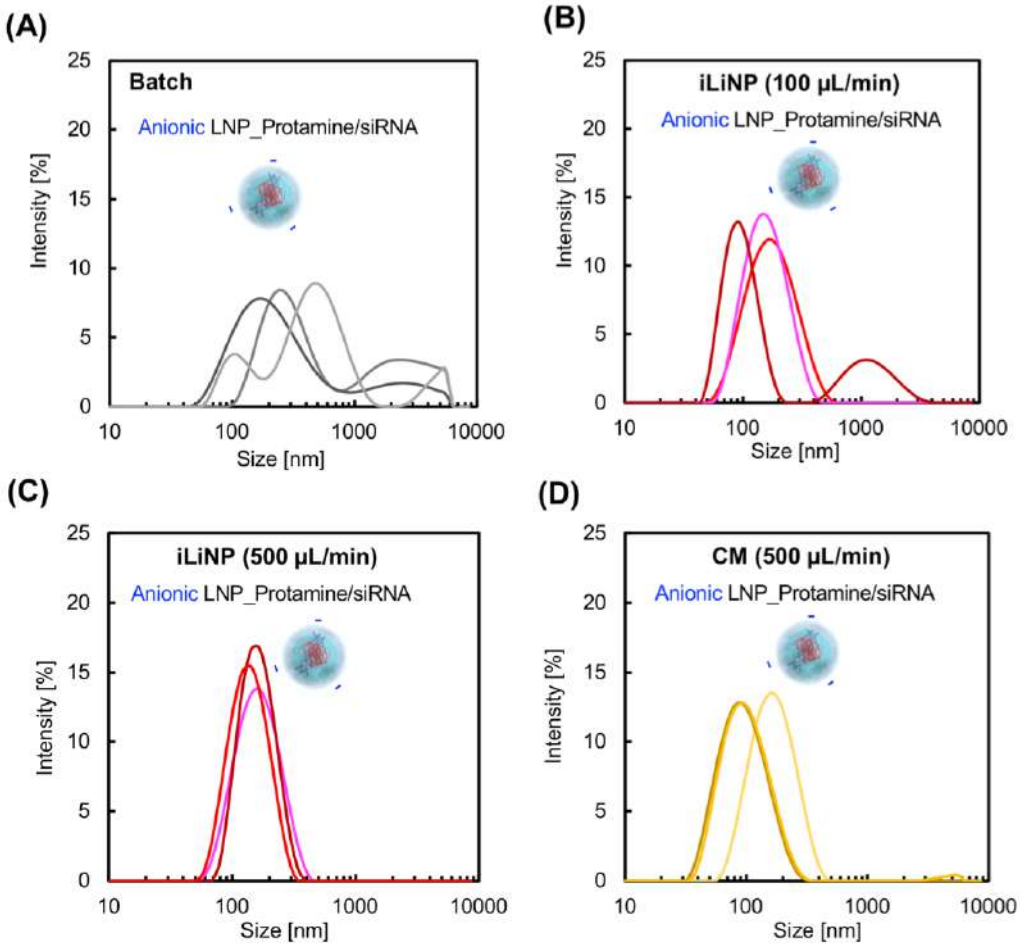

Figure 5.4 Size distributions of the anionic LNPs prepared by using (A) a batch method and (B–D) microfluidic methods. Experiments were repeated three times. CM: chaotic mixing.

Table 5.2 Average sizes, PDI, zeta-potential and siRNA encapsulation efficiency of the protamine/siRNA complex-loaded neutral and anionic LNPs.

protamine/siRNA complex-loaded neutral LNP	Number mean [nm]	SD[a]	Z-average [nm]	SD	Peak [nm]	SD	PDI[b]	SD	Zeta potential [mV]	SD	E.E.[c] [%]	SD
protamine/siRNA complex	65	9.4	98	7.0	97	7.7	0.09	0.053	30	7.1		
Batch	147	65.8	491	290.7	1585	804.2	0.77	0.391	-8	2.0	67	12.5
CM (Q_t [d]100)	119	64.1	332	159.4	1009	315.6	0.75	0.255	-7	2.5	11	4.5
CM (Q_t 500)	76	12.3	401	169.5	134	14.0	0.38	0.164	-6	2.1	16	11.7
iLiNP (Q_t 100)	102	12.6	317	149.2	934	695.9	0.63	0.366	-8	1.7	31	3.5
iLiNP (Q_t 500)	64	12.0	101	19.9	94	22.2	0.15	0.047	-6	1.9	78	8.3

protamine/siRNA complex-loaded anionic LNP	Number mean [nm]	SD	Z-average [nm]	SD	Peak [nm]	SD	PDI	SD	Zeta potential [mV]	SD	E.E. [%]	SD
Batch	122	63.8	301	83.4	1190	352.4	0.51	0.131	-19	2.3	56	5.0
CM (Q_t 100)	104	14.2	210	36.5	1152	535.6	0.56	0.405	-17	7.7	58	24.5
CM (Q_t 500)	85	10.3	186	40.8	135	43.7	0.29	0.186	-18	10.0	83	2.6
iLiNP (Q_t 100)	103	14.8	145	11.7	147	15.9	0.13	0.053	-25	3.0	76	14.4
iLiNP (Q_t 500)	72	5.4	142	7.2	142	9.5	0.07	0.010	-22	0.6	93	6.6

[a]SD: standard deviation; [b]PDI: polydispersity index; [c]E.E.: encapsulation efficiency; [d]Q_t: total flow rate.

5.3.2 Calcium-ion-mediated method for siRNA-loaded LNPs

As described, as a proof of concept experiment, I have confirmed the feasibility of the iLiNP device for the production of size-controlled siRNA-loaded noncationic LNPs by protamine addition. However, the protamine/siRNA-complex-based method requires the preparation of the protamine/siRNA complex before LNP production. To simplify production, I developed a Ca^{2+}-mediated method for one-step iLiNP-based production (Figure 5.5(A)) [12]. First, I identified the most suitable Ca^{2+} concentration and flow conditions for controlling the LNP size and encapsulating the siRNA (Figure 5.5(B)). At a total flow rate of 500 μL/min and

an FRR of 2, 13 mM Ca^{2+} was the optimal concentration for LNP preparation. The siRNA encapsulation efficiency reached almost 90%, and the size of the LNPs was 89 nm. In the Ca^{2+}-mediated method, the effect of the flow conditions showed a similar trend to that of the protamine/siRNA complex-based method concerning the LNP size and the siRNA encapsulation efficiency (Figure 5.6). Specifically, using the iLiNP device, the use of a total flow rate of 500 μL/min and an FRR of 2 was the best condition to produce size-controlled siRNA-loaded noncationic LNPs. Figures 5.5(C) and 5.5(D) show a comparison of the neutral and anionic LNP sizes and siRNA encapsulation efficiencies produced by the batch and microfluidic-based methods. The batch method produced LNPs of 300–400 nm and the siRNA encapsulation efficiency was lower than 20%. Although both the CM and iLiNP devices were able to control the LNP size by varying the total flow rate (Figures 5.7(C) and 5.7(D)), the sizes of neutral and anionic LNPs produced by the CM device were larger than 200 nm, even at a high total flow rate. In addition, in the LNP size distributions obtained by dynamic light scattering (DLS), I observed double peaks corresponding to particles more than 100 nm in size (Figures 5.8(B) and 5.8(E)). On the other hand, the iLiNP device produced LNPs of 89 and 124 nm at a flow rate of 500 μL/min for neutral and anionic lipid systems, respectively. Furthermore, there is a single peak in the particle size distributions for each lipid system (Figures 5.8(C) and 5.8(F)). In addition, the number-weighted particle size distribution of the iLiNP device overlaps the intensity-weighted particle size distribution (Figures 5.5(E) and 5.5(F))).

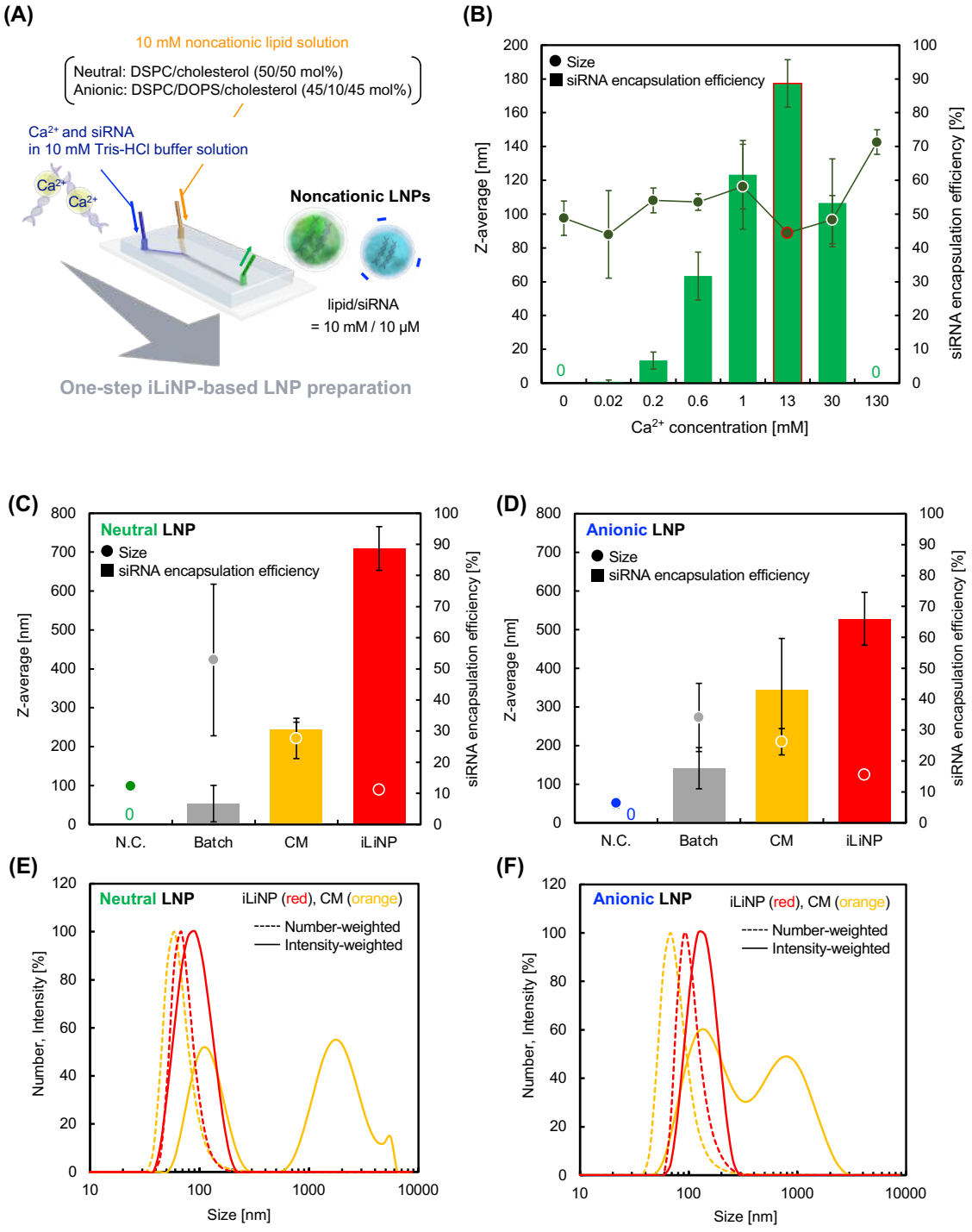

Figure 5.5 (A) One-step iLiNP-based noncationic LNP production. (B) Effects of Ca^{2+} concentration on the neutral LNP size and siRNA encapsulation efficiency. The total flow rate was 500 μL/min and the FRR was 2. (C) Z-average sizes and siRNA encapsulation efficiency of the neutral LNP and (D) the anionic LNP. (E) Intensity-weighted size distributions (solid line) and number-weighted size distributions (dashed line) of the neutral LNPs and (F) the anionic LNPs prepared by the CM device (orange) and the iLiNP device (red). DSPC: 1,2-Distearoyl-sn-glycero-3-phosphocholine (DSPC); DOPS: 1,2-dioleoyl-sn-glycero-3-phospho-L-serine (sodium salt).

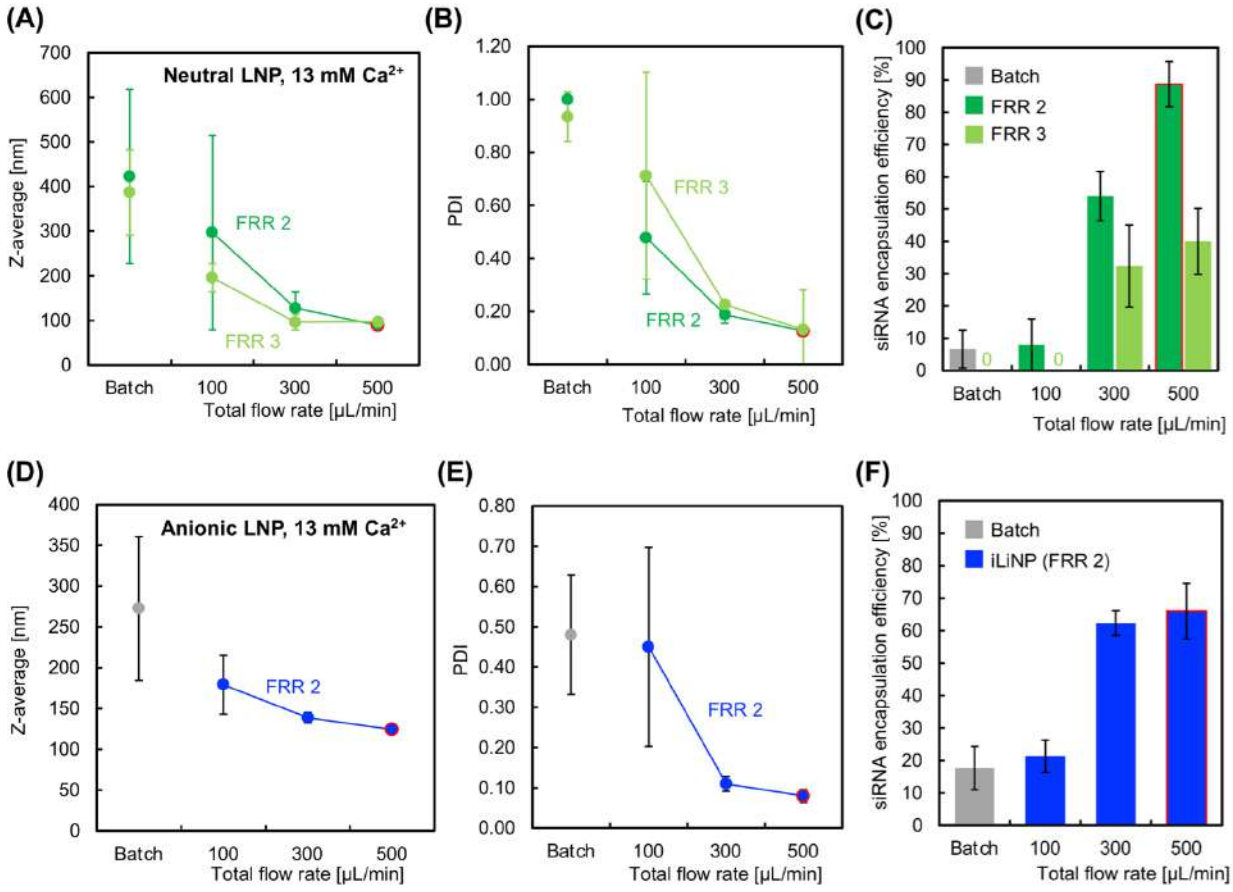

Figure 5.6 Effect of the total flow conditions on (A, D) average NP size, (B, E) polydispersity index (PDI), and (C, F) siRNA encapsulation efficiency for (A–C) neutral LNPs and (D–E) anionic LNPs.

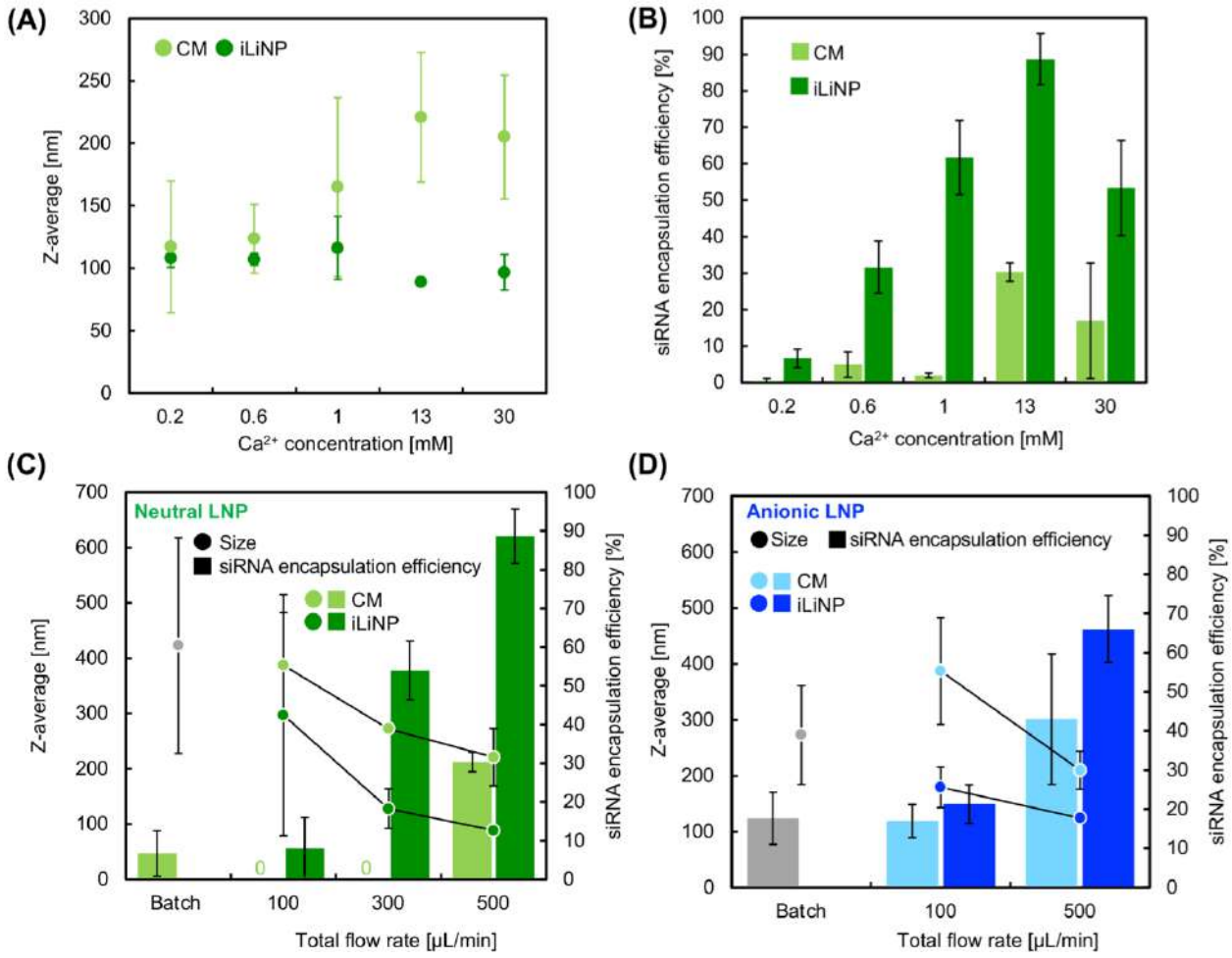

Figure 5.7 Comparison of the size controllability and siRNA encapsulation efficiency of LNPs prepared by the microfluidic devices. (A) Z-average sizes and (B) siRNA encapsulation efficiency of the neutral LNPs. (C-D) Z-average sizes and siRNA encapsulation efficiency of (C) neutral LNPs and (D) anionic LNPs. CM: chaotic mixing.

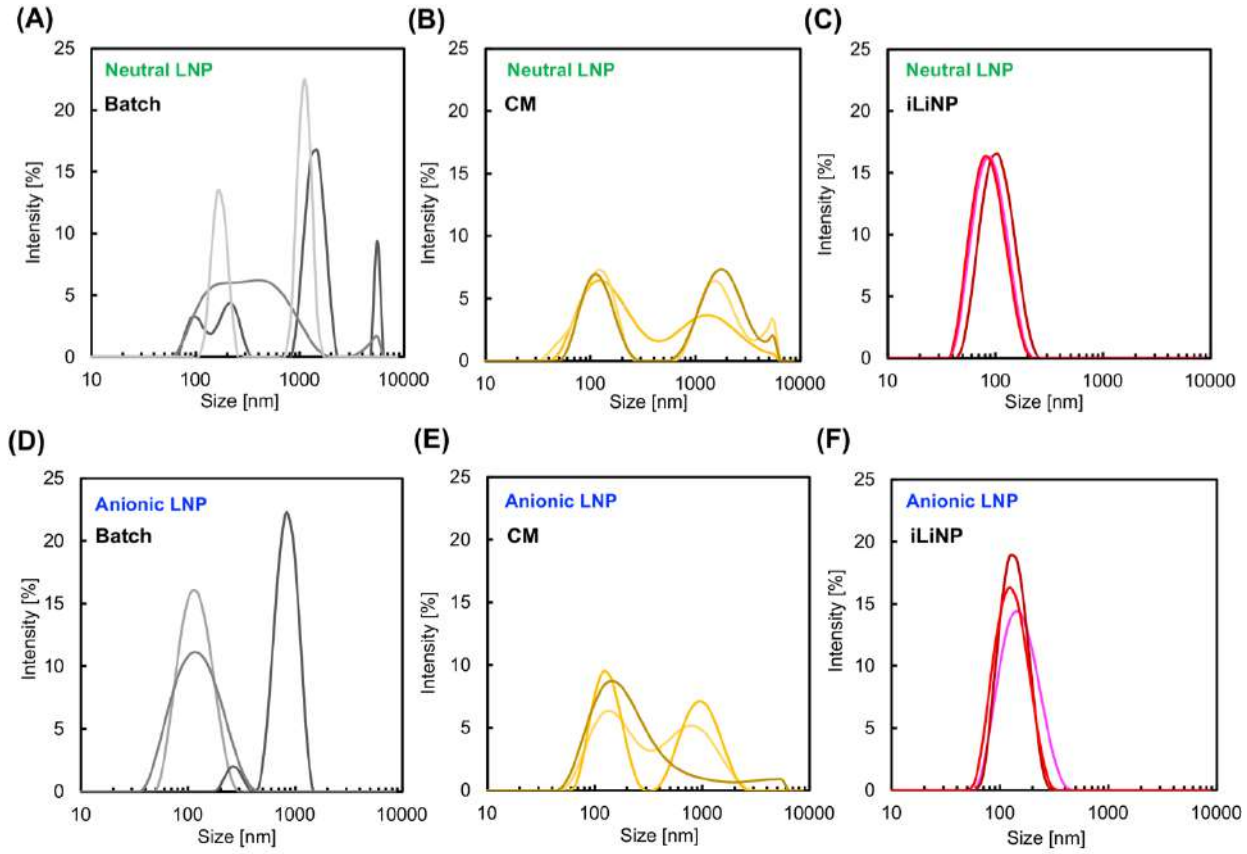

Figure 5.8 Size distributions of (A–C) neutral LNPs and (D–F) anionic LNPs prepared by the batch method and microfluidic devices. In the microfluidic methods, LNPs were produced at the total flow rate of 500 μL/min and a ratio of the flow rates of the aqueous and lipid phases (FRR) of 2. Experiments were repeated three times. CM: chaotic mixing.

These results suggest the iLiNP device produced homogeneously sized LNPs in both lipid system. Similar to that for the protamine/siRNA complex-based method, a total flow rate of 500 μL/min enabled high siRNA encapsulation in both microfluidic devices. The siRNA encapsulation efficiencies of the iLiNP device were 89% and 66% for the neutral and anionic LNPs, respectively, whereas those of the CM device were 30% and 43%, respectively. Previously, I reported the differences in the fluid dynamics of the CM and iLiNP devices.[28] The iLiNP device does not provide homogeneous mixing based on chaotic convection, and I observed an ordered aqueous–lipid solutions interface in the microchannels, although the baffle-like structure induced secondary circulation that diluted the ethanol at the interface. However, the aqueous–lipid solution interface is not disturbed by secondary circulation. In particular, the hydrophilic lipid head groups are oriented toward the

aqueous phase and interact with Ca^{2+} and siRNA. Therefore, I assume that the lipid–siRNA complexes acted as nuclei to form the LNPs. In the strategy based on microfluidic ethanol dilution for LNP production and the Ca^{2+}-mediated method for siRNA encapsulation, the formation of siRNA-loaded LNPs and siRNA precipitation with Ca^{2+} and ethanol are competitive processes. Therefore, a high Ca^{2+} concentration or low flow rate could induce siRNA precipitation before the interaction of the siRNA with the lipids. Thus, I have demonstrated the one-step size-controlled siRNA-loaded LNPs using the iLiNP device, but further investigation is required to understand the formation mechanism; nevertheless, the iLiNP method has great potential for the production of noncationic exosome-like NPs.

Table 5.3 Average sizes, PDI, zeta-potential and siRNA encapsulation efficiency of the siRNA-loaded neutral and anionic LNPs prepared using the Ca^{2+}-mediated method.

siRNA-loaded neutral LNP (Ca^{2+}-mediated)	**Number mean [nm]**	**SD**	**Z-average [nm]**	**SD**	**Peak [nm]**	**SD**	**PDI**	**SD**	**Zeta potential [mV]**	**SD**	**E.E. [%]**	**SD**
Batch	92	11.5	423	194.9	1463	210.6	1.00	0.002	-2	0.6	7	5.9
CM(Q_t 500)	67	14.6	221	51.9	244	38.3	0.78	0.271	-8	2.4	30	2.5
iLiNP(Q_t 100)	62	9.5	297	218.0	123	13.1	0.23	0.080	-4	2.7	10	5.1
iLiNP(Q_t 300)	59	10.8	128	35.7	108	25.4	0.17	0.053	-11	1.9	72	8.3
iLiNP(Q_t 500)	71	4.7	89	2.1	98	1.2	0.12	0.031	-8	1.6	89	7.0

siRNA-loaded anionic LNP (Ca^{2+}-mediated)	**Number mean [nm]**	**SD**	**Z-average [nm]**	**SD**	**Peak [nm]**	**SD**	**PDI**	**SD**	**Zeta potential [mV]**	**SD**	**E.E. [%]**	**SD**
N.C. ([Ca^{2+}] = 0 mM)	58	8.8	51	13.0	58	5.1	0.18	0.037	-44	5.7	0	0.0
Batch	129	57.3	273	88.3	801	144.0	0.48	0.148	-42	2.3	18	6.7
CM(Q_t 500)	85	11.9	210	34.0	123	33.2	0.44	0.074	-51	1.5	43	16.6
iLiNP(Q_t 100)	95	3.1	179	36.2	670	484.0	0.45	0.247	-46	4.4	21	4.9
iLiNP(Q_t 300)	86	3.2	139	6.5	134	3.6	0.11	0.018	-38	5.3	62	3.8
iLiNP(Q_t 500)	92	5.7	124	3.9	137	14.4	0.08	0.016	-34	2.6	66	8.5

5.3.3 Microfluidic preparation of the siRNA-loaded exosome-like NPs

Toward the final goal of producing artificial exosomes containing cell-derived lipids, membrane proteins, and RNA, I next focused on the production of a simple artificial exosome model. The siRNA-loaded exosome-like NPs without membrane proteins were produced using the iLiNP device and the Ca^{2+}-mediated method (Figure 5.9(A)). For the exosome-like lipid system, I optimized the flow conditions (Figures 5.9(B) and 5.9(C) and Figure 5.10) based on the simple neutral and anionic LNP systems. In this system, a total flow rate of 500 μL/min was also the best for controlling the LNP size and achieving a high siRNA encapsulation efficiency. The iLiNP device produced LNPs of 174 and 139 nm in Z-average size at FRRs of 1.5 and 2, respectively, making these values suitable for use. Further, the siRNA encapsulation efficiency was higher than 50%, regardless of the FRR. Figures 5.9(D) and 5.9(E) show the intensity and number-weighted LNP size distributions produced at FRRs of 1.5 and 2. As shown by these results, large, homogeneous exosome-like NPs were produced at an FRR of 1.5. At an FRR of 2, I observed two sharp peaks in the intensity-weighted size distribution. The peak at 40 nm is consistent with that of the number-weighted size distribution. According to DLS theory, large NPs exhibit a stronger scattering peak in the intensity-weighted size distribution than that of the small-sized NPs. Therefore, the size distribution analysis suggests that 40-nm-sized exosome-like NPs dominate when prepared at an FRR of 2. Thus, I carried out transmission electron microscopy (TEM) analysis of the NPs prepared at an FRR of 2 and confirmed the formation of almost 40 to 50-nm-sized NPs (Figure 5.9 (F)). From the results of the size measurement by dynamic light scattering and TEM, I consider the 40 to 50-nm-sized NPs are the majority of NPs produced by the iLiNP at the FRR of 2. Concerning the NPs produced using the batch method and the CM device, the size distributions of exosome-like NPs were broad and the sharp peak at 40 nm was not observed (Figure 5.11).

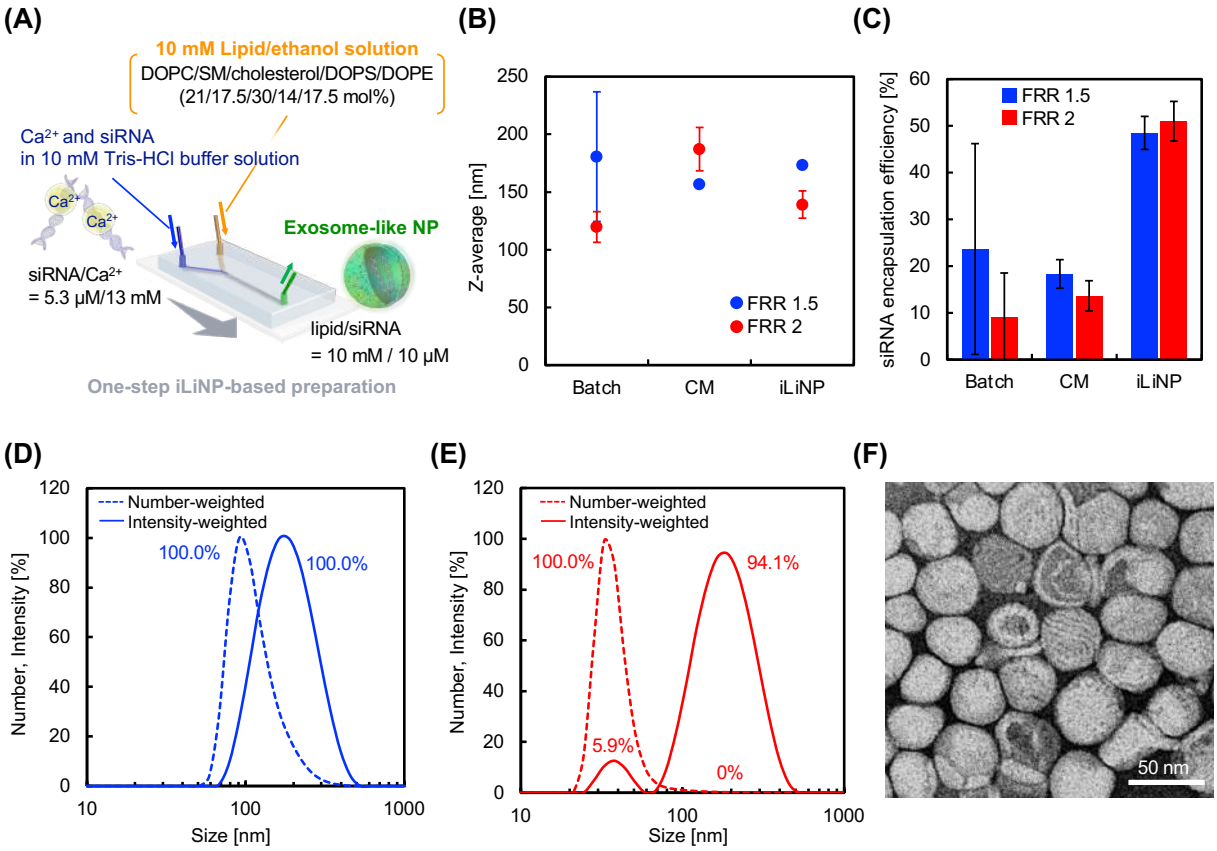

Figure 5.9 (A) One-step iLiNP-based preparation of the exosome-like NPs. (B) Effects of the preparation method on the LNP size and (C) siRNA encapsulation efficiency. (D, E) Intensity-weighted size distributions (solid line) and number-weighted size distributions (dashed line) of the exosome-like LNPs prepared by the iLiNP device at the total flow rate of 500 μL/min and FRRs of 1.5 (blue) and 2 (red). (F) TEM image of the exosome-like NPs prepared by the iLiNP device at 500 μL/min and FRR of 2.

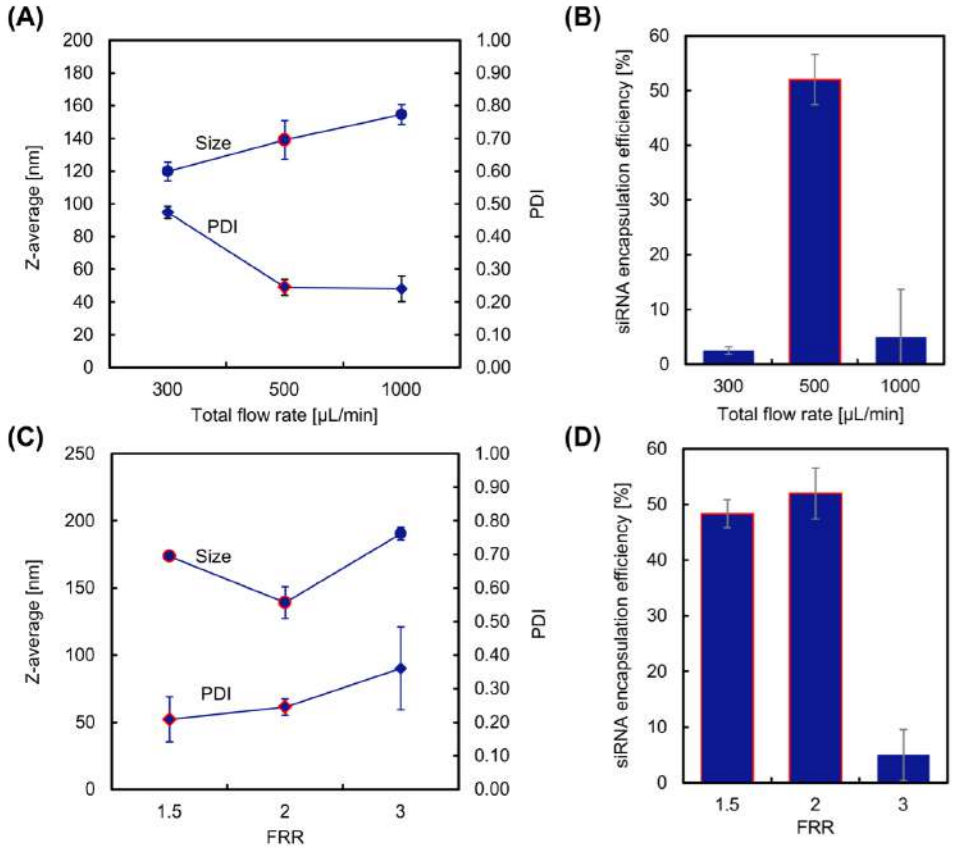

Figure 5.10 Effect of the flow conditions on the size controllability and siRNA-encapsulation efficiency of the exosome-like NPs prepared by the iLiNP device. For the exosome-like NPs, a 10 mM lipid solution composed of DOPC/ SM/cholesterol/DOPS/DOPE (21/17.5/30/14/17.5 mol.%) and 10 mM Tris-HCl buffer solution containing siRNA was used. (A) Effect of the total flow rate on the LNP sizes and PDI and (B) siRNA encapsulation efficiency. The FRR was fixed at 2. Effect of (C) the FRR on the LNP size and PDI and (D) siRNA encapsulation efficiency. The total flow rate was 500 μL/min.

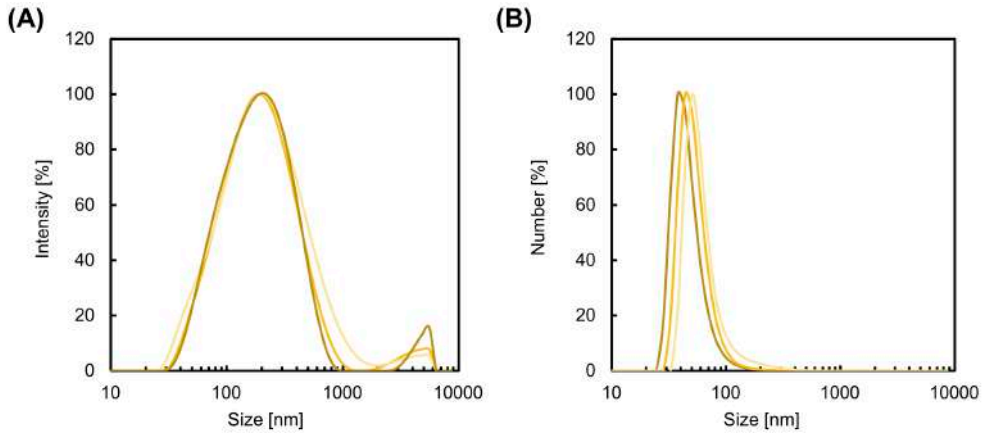

Figure 5.11 (A) Intensity-weighted size distributions and (B) number-weighted size distributions of the exosome-like NPs prepared using the chaotic mixing (CM) device at an FRR of 2. The *y*-axis shows the differential intensity (%) and the differential number (%).

To improve the LNP size distribution, I modified the lipid system with a polyethylene glycol (PEG)-based compound: 1,2-dimyristoyl-*rac*-glycero-3-methylpolyoxyethylene (PEG-DMG 2K) to the lipid system [35]. Figure 5.12(A) shows the average sizes of exosome-like NPs produced at different total flow rate conditions. For the PEG-modified exosome-like NPs, an FRR of 1.5 was optimal for siRNA encapsulation (Figures 5.13(A) and 5.13(B)). Further, as before, the size of the NPs could be controlled from 90 to 121 nm by controlling the total flow rate of the iLiNP device. In contrast, the NP size did not change on varying the flow conditions using the CM device. Importantly, the intensity-weighted size distributions were improved, yielding a single peak, after the addition of PEG-DMG 2K (Figures 5.12(B–D)). However, the size distributions of the NPs were broad, and I could not confirm the effect of the PEG-lipid on NP size controllability. In addition, the sharp peak at 40 nm in the intensity-weighted size distribution disappeared after adding PEG-DMG 2K. Further, the siRNA encapsulation efficiencies were 50% and 30% for the NPs produced by the iLiNP device and the batch/CM device, respectively (Figure 5.12(E)). These results indicate that the iLiNP device can produce a variety of size-controlled exosome-like NPs, including surface-modified exosome-like NPs encapsulating siRNA, in a one-step reaction.

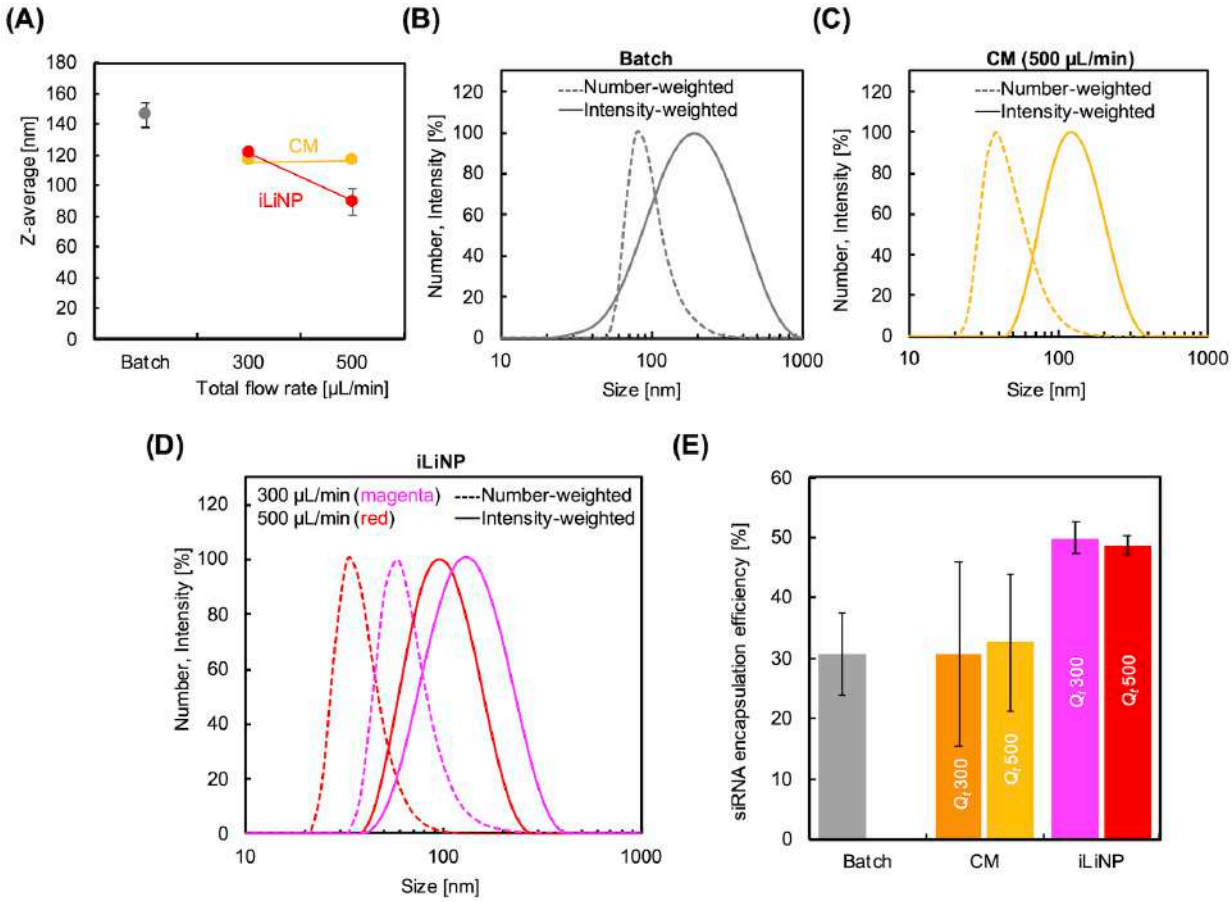

Figure 5.12 (A) Z-average sizes, (B–D) size distributions, and (E) siRNA encapsulation efficiency of the PEG-DMG 2K modified exosome-like NPs. For the microfluidic devices, the total flow rates were 300 and 500 μL/min at an FRR of 1.5.

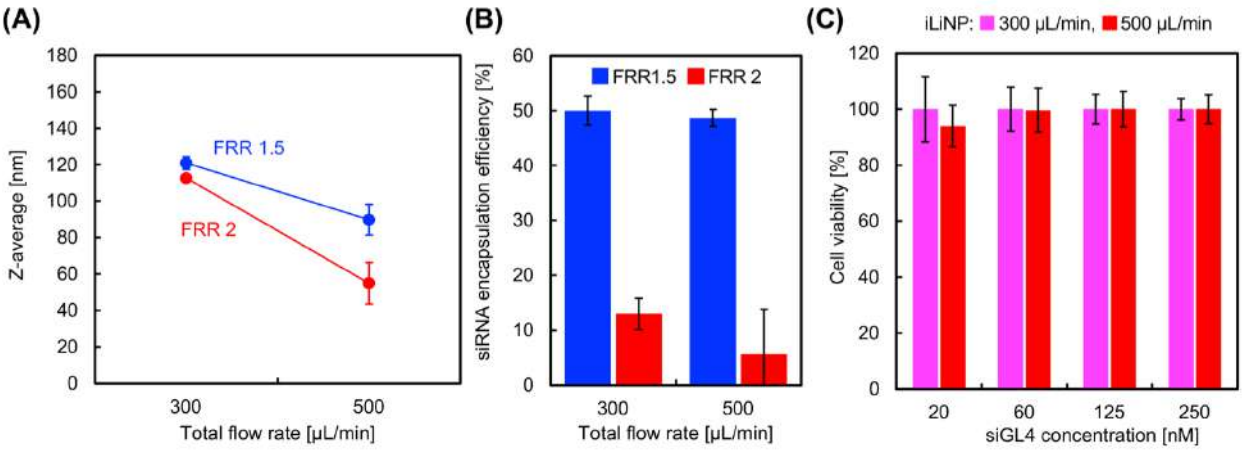

Figure 5.13 One-step iLiNP-based PEG-modified exosome-like NP preparation. Effect of the flow conditions on (A) the Z-average and (B) siRNA encapsulation efficiency. (C) Cytotoxicity of the NPs prepared at total flow rates of 300 (magenta) and 500 μL/min (red).

Next, I evaluated cell viability and the luciferase knockdown activity of the exosome-like NPs. Figure 5.14(A) shows fluorescence microscopy images of the intercellular distribution of exosome-like NPs prepared by the iLiNP device (FRR: 2), Lipofectamine RNAiMAX, and cationic LNPs. The exosome-like NPs were taken up into the HeLa cells. The Lipofectamine RNAiMAX and cationic LNPs achieved higher intercellular distributions than the exosome-like NPs. The dose-dependent cell viability for each NP at different siRNA concentrations was then determined (Figure 5.14(B)). The exosome-like NPs showed no significant cytotoxicity, even at a high siRNA dose of 250 nM. In contrast, cell viability was decreased to 60% at an siRNA dose of 250 nM when using the cationic LNPs. Figure 5.14(C) shows a comparison of the luciferase knockdown activity using Lipofectamine RNAiMAX, the cationic LNPs, and the exosome-like NPs. Lipofectamine and the cationic LNPs showed 80% luciferase knockdown at a dose of 20 nM siRNA. In contrast, the luciferase expression was reduced to 50% at a dose of 20 nM siRNA by the exosome-like NPs (FRR 2). However, a dose of 60 nM siRNA introduced by the exosome-like NPs did not increase the knockdown activity, suggesting that 50% luciferase expression was the maximum knockdown activity in this lipid formulation. Interestingly, the exosome-like NPs produced at an FRR of 1.5, which exhibited a single peak in the intensity-weighted size distribution (Figure 5.9(D)), could not suppress luciferase expression at a dose of 20 nM siRNA, but, at a 60 nM siRNA dose, 30% luciferase expression was suppressed by the NPs. In addition, the exosome-like NPs prepared by other methods also showed similar luciferase knockdown activities (Figure 5.15(B)). As shown in Figures 5.9(D) and 5.9(E), the homogeneity of the NPs produced at an FRR of 1.5 was higher than that of the NPs produced at an FRR of 2. This result indicates that luciferase knockdown was induced by the 40 to 50-nm-sized NPs formed at an FRR of 2 rather than the homogeneously sized NPs ranging from 100 to 200 nm.

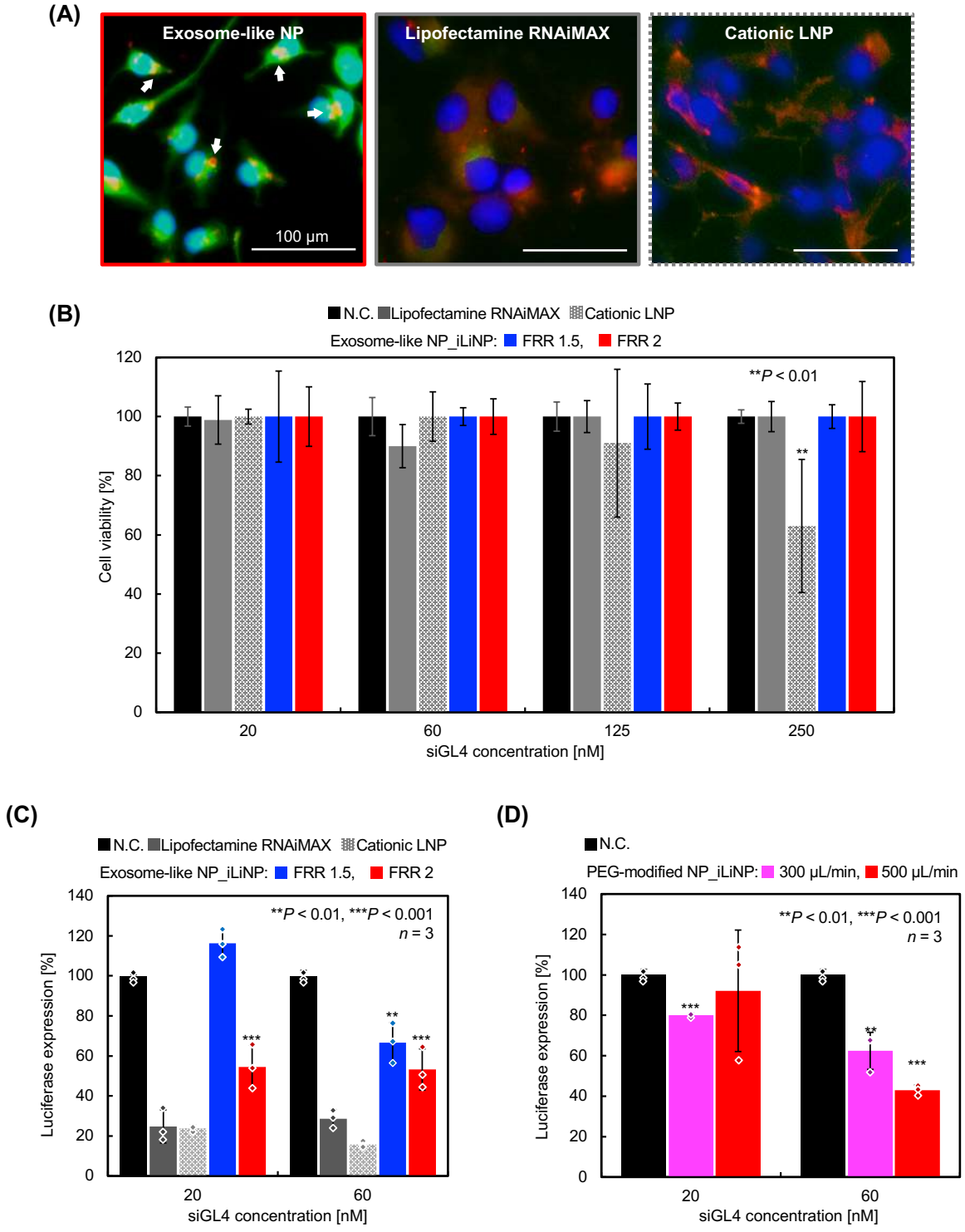

Figure 5.14 (A) Fluorescence microscopy images of HeLa-dluc cells treated with siGL4-loaded exosome-like NPs (without PEGylated lipid) at a dose of 100 nM siGL4. NPs were prepared by using the iLiNP device at the total flow rate of 500 μL/min and FRR of 2. Green, blue, and red represent the cytoplasm, nuclei, and siGL4, respectively. (B) Cell viability assay of the exosome-like NPs. (C, D) Gene-silencing activity of (C) the exosome-like NPs (without PEGylation) and (D) the PEGylated-exosome-like NPs. $^{**}P < 0.01$ (vs. N.C.), $^{***}P < 0.001$ (vs. N.C.), $n = 3$, Student's t-test. Scale bar: 100 mm.

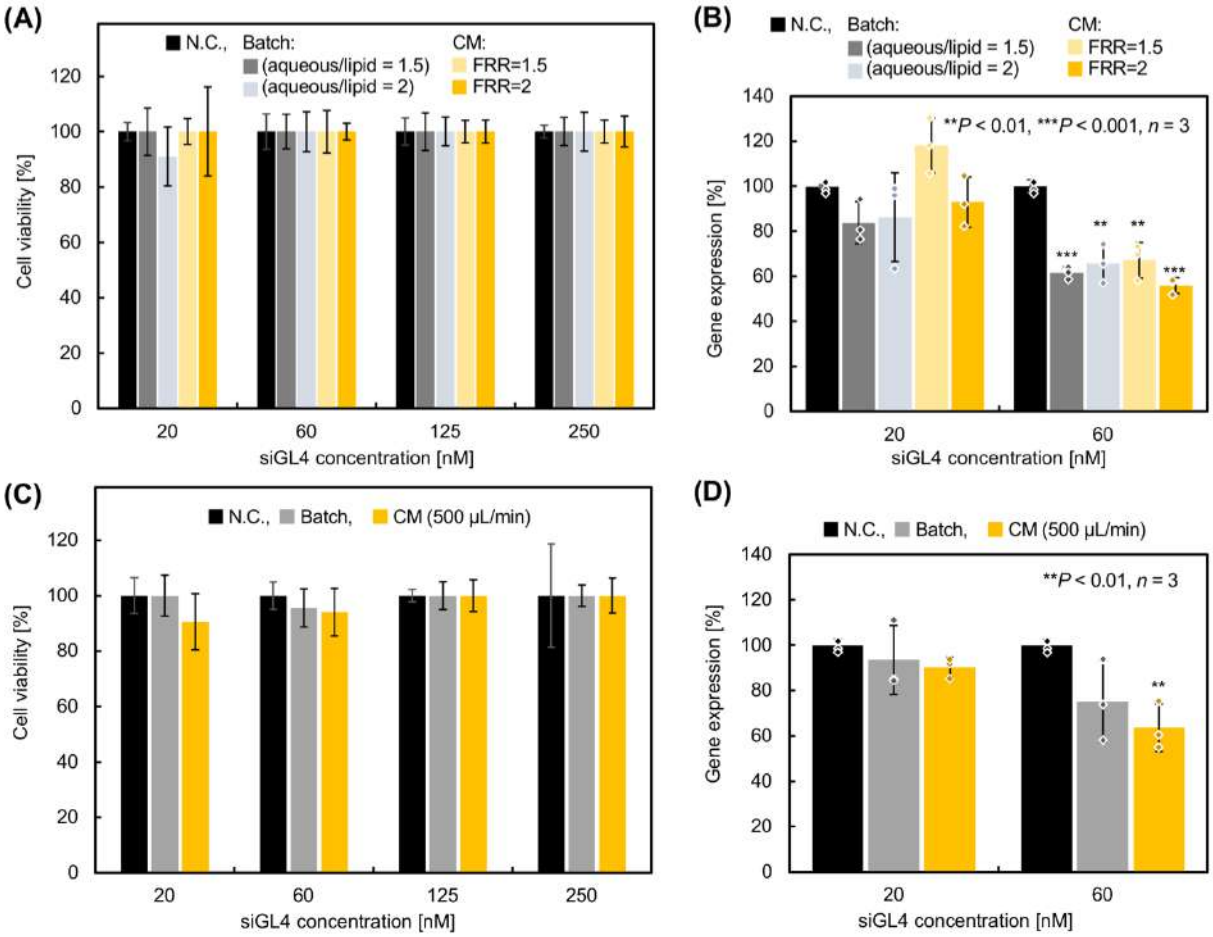

Figure 5.15 Cytotoxicity and gene-silencing activity of (A, B) exosome-like NPs and (C, D) PEG-modified exosome-like NPs. NPs were prepared using the batch method and the CM device. $^{**}P < 0.01$, $^{***}P < 0.001$, $n = 3$, Student's *t*-test. CM: chaotic mixing.

I also evaluated the luciferase knockdown activity using the PEG-modified exosome-like NPs. As shown in Figures 5.12(B–D), the size distribution of the NPs was improved, yielding a single peak, by addition of the PEG-DMG 2K to the lipid system. The median effective dose was shifted to higher concentration compared to that of the exosome-like NPs without PEG-DMG 2K (Figure 5.14(D)). In the PEG-modified NPs, the small NPs (90 nm) prepared at 500 µL/min suppressed 60% luciferase expression at a dose of 60 nM siRNA, whereas the large NPs (121 nm) suppressed 40% luciferase expression. This result also supports the hypothesis that 40-

nm NPs show effective luciferase knockdown activity. The cytotoxicity of the modified NPs was the same as that of exosome-like NPs without PEG-DMG 2K (Figures 5.13(C), Figure 5.15(A) and 5.15(C)).

As a result, the approach using the iLiNP device produces not only highly biocompatible and size-controlled exosome-like NPs but also modified artificial exosome-like NPs encapsulating siRNA. This technique allows the production of artificial exosomes and virus mimetic NPs for use as RNA delivery systems.

Table 5.4 Average sizes, PDI, zeta-potential, siRNA encapsulation efficiency and recovery rate of the exosome-like NPs and the PEG-modified exosome-like NPs. R.R.: recovery rate.

Exosome-like NPs		**Number mean [nm]**	**SD**	**Z-average [nm]**	**SD**	**Peak [nm]**	**SD**	**PDI**	**SD**	**Zeta potential [mV]**	**SD**	**E.E. [%]**	**SD**	**R.R. [%]**	**SD**
Lipofectamine RNAiMAX		21	0.3	78	1.0	114	5.1	0.30	0.009	46	2.0				
DOTAP-LNP		50	5.3	126	4.5	150	5.4	0.15	0.003	38	0.5	76	7.8	100	0
Batch	Aqueous/lipid = 1.5/1 [v/v]	42	10.8	181	56.2	160	146.7	0.49	0.035	-43	1.6	35	17.7	84	19.8
	2/1 [v/v]	42	9.2	120	13.3	164	157.3	0.48	0.341	-43	0.9	9	9.5	99	2.3
CM	FRR = 1.5	42	6.9	157	1.2	235	28.5	0.35	0.082	-48	0.5	18	3.1	70	17.6
	FRR = 2	47	7.1	187	18.8	275	47.2	0.41	0.186	-29	6.4	14	3.2	76	20.4
iLiNP	FRR = 1.5	111	6.4	174	2.2	224	41.2	0.21	0.067	-55	0.3	48	2.5	71	5.8
	FRR = 2	40	7.3	139	11.8	40	3.5	0.25	0.024	-31	6.6	52	4.6	84	4.6

PEG-modified exosome-like NPs		**Number mean [nm]**	**SD**	**Z-average [nm]**	**SD**	**Peak [nm]**	**SD**	**PDI**	**SD**	**Zeta potential [mV]**	**SD**	**E.E. [%]**	**SD**	**R.R. [%]**	**SD**
Batch		104	5.5	146	8.1	177	15.7	0.12	0.019	-25	0.7	31	6.8	69	2.6
CM	Q_t 300	58	12.2	116	0.9	135	5.8	0.16	0.008	-27	0.8	33	11.4	69	5.3
	Q_t 500	63	4.4	97	6.9	108	4.2	0.14	0.028	-23	0.6	23	3.2	76	17.0
iLiNP	Q_t 300	61	8.1	121	3.5	150	8.9	0.20	0.031	-31	0.7	50	2.6	54	5.3
	Q_t 500	42	0.7	90	8.4	113	8.1	0.19	0.040	-35	1.3	49	1.5	62	6.1

5.4 Conclusion

I developed a one-step production method for noncationic size-controlled exosome-like NPs using the iLiNP device. The iLiNP device produced the NPs with precise size controllability and high siRNA encapsulation efficiency in neutral and anionic lipid systems. Two methods are available to produce the noncationic NPs encapsulating siRNA using the iLiNP device: (1) protamine/siRNA complexation and (2) a Ca^{2+}-mediated method. In both methods, the flow conditions affected the NP size controllability and the siRNA encapsulation efficiency. After the optimization of the NP preparation conditions, I applied the one-step method for the production of exosome-like NPs encapsulating siRNA and evaluated their cytotoxicity and luciferase knockdown activity. The exosome-like NPs showed no cytotoxicity, even at high siRNA doses. In addition, the size-controlled NPs suppressed the luciferase expression at a low dosage of siRNA. The microfluidic approach is the only way to produce the size-controlled and highly siRNA-loaded exosome-like NPs via a one-step reaction. I expect that the approach will be applied to the production of the functional and artificial exosomes, and it will be a useful technique for exosome research such as understanding the exosome role, targeting, and functionalization.

References

[1] S. C. Semple, A. Akinc, J. Chen, A. P. Sandhu, B. L. Mui, C. K. Cho, D. W. Sah, D. Stebbing, E. J. Crosley, E. Yaworski, I. M. Hafez, J. R. Dorkin, J. Qin, K. Lam, K. G. Rajeev, K. F. Wong, L. B. Jeffs, L. Nechev, M. L. Eisenhardt, M. Jayaraman, M. Kazem, M. A. Maier, M. Srinivasulu, M. J. Weinstein, Q. Chen, R. Alvarez, S. A. Barros, S. De, S. K. Klimuk, T. Borland, V. Kosovrasti, W. L. Cantley, Y. K. Tam, M. Manoharan, M. A. Ciufolini, M. A. Tracy, A. de Fougerolles, I. MacLachlan, P. R. Cullis, T. D. Madden and M. J. Hope, *Nat. Biotechnol.*, **28**, 172-176 (2010)

[2] A. Schroeder, C. G. Levins, C. Cortez, R. Langer and D. G. Anderson, *J. Intern. Med.*, **267**, 9-21 (2010)

[3] P. R. Cullis and M. J. Hope, *Mol. Ther.*, **25**, 1467-1475 (2017)

[4] T. Ren, Y. K. Song, G. Zhang and D. Liu, *Gene Ther.*, **7**, 764-768 (2000)

[5] D. A. Balazs and W. Godbey, *J Drug Deliv*, **2011**, 326497 (2011)

[6] D. Zhi, S. Zhang, B. Wang, Y. Zhao, B. Yang and S. Yu, *Bioconjug. Chem.*, **21**, 563-577 (2010)

[7] K. Lappalainen, I. Jaaskelainen, K. Syrjanen, A. Urtti and S. Syrjanen, *Pharm. Res.*, **11**, 1127-1131 (1994)

[8] M. C. Filion and N. C. Phillips, *Biochim. Biophys. Acta*, **1329**, 345-356 (1997)

[9] S. Krasnici, A. Werner, M. E. Eichhorn, M. Schmitt-Sody, S. A. Pahernik, B. Sauer, B. Schulze, M. Teifel, U. Michaelis, K. Naujoks and M. Dellian, *Int. J. Cancer*, **105**, 561-567 (2003)

[10] M. Schlich, F. Longhena, G. Faustini, C. M. O'Driscoll, C. Sinico, A. M. Fadda, A. Bellucci and F. Lai, *Nano Research*, **10**, 3496-3508 (2017)

[11] A. D. Tagalakis, D. H. Lee, A. S. Bienemann, H. Zhou, M. M. Munye, L. Saraiva, D. McCarthy, Z. Du, C. A. Vink, R. Maeshima, E. A. White, K. Gustafsson and S. L. Hart, *Biomaterials*, **35**, 8406-8415 (2014)

[12] M. Somiya, K. Yamaguchi, Q. Liu, T. Niimi, A. D. Maturana, M. Iijima, N. Yoshimoto and S. Kuroda, *Int. J. Pharm.*, **490**, 316-323 (2015)

[13] M. Lu, X. Zhao, H. Xing, Z. Xun, S. Zhu, L. Lang, T. Yang, C. Cai, D. Wang and P. Ding, *Int. J. Pharm.*, **550**, 100-113 (2018)

[14] M. Lu, X. Zhao, H. Xing, H. Liu, L. Lang, T. Yang, Z. Xun, D. Wang and P. Ding, *Acta Biomater.*, **96**, 517-536 (2019)

[15] H. Cabral, Y. Matsumoto, K. Mizuno, Q. Chen, M. Murakami, M. Kimura, Y. Terada, M. R. Kano, K. Miyazono, M. Uesaka, N. Nishiyama and K. Kataoka, *Nat Nanotechnol*, **6**, 815-823 (2011)

[16] T. Nakamura, M. Kawai, Y. Sato, M. Maeki, M. Tokeshi and H. Harashima, *Mol. Pharm.*, **17**, 944-953 (2020)

[17] Y. Sato, Y. Note, M. Maeki, N. Kaji, Y. Baba, M. Tokeshi and H. Harashima, *J. Control. Release*, **229**, 48-57 (2016)

[18] S. Khadke, C. B. Roces, A. Cameron, A. Devitt and Y. Perrie, *J. Control. Release*, **307**, 211-220 (2019)

[19] M. Maeki, N. Kimura, Y. Sato, H. Harashima and M. Tokeshi, *Adv Drug Deliv Rev*, **128**, 84-100 (2018)

[20] Q. Cheng, T. Wei, L. Farbiak, L. T. Johnson, S. A. Dilliard and D. J. Siegwart, *Nat Nanotechnol*, **15**, 313-320 (2020)

[21] J. A. Kulkarni, M. M. Darjuan, J. E. Mercer, S. Chen, R. van der Meel, J. L. Thewalt, Y. Y. C. Tam and P. R. Cullis, *ACS Nano*, **12**, 4787-4795 (2018)

[22] M. A. Oberli, A. M. Reichmuth, J. R. Dorkin, M. J. Mitchell, O. S. Fenton, A. Jaklenec, D. G. Anderson, R. Langer and D. Blankschtein, *Nano Lett.*, **17**, 1326-1335 (2017)

[23] N. Kimura, M. Maeki, Y. Sato, A. Ishida, H. Tani, H. Harashima and M. Tokeshi, *ACS Appl Mater Interfaces*, **12**, 34011-34020 (2020)

[24] A. Hashiba, M. Toyooka, Y. Sato, M. Maeki, M. Tokeshi and H. Harashima, *J. Control. Release*, **327**, 467-476 (2020)

[25] M. Maugeri, M. Nawaz, A. Papadimitriou, A. Angerfors, A. Camponeschi, M. Na, M. Holtta, P. Skantze, S. Johansson, M. Sundqvist, J. Lindquist, T. Kjellman, I. L. Martensson, T. Jin, P. Sunnerhagen, S. Ostman, L. Lindfors and H. Valadi, *Nat Commun*, **10**, 4333 (2019)

[26] M. J. W. Evers, J. A. Kulkarni, R. van der Meel, P. R. Cullis, P. Vader and R. M. Schiffelers, *Small Methods*, **2**, 1700375 (2018)

[27] M. Yanez Arteta, T. Kjellman, S. Bartesaghi, S. Wallin, X. Wu, A. J. Kvist, A. Dabkowska, N. Szekely, A. Radulescu, J. Bergenholtz and L. Lindfors, *Proc. Natl. Acad. Sci. U. S. A.*, **115**, E3351-E3360 (2018)

[28] N. Kimura, M. Maeki, Y. Sato, Y. Note, A. Ishida, H. Tani, H. Harashima and M. Tokeshi, *ACS Omega*, **3**, 5044-5051 (2018)

[29] M. Maeki, Y. Fujishima, Y. Sato, T. Yasui, N. Kaji, A. Ishida, H. Tani, Y. Baba, H. Harashima and M. Tokeshi, *PLoS One*, **12**, e0187962 (2017)

[30] W. Alshaer, H. Hillaireau, J. Vergnaud, S. Mura, C. Delomenie, F. Sauvage, S. Ismail and E. Fattal, *J. Control. Release*, **271**, 98-106 (2018)

[31] S. Stremersch, R. E. Vandenbroucke, E. Van Wonterghem, A. Hendrix, S. C. De Smedt and K. Raemdonck, *J. Control. Release*, **232**, 51-61 (2016)

[32] Y. Sato, K. Hashiba, K. Sasaki, M. Maeki, M. Tokeshi and H. Harashima, *J. Control. Release*, **295**, 140-152 (2019)

[33] I. V. Zhigaltsev, N. Belliveau, I. Hafez, A. K. K. Leung, J. Huft, C. Hansen and P. R. Cullis, *Langmuir*, **28**, 3633-3640 (2012)

[34] D. Chen, K. T. Love, Y. Chen, A. A. Eltoukhy, C. Kastrup, G. Sahay, A. Jeon, Y. Dong, K. A. Whitehead and D. G. Anderson, *J. Am. Chem. Soc.*, **134**, 6948-6951 (2012)

[35] A. S. Nosova, O. O. Koloskova, A. A. Nikonova, V. A. Simonova, V. V. Smirnov, D. Kudlay and M. R. Khaitov, *Medchemcomm*, **10**, 369-377 (2019)

CHAPTER 6 Conclusion and Future Prospects

6.1 Conclusions

This research was designed to develop microfluidic devices to produce size-controlled, lipid nanoparticles (LNPs) to aid LNP-based drug development. Effective ethanol dilution is one of the key techniques for the precise size controllability of LNPs. The developed microfluidic devices were equipped with optimized baffle structures and allowed effective ethanol dilution by the induced secondary flow. Therefore, the baffle devices showed more precise size controllability of LNPs than other methods for producing LNPs and could be applied for DDS applications. The baffle device was also applicable for the production of size-controlled, exosome-like LNPs, indicating the developed devices could be used for developing LNP-based nanomedicines and exosome-inspired drugs. A brief overview of the present research is described in the following text.

In Chapter 2, the development of invasive lipid nanoparticle production (iLiNP) device was described, and this device allowed the first-reported LNP size tuning at 10 nm intervals in the size range of 20 to 100 nm. Thus, the iLiNP device has useful practical applications. From the viewpoint of the LNP formation mechanism, rapid ethanol solvent dilution is important for precise size controllability. The optimized baffle structures induced effective secondary flow in the iLiNP device at the total flow rate of 500 μL/min and enabled precise size controllability and 20-nm-sized LNP production. Compared to the current gold-standard microfluidic device called the CM device, the iLiNP device showed better LNP size controllability, robust device design, and LNP mass productivity. In addition, the iLiNP device-assisted LNP production method was applicable for small interfering RNA (siRNA)-loaded LNP production composed of the pH-sensitive, cationic lipid-based system. The prepared siRNA-loaded LNPs effectively performed as drug delivery system (DDS)-nanocarriers in vivo. Therefore, the developed iLiNP device is expected to be applied as a novel DDS-nanocarrier production apparatus.

In Chapter 3, the improvement of LNP size controllability of the iLiNP device at low flow rate conditions with an aim of precise size control of large-sized LNPs is narrated. The three-dimensional symmetrically

assembled microfluidic device named the 3D-iLiNP device was developed based on the design of the conventional iLiNP device. The 3D-iLiNP device allowed a homogeneous and slow rate ethanol dilution by induced secondary flow and achieved precise size control of the 20–100-nm-sized LNPs with low coefficient variation (CV) values (< 10%). The influence of the average size and size distribution of siRNA-loaded, pH-sensitive, cationic lipid-based NPs on gene-silencing activity was also evaluated using in vitro and in vivo experiments. The results revealed that LNPs with a size between 90 and 120 nm showed higher gene-silencing activity than those with other sizes. Therefore, the 3D-iLiNP device is expected to improve DDS performance by the precise size controllability of LNPs. Detailed effect of the post-treatment processes on the final product size of LNPs was investigated to develop the integrated baffle device composed of an LNP production region and a post-treatment region, which has been described in Chapter 4. After microfluidic LNP preparation, including the iLiNP device-assisted method, some post-treatments are needed to remove the remaining ethanol. Conventionally, overnight dialysis or direct dilution with a buffer solution are used as post-treatments. However, the kinetics of ethanol removal from the inner and outer membranes of LNPs could induce a structural change in the lipid membrane that could lead to the fusion of LNPs. As expected, the flow conditions of the post-treatment that dilutes the remaining ethanol in the LNP suspension affected the final product size of LNPs. Based on this finding, the integrated baffle device was developed, and the device could prevent the undesirable aggregation or fusion of LNPs. Moreover, the iLiNP device-assisted microfluidic post-treatment method was applied to siRNA delivery with the pH-sensitive, cationic lipid system. Thirty-nanometer-sized siRNA-loaded LNPs were produced using the integrated baffle device. There were no significant effects because of the continuous microfluidic process on the siRNA encapsulation efficiency, biological distribution, and gene-silencing activity. These results suggest that the continuous post-treatment process using the microfluidic devices equipped with baffle structures is expected to contribute to the production of LNPs with practical applications and development of novel LNP-based nanomedicines.

In Chapter 5, the application of iLiNP device-assisted LNP production method for RNA delivery using noncationic, size-controlled, exosome-like NPs is outlined. As described in Chapters 2–4, siRNA-loaded LNP

components contain cationic lipids. Noncationic, lipid-based NPs, such as exosomes, are also ideal nanocarriers for drug delivery because of their excellent biocompatibility. However, reasonable simultaneous production of size-controlled, noncationic LNP and effective RNA encapsulation is difficult because of the lack of electrostatic interactions. To cancel the negative charge of siRNA, the protamine/siRNA complexation and the Ca^{2+}-mediated method were employed. The iLiNP device produced the NPs with precise size controllability and high siRNA encapsulation efficiency in the simple, neutral, and anionic lipid-based systems, whereas the batch method and the chaotic micromixer (CM) device did not. Based on the optimized conditions for noncationic LNP production, the iLiNP device-assisted production method was applied to produce size-controlled, siRNA-loaded, exosome-like NPs. The iLiNP device only produced 40–50-nm-sized, exosome-like, NPs with 50% of siRNA encapsulation efficiency, and the NPs showed no cytotoxicity and better gene-silencing activity than other NPs. Therefore, the iLiNP device-assisted, one-step production method for RNA-encapsulated size-controlled, noncationic NP is a promising method to produce artificial exosomes and functionally modified exosomes for gene and cell therapies.

6.2 Implications of the Research and Relationship to Previous Research

This section gives an overview of the research implications and their relationship to previous works in this field. In addition to the practical application of the developed microfluidic device (iLiNP^{TM} device), the present research has provided a compelling direction for developing microfluidic devices to produce various size-controlled LNPs, including artificial exosomes. Precise size controllability of LNPs with a wide range, robust device design, scale-up performance, and effective payload trapping into noncationic LNPs will contribute to various research fields.

The size-controlled LNP producing technologies using the microfluidic devices described in Chapter 2 and Chapter 3 are in corroboration with previous studies, such as those of Chen et al., in 2012, [1] and Zhigaltsev et al., in 2012 [2]. Size-controlled LNP production methods described in the literature use microfluidic devices

called CM devices developed to achieve complete mixing in the microchannel. However, effective dilution of ethanol from lipid solutions is expected more important for the size controllability of LNPs than the complete mixing of lipid solution and an aqueous solution (Maeki et al. in 2017 [3]). Unlike the CM design, the baffle devices have been designed to achieve effective ethanol dilution. Therefore, these devices achieve precise size control of sub-100 nm LNPs with a broader range than the CM device. In addition to the production of LNPs, solvent dilution dynamics in the device will be applicable for other biocompatible nanoparticles formed by self-assembly.

Although the microfluidic post-treatment methodology described in Chapter 4 was developed based on structural dynamics of LNPs reported in the literature reviewed in the chapter, the influences of the indispensable post-treatment process on the final products have not been investigated in detail. The findings regarding the kinetic effects of microfluidic ethanol dilution at the post-treatment process on the final products will contribute to material sciences and biosciences. The development of integrated device with several functions is an effective strategy for improving throughput [4]. However, the integrated microfluidic device has limited utility for microfluidic remote loading in the post-treatment process. Unlike conventional off-device treatments, the developed integrated baffle devices allow high-throughput production of LNPs and improved precise size controllability by preventing undesirable LNPs aggregation and fusion through the microfluidic post-treatment. The microfluidic post-treatment process-assisted integration concept is expected to be widely applicable for various lipid systems and will enable the high-throughput practical production under strict hygiene-controlled conditions.

Exosome-like NPs are expected to have great applicability in developing non-toxic nanomedicines, as described in Chapter 5. Although several studies reviewed in the chapter reported the production of RNA-loaded, noncationic LNPs including artificial exosomes, these NPs are produced using multi-step processes composed of hydration and size adjustment. Conversely, the iLiNP device-assisted production of noncationic LNPs allows simultaneous size controllability and effective RNA encapsulation, as discussed in Chapter 5. The seamless

process and the applicability to produce size-controlled exosome-like LNPs will contribute to exosome-inspired drug development and biological analysis systems.

6.3 Limitations of the Research and Future Prospects

The limitations of this study and suggested directions for future research are described below.

First, only ethanol was used as the lipid solvent in this study. Ethanol is an organic solvent with low toxicity that is used for pharmaceutical production [ICH guideline Q3C (R6) on impurities: guideline for residual solvents-step 5, (2019)]; however, the solvent selection could have affected the size controllability and the encapsulation efficiency. Applicability to produce lipophilic, drug-loaded LNPs is also limited by the low solubility of lipophilic drugs into ethanol. Therefore, it would be interesting to expand the lipid solvent type, which could allow further applications.

Second, almost all LNPs produced in this study were characterized with the dynamic light scattering (DLS) measurement. Although the DLS is widely used for measuring the size of NPs in various research fields, it is better to analyze the LNPs with several methods, such as nano tracking analysis (NTA) and transmission electron microscopy (TEM), for a detailed evaluation, as discussed in Chapter 4 and Chapter 5. Furthermore, analysis of the LNP structural details under biological conditions is expected to contribute to the development of novel nanocarriers and understanding structural dynamics.

Third, siRNA, mainly used as a payload in this study, is a small-sized genetic drug compared with other genetic drugs, such as mRNA and plasmid DNA. Therefore, additional optimization processes of the device design and the production conditions may be needed to produce other genetic, drug-loaded LNPs. In addition, the exosome-like NPs produced in this study are imperfect because of a lack of functional modifications. To be applicable in exosome-inspired drug development, further investigations for surface modifications such as using membrane proteins are also essential.

Despite several limitations mentioned above, the developed microfluidic devices and established concept for designing microfluidic devices to produce size-controlled LNPs have great potential for producing various nanomedicines composed of amphipathic molecules and promoting individualized medications. In particular, the microfluidic techniques are expected to contribute to the effective development of mRNA vaccines against the severe respiratory syndrome coronavirus 2 (SARS-CoV-2), which are in clinical trials. Furthermore, this research provides valuable findings of the structural dynamics of LNPs and the effect of size distributions on the gene-silencing activity. Therefore, this study is expected to contribute to drug development technologies and various life science fields.

References

[1] D. Chen, K. T. Love, Y. Chen, A. A. Eltoukhy, C. Kastrup, G. Sahay, A. Jeon, Y. Dong, K. A. Whitehead and D. G. Anderson, *J. Am. Chem. Soc.*, **134**, 6948-6951 (2012)

[2] I. V. Zhigaltsev, N. Belliveau, I. Hafez, A. K. K. Leung, J. Huft, C. Hansen and P. R. Cullis, *Langmuir*, **28**, 3633-3640 (2012)

[3] M. Maeki, Y. Fujishima, Y. Sato, T. Yasui, N. Kaji, A. Ishida, H. Tani, Y. Baba, H. Harashima and M. Tokeshi, *PLoS One*, **12**, e0187962 (2017)

[4] R. R. Hood, W. N. Vreeland and D. L. DeVoe, *Lab Chip*, **14** (2014)

List of Publications

[1] **Niko Kimura**, Masatoshi Maeki, Yusuke Note, Yusuke Sato, Akihiko Ishida, Hirofumi Tani, Hideyoshi Harashima, and Manabu Tokeshi, "Development of the iLiNP Device: Fine Tuning the Lipid Nanoparticle Size within 10 nm for Drug Delivery," *ACS Omega*, 3, 5044-5051 (2018) doi: 10.1021/acsomega.8b00341

[2] **Niko Kimura**, Masatoshi Maeki, Yusuke Sato, Akihiko Ishida, Hirofumi Tani, Hideyoshi Harashima, and Manabu Tokeshi, "Development of a Microfluidic-Based Post-Treatment Process for Size-Controlled Lipid Nanoparticles and Application to siRNA Delivery," *ACS Applied Materials & Interfaces*, 12, 34011-34020 (2020) doi: 10.1021/acsami.0c05489

[3] **Niko Kimura**, Masatoshi Maeki, Kosuke Sasaki, Yusuke Sato, Akihiko Ishida, Hirofumi Tani, Hideyoshi Harashima, Manabu Tokeshi, "Three-Dimensional, Symmetrically Assembled Microfluidic Device for Lipid Nanoparticle Production", *RSC Advances*, 11, 1430-1439 (2021) doi: 10.1039/d0ra08826a

[4] **Niko Kimura**, Masatoshi Maeki, Akihiko Ishida, Hirofumi Tani, Manabu Tokeshi, "One-Step Production of Highly Biocompatible Size-Controlled Non-Cationic Exosome-Like Nanoparticles for RNA Delivery Using a Microfluidic Device", *ACS Applied Bio Materials*, 4, 1783-1793 (2021) doi: 10.1021/acsabm.0c01519

[5] **Niko Kimura**, Masatoshi Maeki, Yusuke Note, Yusuke Sato, Akihiko Ishida, Hirofumi Tani, Hideyoshi Harashima, and Manabu Tokeshi, "A Small-Sized Lipid Nanoparticles Production Method Using Microfluidic Devices with Baffle Structures," *Proceedings of Micro Total Analysis System 2017,* 1, 965-966 (2017)

[6] **Niko Kimura**, Masatoshi Maeki, Nana Okabe, Yusuke Sato, Akihiko Ishida, Hirofumi Tani, Hideyoshi Harashima, and Manabu Tokeshi, "Microfluidic Stepwise and Rapid Ethanol Dilution for Precise Size Control of Lipid Nanoparticles," *Proceedings of Micro Total Analysis System 2018*, 1, 1404-1405 (2018)

[7] **Niko Kimura**, Masatoshi Maeki, Yusuke Sato, Kosuke Sasaki, Akihiko Ishida, Hirofumi Tani, Hideyoshi Harashima, and Manabu Tokeshi, "Development of a Three-Dimensional Micromixer Device for Production of Various Lipid-Based Nucleic Acid Nanocarriers," *Proceedings of Micro Total Analysis System 2019*, 1, 368-369 (2019)

[8] Masatoshi Maeki, **Niko Kimura**, Kazuki Shimizu, Kento Yonezawa, Nobutaka Shimizu, Akihiko Ishida, Hirofumi Tani, Manabu Tokeshi, "Understanding the Lipid Nanoparticles Structure Dynamics Using a Time-Resolved SAXS Measurement," *Proceedings of Micro Total Analysis System 2019*, 1, 1478-1479 (2019)

[9] **Niko Kimura**, Masatoshi Maeki, Akihiko Ishida, Hirofumi Tani, Hideyoshi Harashima, and Manabu Tokeshi, "An Aprotic Polar Solvent Assisted Size-Tuning Method for Microfluidic Production of Lipid-Based Drug Nanocarriers," *Proceedings of Micro Total Analysis System 2020*, 1, 1021-1022 (2020)

[10] **Niko Kimura**, Masatoshi Maeki, Akihiko Ishida, Hirofumi Tani, Hideyoshi Harashima, and Manabu Tokeshi, "Lipid Nanoparticle-Size Control by Microchannel with Baffle Structures," *Chemistry and Micro-Nano Systems* (in Japanese), 16, 30-31 (2017)

[11] Masatoshi Maeki, **Niko Kimura**, Yusuke Sato, Hideyoshi Harashima, Manabu Tokeshi, "Advances in Microfluidics for Lipid Nanoparticles and Extracellular Vesicles and Applications in Drug Delivery Systems," *Advanced Drug Delivery Reviews*, 128, 84-100 (2018) doi: 10.1016/j.addr.2018.03.008

[12] **Niko Kimura**, Masatoshi Maeki, and Manabu Tokeshi, "Microfluidic Devices for Lipid Nanoparticle Preparation," *Chemical Engineering* (in Japanese), 63, 31-37 (2018)

[13] Keine Nishiyama, **Niko Kimura**, Masatoshi Maeki, and Manabu Tokeshi, "Microfluidic Device: As a Tool of Pharmaceutical Research and Development," *Journal of Pharmaceutical Science and Technology, Japan* (in Japanese), 79, 124-129 (2019) doi: 10.14843/jpstj.79.124

[14] **Niko Kimura** and Manabu Tokeshi, “Development of Microfluidic Devices for Precise Size Control of Lipid Nannoparticles,” *Hosokawa Powder Technology Foundation Annual Report*, 27, 154-156 (2020) doi: 10.14356/hptf.18505

[15] **Niko Kimura**, Masatoshi Maeki, Manabu Tokeshi, “Microfabrication and Microfluidic Devices for Drug Delivery,” *Microfluidics for Pharmaceutical Applications: From Nano/Micro Systems Fabrication to Controlled Drug Delivery*, Hélder A. Santos, Dongfei Liu, Hongbo Zhang, eds., 123-136, Elsevier, (2019) doi: 10.1016/B978-0-12-812659-2.00005-3

Patent

[1] 3D-channel structure and nanoparticle formation method using same, Masatoshi Maeki, Manabu Tokeshi, **Niko Kimura**, Yusuke Sato, Hideyoshi Harashima, PCT/JP2019/039347 (International filling date: October 4th, 2019)

[2] Method for producing particle-containing aqueous solution, Masatoshi Maeki, Manabu Tokeshi, **Niko Kimura**, Yusuke Sato, Hideyoshi Harashima, PCT/JP2019/043420 (International filing date: November 6th, 2019)

Acknowledgement

This thesis is the result of the author's research in the Bioanalytical Chemistry Laboratory, Graduate School of Chemical Sciences Engineering, Hokkaido University. Getting to this point of my life would have been impossible without the several important people who have supported me along the way, and my deepest gratitude goes out to all of them.

First, I would like to express my sincerest respect and gratitude to my supervisor, Professor Manabu Tokeshi of the Division of Applied Chemistry, Faculty of Engineering, Hokkaido University, for his guidance, wisdom, meaningful advice, continuous support, and encouragement as I take on the challenges of pursuing my Ph.D. degree. He provided me not only with my view of research but also views of life. I doubt that I will ever be able to fully convey my appreciation, but I owe him my eternal gratitude.

I am deeply grateful and proud that I am part of the Bioanalytical Chemistry Laboratory (Tokeshi Lab). I am especially grateful to Associate Professor Hirofumi Tani, Assistant Professor Akihiko Ishida, and Assistant Professor Masatoshi Maeki of the lab for the valuable assistance, advice, and discussions. A very special thank you goes out to Professor Ishida for providing me with his precious advice that was like a father's guidance and to Professor Maeki for providing me with his valuable technical advice and our journeys together to many academic conferences.

I would like to acknowledge Associate Professor Hirofumi Tani and Professor Toshifumi Satoh of Faculty of Engineering, Hokkaido University and Professor Kazuki Sada of the Faculty of Science, Hokkaido University for accepting the responsibility of being my official co-supervisors.

I also want to acknowledge Professor Hideyoshi Harashima and Assistant Professor Yusuke Sato of Faculty of Pharmaceutical Sciences, Hokkaido University.

I would like to thank Dr. Kobayashi and Nikon Imaging Center at Hokkaido University for the use of the confocal microscope system and for carrying out the image analysis.

I would like to acknowledge the Grant-in-Aid for the Japan Society for the Promotion of Science Fellows, Hosokawa Powder Technology Foundation, and Kato Memorial Bioscience Foundation, the Special Education and Research Expenses from the Ministry of Education, Culture, Sports, Science and Technology, 2020 Feasibility Study Program of the Frontier Chemistry Center, Faculty of Engineering, Hokkaido University, JST-PRESTO, and JST-CREST program.

Because of my research, I attended many academic conferences. Thanks to all the professors, students, and participants, I had great inspiration and experiences through the conference presentations and traveling for international conferences. I would especially like to thank Eriko Kamata of Japan Women's University and Yumi Moriya of Toyo University, who discussed scientific techniques at academic conferences and made me laugh whenever I was feeling low. I sincerely thank each member of Baba Lab of Nagoya University, Kitamori Lab of the University of Tokyo, Sato Lab of Gunma University, Seki Lab of Chiba University, Sato Lab, and many other people with whom I had delightful dinners. I have lovely memories of the conferences.

I would also like to thank my lab mates, Takeshi Komatsu and Keine Nishiyama, who worked in the lab with me and made my lab life exceptionally fulfilling, Taiga Ajiri, Osamu Wakao, Donny Nugraha Mazaafrianto, Lori Shayne A. Busa, Saeed Mohammadi, Yuka Fujishima, Yuto Kikuchi, Seiya Nakamata, Daichi Fujii, Shohei Yamazaki, Akinori Yamaguchi, Yuka Matsuura, Kota Kikuchi, Yuki Kudo, Saya Sato, Ryohei Mizukami, Yi Bao, Yuri Moratelli Piske, Shingo Ikeda, Kazuki Shimizu, Ayano Nakamura, Koki Hoshikawa, Yang Yi, Issei Takata, Reo Takeda, Takuma Nishimura, Ryoga Maeda, Chen po-sheng, Yuto Okada, Tomoaki Funakubo, Shizuka Kuki, Yasunobu Nonaka, Kazuki Takahashi, Shuya Uno, Asuka Koza, Rikuro Saiki, Ayuka Niwa, our lab secretary Kokoro Haruki-San, and research fellow Hiroko Matsumura-san. I would also like to thank Michiko Tani-san of Lilac Pharma Inc.

Finally, I would like to extend a big thank you to my family; they provided me with the opportunity to study, while providing unwavering support.